VOLUME 34 MAY 1956 NUMBER 3

UNIVERSITY
OF MICHIGAN
MAY 7 1956
ENGINEERING
LIBRARY

Canadian Journal of Technology

Editor: G. A. LEDINGHAM

Published by THE NATIONAL RESEARCH COUNCIL
OTTAWA CANADA

CANADIAN JOURNAL OF TECHNOLOGY

(Formerly Section F, Canadian Journal of Research)

Under the authority of the Chairman of the Committee of the Privy Council on Scientific and Industrial Research, the National Research Council issues THE CANADIAN JOURNAL OF TECHNOLOGY and six other journals devoted to the publication, in English or French, of the results of original scientific research. Matters of general policy concerning these journals are the responsibility of a joint Editorial Board consisting of: members representing the National Research Council of Canada; the Editors of the Journals; and members representing the Royal Society of Canada and four other scientific societies.

The Chemical Institute of Canada has chosen the Canadian Journal of Technology and the Canadian Journal of Chemistry as its medium of publication for scientific papers.

EDITORIAL BOARD

Representatives of the National Research Council

A. N. Campbell, *University of Manitoba*
G. E. Hall, *University of Western Ontario*
E. G. D. Murray, *McGill University*
D. L. Thomson, *McGill University*
W. H. Watson (Chairman), *University of Toronto*

Editors of the Journals

D. L. Bailey, *University of Toronto*
T. W. M. Cameron, *Macdonald College*
J. B. Collip, *University of Western Ontario*
G. A. Ledingham, *National Research Council*
Léo Marion, *National Research Council*
R. G. E. Murray, *University of Western Ontario*
G. M. Volkoff, *University of British Columbia*

Representatives of Societies

D. L. Bailey, *University of Toronto*
Royal Society of Canada
T. W. M. Cameron, *Macdonald College*
Royal Society of Canada
J. B. Collip, *University of Western Ontario*
Canadian Physiological Society
R. G. E. Murray, *University of Western Ontario*
Canadian Society of Microbiologists
H. G. Thode, *McMaster University*
Chemical Institute of Canada
T. Thorvaldson, *University of Saskatchewan*
Royal Society of Canada
G. M. Volkoff, *University of British Columbia*
Royal Society of Canada; Canadian Association of Physicists

Ex officio

Léo Marion (Editor-in-Chief), *National Research Council*
F. T. Rosser, Director, Division of Administration, *National Research Council*

Manuscripts for publication should be submitted to Dr. Léo Marion, Editor-in-Chief, Canadian Journal of Technology, National Research Council, Ottawa 2, Canada.
(For instructions on preparation of copy, see **Notes to Contributors** (inside back cover).)

Proof, correspondence concerning proof, and orders for reprints should be sent to the Manager, Editorial Office (Research Journals), Division of Administration, National Research Council, Ottawa 2, Canada.

Subscriptions, renewals, requests for single or back numbers, and all remittances should be sent to Division of Administration, National Research Council, Ottawa 2, Canada. Remittances should be made payable to the Receiver General of Canada, credit National Research Council.

The journals published, frequency of publication, and prices are:

Canadian Journal of Biochemistry and Physiology	Bimonthly	$3.00 a year
Canadian Journal of Botany	Bimonthly	$4.00 a year
Canadian Journal of Chemistry	Monthly	$5.00 a year
Canadian Journal of Microbiology	Bimonthly	$3.00 a year
Canadian Journal of Physics	Monthly	$4.00 a year
Canadian Journal of Technology	Bimonthly	$3.00 a year
Canadian Journal of Zoology	Bimonthly	$3.00 a year

The price of single numbers of all journals is 75 cents.

Canadian Journal of Technology

Issued by THE NATIONAL RESEARCH COUNCIL OF CANADA

VOLUME 34 MAY 1956 NUMBER 3

NICKEL–CADMIUM BATTERIES

I. SINTERED PLATES FROM A NEW CANADIAN NICKEL POWDER[1]

BY E. J. CASEY, P. L. BOURGAULT, AND PHYLLIS E. LAKE

ABSTRACT

Sintered plaques of high porosity and good mechanical strength have been made from a new domestic nickel powder. The plaques, when impregnated and given electrolytic oxidations and reductions in a test cell, gave electrical capacities at low rates of discharge equal to those of plates produced commercially from carbonyl nickel powder; and at extremely high rates gave 15–20% less than the commercial plates. Physical and electrical characteristics of the plates are interpreted in terms of the physical properties of the new powder and various factors in the processing. Certain problems which need detailed investigation are pointed out.

INTRODUCTION

The conventional nickel–cadmium battery was invented in Sweden about 1900, and has since been used widely in Europe for various industrial applications. Porous plaques of sintered nickel to contain the electrically active material were developed in Germany about 1935 (8). The plaque was made by sintering fine, irregular carbonyl nickel powder in a reducing atmosphere for a few minutes at about 1650° F. The nickel metal matrix so formed was about 80% free volume, and into the pores were impregnated the electrically active materials, nickel hydroxide to form positives and cadmium hydroxide to form negatives.

The advantages of the nickel–cadmium system have been adequately described in the trade literature. Some electrical characteristics of early U.S. sintered-plate batteries were published recently by Ellis, Mandel, and Linden (2). Mounting evidence obtained in these Laboratories as well as elsewhere shows that in this construction the battery is a versatile, dependable, and rugged power source.

To be suitable for making sintered plaques, nickel powder must be quite pure and inert to caustic; physically, it must sinter to give a mechanically strong matrix which does not crumble during the impregnation process nor during the subsequent expansions and contractions of the active material

[1]*Manuscript received December 5, 1955.*
Contribution from Defence Research Chemical Laboratories, Ottawa. Issued as D.R.C.L. Report No. 187.

which occur while the plate is being charged and discharged. Pores must be so interconnected that an electrolytic path exists between each pore and the bulk electrolyte. Pore size distribution must be optimum—not so large that the solid layer of active material on the surface of the pore is thick, nor so small that the electrolyte channels within the plaque are severely constricted; either of these extremes would result in high electrical resistance. Nickel powder made by the carbonyl process has the desired characteristics. In this survey work it was found that it is possible to make satisfactory sintered plates on a laboratory scale from seed nickel powders made by Sherritt Gordon Mines Ltd. by catalytic hydrogenation of an aqueous nickel ion solution (5). Several fundamental and applied problems encountered in the formulation of finished plates from the raw powder are pointed out in the following sections. Certain of the more important of these problems are now being studied in more detail.

MATERIALS AND METHODS

Powders

The powders surveyed in this work are listed in Table IA.

TABLE IA

Type of powder	Source	Apparent density (gm./cc.)	Analysis (%)		
			Fe	Co	S
NiO	Nicaro Nickel Co.	2.0	0.34	0.45	0.02
NiO	Sherritt Gordon Mines Ltd.	0.73–0.86	—	0.07	0.18
Ni(fine) A	Sherritt Gordon Mines Ltd.	0.72	0.33	0.10	0.014
Ni(fine) B	Sherritt Gordon Mines Ltd.	0.92	0.052	0.26	0.011
Ni(fine) C	Sherritt Gordon Mines Ltd.	1.28	0.046	0.32	0.012
Ni(heavy)	Sherritt Gordon Mines Ltd.	3.5–4.5	0.1–0.2	0.10	0.09–0.10

TABLE IB

PARTICLE SIZE DISTRIBUTION OF NICKEL POWDERS

Particle diameter (microns)	% by wt.						
	Nicaro NiO	S.G. NiO	Ni(fine) A	Ni(fine) B	Ni(fine) C	Ni(fine) A+C	Ni(heavy)
>150*	12.6	4.4	0.5	0.1	0.2	0.3	0.2
125–150	2.3	0.7	0.6	0.3	0.2	0.4	0.3
105–125	1.9	2.1	1.3	0.8	0.2	0.7	0.9
88–105	1.1	5.5	2.5	3.9	0.2	1.4	3.5
74–88	1.1	8.6	11.6	7.3	1.1	6.3	10.0
64–74	1.1	14.0	21.3	15.8	2.8	12.0	30.5
53–64	0.9	6.4	16.2	12.7	4.4	10.3	26.0
43–53	1.7	15.8	20.0	18.0	9.0	14.5	29.8
32–43†	0.3	0.8	3.0	3.3	8.0	9.2	1.6
16–32	29.0	33.3		4.1	25.4	7.2	0.1
10–16	25.4	4.8	10.5			3.6	—
5–10	8.5	1.3		17.0	47.0	27.8	—
<5	11.5	1.0	16.5	16.5	9.5	11.7	—

**Diameters above 43 microns, U.S. National Bureau of Standards sieve size specifications.*
†Diameters below 43 microns, Stokes equivalent diameters as obtained on Roller air separator.

Sintering

The first survey work was done by R. C. Shnay, Mines Branch, Department of Mines and Technical Surveys. The sintering was done under coke, in a CO atmosphere. The results showed promise, especially for the fine nickel powders. The chief problems encountered were (i) brittleness, ascribed to high sulphur in the atmosphere of the furnace, and (ii) unsatisfactory bonding in the sinter, ascribed to the heat capacity and chemical properties of the atmosphere. The survey was continued and expanded by P. H. White and J. Maisonneuve at A. C. Wickman Ltd., using a furnace with an electrolytic hydrogen atmosphere.

After preliminary experiments the following procedure was adopted. Sintering was done in carbon molds of internal dimensions 4.50 in. × 3.25 in. × 0.070 in. About 0.030 in. of powder was placed in the mold, an annealed and flattened nickel wire screen laid on top, and then the mold filled to overflowing with powder. Excess was scraped off with a straightedge. Best results were obtained if the mold cover was provided with an undercut, which allowed the cover to rest on the powder and provide a light, steady pressure during sintering. The undercut was deep enough to force no more than 20% compression. The molds were fed through the furnace in a continuous operation, each one pushing the one ahead of it.

Sintering was done over a wide range of time and temperature for each powder individually, and then for various mixtures of the powders. Physically satisfactory* plates were obtained only under the sets of conditions given in Table II. Sintering time is here expressed as time spent in the hot zone of the furnace, and the temperature recorded is that of the hot zone.

TABLE II

CONDITIONS PRODUCING PHYSICALLY SATISFACTORY PLAQUES

Plaque type No.	Composition (% by volume)	Temp. (° F.)	Time (hr.)	Porosity*
1	100% NiO—Nicaro	1900–2000	1.0	77–79
2	55% NiO+45% Ni(heavy)—Sherritt	1900	1.0	80
3	100% Ni(fine) A—Sherritt	1900	2.0	80
4	100% Ni(fine) B—Sherritt	1900	2.0	79
5	50% Ni(fine) A+50% Ni(fine) C—Sherritt	1900	1.0	79

**% holes—determined from bulk density of plaque and density of nickel metal, allowance being made for the metal grid.*

Impregnation

The active materials of the battery, nickel hydroxide for the positive and cadmium hydroxide for the negative, were impregnated into the pores of the plaques by a modification of the vacuum method described by Fleischer (4) and by Koren and Baumstark (7). The pores were evacuated, then flooded with the appropriate aqueous nitrate. The plates were then cathodized in

**By arbitrarily chosen minimum standards of high porosity, small shrinkage, and good resistance to crumbling while being abraded with a soft rubber policeman attached to a stirring rod.*

caustic, during which operation the conversion to the hydroxide occurs. Washing in distilled water to constant pH, and then drying, completed one impregnation "cycle". Each plate was given four impregnation cycles so that sufficient active material might be incorporated into the plaque. Because reproducibility of end product has been found, both in this and in other Laboratories, to depend to a marked extent upon technique, thus indicating variables still uncontrolled, the conditions used for the present work are given below in as much detail as possible: Temperature of nitrate bath: 25° C.; reduced pressure: 12 mm. Hg; sp. gr. of aqueous nitrate: 1.55–1.60; pH: 0.8–1.2; immersion time: five minutes; temperature of KOH polarizing bath: 75–85° C.; sp. gr. of KOH: 1.25; current density: 0.13–0.18 amp. cm.$^{-2}$; time of polarization: until voltage is flat (approximately five minutes/gram weight gain).

Testing of Plates

The test cell was contained in a lucite case 3 in. × 6½ in. × 7½ in. The test plate was mounted between two plates of opposite polarity. The plates were covered with 1.30 sp. gr. KOH, and protected from evaporation and CO_2 absorption by a ¼ in. layer of mineral oil.

Voltage characteristics of the test plate were measured against Hg/HgO/KOH (aqueous) electrodes, and were traced on recording voltmeters of ~200,000 ohms input resistance. The end voltage of discharge was chosen to be 0.0 volts with respect to the Hg/HgO electrode (i.e. approximately 0.80 volts and 0.30 volts below the flat voltage of negative and positive plates, respectively). Three forming charges and discharges were given to each plate in the manner suggested in Fleischer's paper (4). During the test program the charging was done at the convenient one-hour rate, with 100% overcharge. Discharges were done at currents between 0.00073 and 0.073 amp. cm.$^{-2}$, a range which includes all normal discharge rates to be expected during operation.

RESULTS

Low Rate Capacity of Plates

It was found that the ampere-hour (AH) capacities of plates made from 100% Nicaro NiO (see Table II) were higher than those made from the other powders, but that these plates shed material and slowly disintegrated during cycling. This was also true, although to a lesser extent, for plates made from the 55% NiO + 45% Ni(heavy)—Sherritt powder. Plates made from the other three powders listed in Table II had no apparent tendency to disintegrate, at least in the first 30 cycles, and all gave quite good electrical capacities. Table III shows typical low rate capacities of these plates as compared with those from plaques made by the Amplex Division, Chrysler Corporation, from carbonyl nickel powder.

High Rate Capacity of Plates

The negatives made from seed nickel powders showed a small loss of capacity with cycling, a phenomenon which is now known to be common and for

TABLE III

MEDIUM-LOW RATE (0.003 AMP. CM.$^{-2}$) CAPACITIES OF TEST PLATES

Plate	Impregnated	Thickness (mm.)	Capacity (AH cm.$^{-2}$ mm.$^{-1}$)	
			Positive	Negative
Seed Ni Type No. 3*	DRCL	1.78	0.0235	0.0355
Seed Ni Type No. 4	DRCL	1.90	0.022	0.036
Seed Ni Type No. 5	DRCL	1.96	0.024	0.0355
Carbonyl Ni Amplex	DRCL	0.64	0.024	0.030
Carbonyl Ni Amplex	Sonotone Corp.	0.64	0.024	0.052
Carbonyl Ni Amplex	NICAD Corp.	2.51	0.021	
		1.90		0.0525 (theoretical (4))

**Reference Table II.*

which cures have been devised (3). Capacities delivered by these negatives at the high rate, 0.070 amp. cm.$^{-2}$ (0.45 amp. in.$^{-2}$), were 75–83% of the low rate capacity. Negatives made commercially gave about the same percentage.

The positives showed a gain in capacity on cycling. It was observed on both the carbonyl and seed nickel plaques that during the electrolysis step the nickel hydroxides gathered near the planar surface of the plate, yet still within the sinter, leaving the middle of the plate devoid of active material. Apparently this material was packed too tightly since initially the high rate capacities were low. Persistent cycling seemed to effect a more even distribution, because the high rate output improved with cycling. The final high rate (at 0.070 amp. cm.$^{-2}$) figures on the seed nickel plates (1.96 mm. thick) were of the order of 0.16 AH cm.$^{-2}$ mm.$^{-1}$, and can be compared with the figures 0.022 and 0.0192 AH cm.$^{-2}$ mm.$^{-1}$ obtained on commercial plates 0.64 mm. thick and 2.51 mm. thick respectively at the same current density.

Results on a 19-Plate Test Cell

In order to obtain the average behavior of several plates under various conditions of current, temperature, etc., a 19-plate cell (PB1) was constructed from plaques of the type 100% Ni(fine) A—Sherritt, impregnated as before. External dimensions of the case were: height 5 in., width 3 in., depth 1 in. The case was lucite, bonded with methylene chloride. Collector tabs and terminal posts were of nickel. The separator was the nylon cloth – unplasticized cellophane – nylon cloth combination now in common use commercially. Based on the weight of active materials in the plate, the theoretical capacity (4) of the positives was 16.3 AH, and that of the negatives 22 AH.

The cell was given three forming cycles, followed by one 24-hr. rate discharge (as had been the single plates), and then cycled on a medium-high rate program based on the theoretical capacity: charged at the 1.0-hr. rate, with 50% overcharge, discharged at the 1.5-hr. rate. After every few cycles a 24-hr. rate discharge was done; the capacity was consistently improved by one of these low-rate discharges. Thus, from cycle 5 to 16 the output was 9–11 AH; the 24-hr. rate discharge 17 gave 19 AH. From cycle 18 to 21 the output was

12–13 AH. Following another 24-hr. rate discharge, the output from cycle 23 to cycle 29 was 13–15 AH. Following a fourth low rate cycle, the output from cycle 31 to cycle 41 gradually increased to become steady at 15–16 AH. Thereafter the full capacity was maintained with cycling.

After conditioning as above, the capacity delivered by the pack of plates of the PB1 was compared directly with that of the best obtainable commercial (carbonyl nickel) cell of comparable size, the type 9800 made by the Sonotone Corporation. Physical characteristics of the two cells are contained in Table IV.

TABLE IV

PHYSICAL CHARACTERISTICS OF EXPERIMENTAL AND COMMERCIAL CELLS

	PB1	9800
Thickness of plates	1.0 mm.	1.0 mm.
Number of positives	10	7
Number of negatives	9	6
Volume of pack of plates	222 $cm.^3$	54 $cm.^3$
Total cell volume	479 $cm.^3$	121 $cm.^3$

Current drains per unit volume chosen for comparing packs of plates were 0.0031, 0.045, and 0.39 amp. $cm.^{-3}$, approximately the 30-, 2-, and 0.2-hr. rates respectively. Capacities per unit volume delivered at various temperatures are listed in Table V. All charging was done at approximately the one-hour rate and at the temperature of the subsequent discharge, and the overcharge in each case mounted to 30–50% of the theoretical capacity.

TABLE V

PERCENTAGE OF LOW RATE CAPACITY AVAILABLE AT MEDIUM AND HIGH RATES

Low rate capacities to 0.6 volts/cell:
Experimental cell PB1—0.086 AH $cm.^{-3}$; 27-hr. rate
Commercial cell 9800—0.110 AH $cm.^{-3}$; 35-hr. rate

	PB1		9800	
Temperature (° F.)	0.045 (amp. $cm.^{-3}$)	0.39 (amp. $cm.^{-3}$)	0.045 (amp. $cm.^{-3}$)	0.39 (amp. $cm.^{-3}$)
77	79%	45	75	65
−20	57	45	65	60
−40	45	40*	54	54%

**To end voltage 0.5/cell.*

After 100 cycles both cells were dissembled and examined. It was observed that there was very little apparent difference in the tendency of the plates to disintegrate. Both shed some material, especially the positives during the low temperature tests. Hence, the strength of the sinter of the seed nickel plate seems to be comparable to that of the carbonyl nickel plate.

DISCUSSION

Electrical Output

In view of the results given on positives in Table III, the difference observed between the low rate capacities of PB1 and the 9800 is not serious. The difference is probably due to compression of the commercial plates either before or after assembling.

The differences observed at high rate, paralleling the single-plate results obtained on positives, are most serious. Fundamentally, they probably are the result of differences in pore size distribution in the sintered nickel plaque. Fig. 1 shows a photomicrograph of both carbonyl nickel and seed nickel plaques. The average pore size seems to be larger in the latter, and if the active material is present to the same weight per unit volume in both cases, the ma-

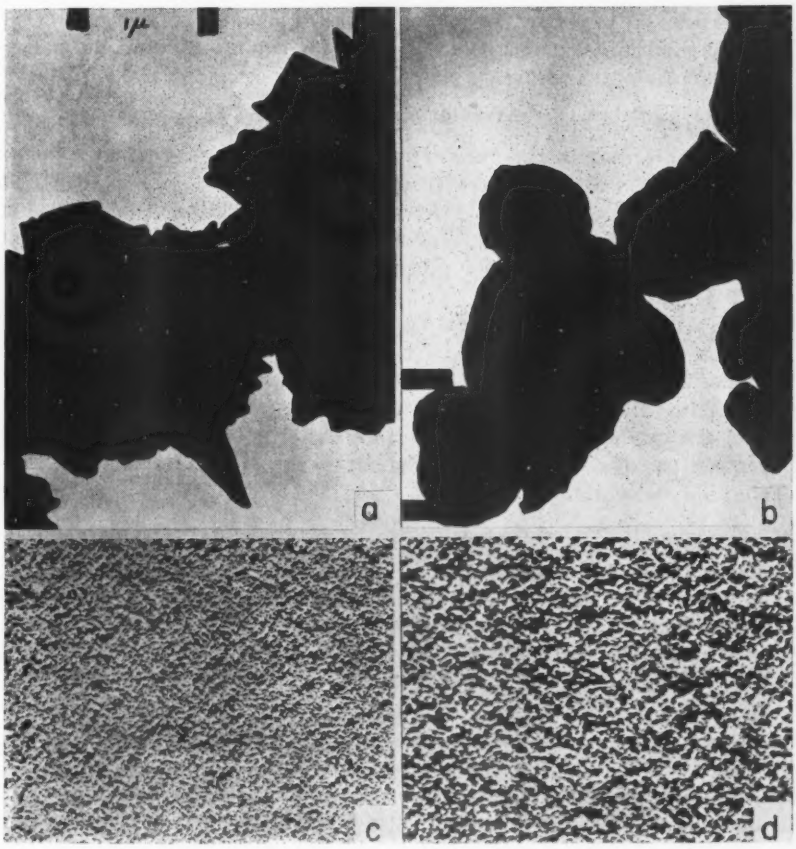

FIG. 1. Electron microscope photograph of (*a*) carbonyl nickel powder particulate, and (*b*) seed nickel powder particulate. Photomicrographs 15× of sintered plaques made from (*c*) carbonyl nickel powder and (*d*) seed nickel powder.

terial must be thicker on the surface in the latter case, and offer higher electrical resistivity. To this might be attributed the poorer high-rate behavior of seed nickel positives.

However, the electrolytic resistance in the pores is probably less in the seed nickel plaque than in the carbonyl nickel plaque because of the higher cross sectional area of the pores. This qualitative observation of Fig. 1*c* and 1*d* is strengthened by two experimental observations: (i) the voltage–time discharge characteristic for negative plates was found to be more flat for seed nickel plates than for carbonyl, even up to currents of 0.15 amp. cm.$^{-2}$ (1.0 amp. in.$^{-2}$); (ii) the output given by PB1 at -20 and $-40°$ F. at the high rate, coupled with previous work (1, 6) on the temperature coefficient of capacity of negative carbonyl nickel plates, indicates that the temperature coefficient of capacity of the seed nickel negatives at high discharge rate is smaller, down to $-40°$. Hence, it might be possible to obtain as good $-40°$ high rate output from the seed nickel plates, which contain far less negative active material per unit volume, than from normally-impregnated carbonyl nickel plates.

Impregnation

Two factors warrant comment. First, the vacuum impregnation technique has been developed over many years to suit carbonyl nickel plaques. The technique developed, however, may not be optimal for seed nickel plaques. Alternatively, the pore size distribution of the sintered nickel plaques may not be the best for the impregnation process used. Thus it has already been noted (Table III) that the impregnation process was found to have uncertainties even for carbonyl nickel plaques. Work on the stoichiometry of the various steps of the over-all process needs to be done first, to be followed by studies on mechanisms. Secondly, iron has been rather inconsistently reported to poison the nickel hydroxide of positive plates, but owing to the complexity of the system the extent of this effect under different experimental conditions has never been clearly defined. The iron content of one of the experimental powders (Table IA) was quite high.

Sintering

A result of some fundamental importance is that the sintering temperature is roughly 200° F. higher for seed nickel than for carbonyl nickel powder; this seems to be directly related to particle shape (Fig. 1). Further, the sintering time in general is much longer with the seed nickel. The results show that sintering time and strength are apparently functions of particle size distribution: thus, heavy seed nickel powder does not produce plaques which are strong and yet highly porous; Ni(fine) A and Ni(fine) B form good plaques in two hours of sintering; and the mixture No. 5 (Table II) forms good plaques in one hour. The practical implication is that the particle size distribution must be optimally controlled if sintering is to be accomplished in minimum time. It is noteworthy as a tentative observation that sintering was accomplished in the shortest time on powders which had an abnormal, two-step particle size distribution—many coarse particles (43 to 105 μ) and many fines ($<16\ \mu$).

With the carbonyl nickel, high strength of sinter and high porosity are not so dependent upon particle size distribution and sintering time because of the spikes radiating from the bulk particle (Fig. 1). Nevertheless the pore size distribution in the plaques must be a function of initial particle size distribution. It is therefore apparent that close quality control of the impregnated battery plate will depend upon careful control of the initial particle size distribution of the nickel powder, whether of the carbonyl or seed nickel type. Further studies on the effects of particle shape and particle size distribution will be reported later.

ACKNOWLEDGMENTS

The contributions of the Department of Mines and Technical Surveys, Consumers Research Laboratories Ltd., A. C. Wickman Ltd., and of Mr. P. H. Trudel and Mr. S. C. O'Brien of this Laboratory during the early stages of this work, are gratefully acknowledged. The co-operation of Sherritt Gordon Mines Ltd., through the development and supply of suitable powders for this work, has been outstanding. The photomicrographs and electron microscope pictures were taken by Mr. L. G. Wilson of Defence Research Chemical Laboratories.

REFERENCES

1. BAARS, E. G. Design factors for alkaline sintered plate storage batteries. U.S. Signal Corps Eng. Lab. Rept. 1949.
2. ELLIS, G. B., MANDEL, H., and LINDEN, D. J. Electrochem. Soc. 99: 250*c*. 1952.
3. FLEISCHER, A. Private communication.
4. FLEISCHER, A. J. Electrochem. Soc. 94: 289. 1948.
5. FORWARD, F. A. Can. Mining Met. Bull. 41: 363. 1953.
6. GEORGE, P. E. and CASEY, E. J. Unpublished results.
7. KOREN, H. W. and BAUMSTARK, G. To Sonotone Corporation, U.S.A.; U.S. Patent No. 2,696,515. 1954.
8. SCHLECT, L. and ACKERMANN, K. To I. G. Farbenindustrie Aktiengesellschaft, Germany; U.S. Patent No. 2,198,042. 1940.

FLUIDIZED SOLIDS COKING OF CANADIAN HEAVY CRUDE OILS[1]

By W. S. Peterson, H. Keller, and P. E. Gishler

ABSTRACT

Three Canadian heavy crude oils, Alberta bitumen, Coleville crude, and Lloydminster crude, were subjected to both thermal and catalytic cracking using the fluidized solids technique. Oil yields were somewhat lower when a catalyst (silica–alumina) bed was used, but gasoline yields were substantially higher and sulphur content was reduced. The gasoline cut of each product was studied in detail. The product of catalytic cracking in each case was substantially higher in aromatic content. There was a similarity in the gasoline cut produced from all three feeds, except that for Coleville and Lloydminster crude there was a higher concentration of low boiling (C_5) fraction. The desirability of extending the work to include other catalysts is indicated. The effect of hydrodesulphurization on gasoline composition was also studied.

PART I. PRODUCTION OF COKER DISTILLATE

Introduction

The purpose of this work was to compare the effect of a catalyst bed with that of an inert solids bed in the upgrading, by cracking, of heavy high-sulphur Canadian crude oils. The reduction of sulphur, the increase in gasoline content, and the change in composition were of interest. Equilibrium synthetic silica–alumina catalyst was used for the catalytic coking. Sand was used as a relatively inert material for fluidized thermal coking.

A regular (but limited) oil inspection was done on the products. A detailed study was made of the gasoline cut involving close fractionation followed by chromatographic analysis of each fraction.

The application of the fluidized solids technique to the separation and coking of Alberta bitumen has been described (5, 7, 9). More recently the application of this technique to the coking of other oils has been reported (11). Extensive use on a commercial scale is indicated. The petroleum industry uses mainly gas oil as feed stock for fluidized catalytic cracking to yield gasoline, and the literature contains a considerable amount of information on this subject. However, very little information is available on the effect of the catalysts on heavy crude or reduced crude oils. A moving bed has been used commercially for the cracking of reduced crude (4). The high cost of silica–alumina catalyst makes its use commercially unattractive. The results described here point out the advantages of a catalyst bed over those of an inert bed and indicate the desirability of further study using other catalysts.

Feed

Three different crude oils were studied. Samples were obtained from (1) the Coleville field in west central Saskatchewan, (2) the Lloydminster field 150

[1]*Manuscript received August 26, 1955.*
Contribution from Division of Applied Chemistry, National Research Council, Ottawa, Canada. Issued as N.R.C. No. 3914.

miles east of Edmonton, and (3) the oil sands deposit at Bitumount, Alberta. The third sample was a hot-water separation product from Alberta bituminous sands and contained 18.7% water and 2.3% solids.

The properties of the three samples are given in Table I.

The sand used as bed material was that remaining after the oil had been separated from the Alberta bituminous sand. It was crushed to 99.6% finer than 100 mesh, to improve its fluidization properties. The solids properties for both sand and equilibrium silica–alumina catalyst are shown in Table II.

TABLE I

INSPECTION OF OIL CHARGE

	Bitumen	Coleville	Lloydminster
Specific gravity	1.01	0.976	0.982
A.P.I. gravity	8.0*	13.9	12.4
Water, %	15–22	0.4–1.4	0.1–0.2
Solids, %	2.3–2.6	0–0.15	0–0.15
Sulphur	4.8*	3.5	3.3
Conradson carbon	14.2*	11.5	8.2
Distillation			
I.B.P., ° F.	390	275	280
10%	670	484	540
20%	750	562	596
30%	—	586	617
50%	—	612	629

**Water and solids free basis.*

TABLE II

PROPERTIES OF CATALYST AND INERT BED MATERIALS

	Catalyst	Sand
Composition	SiO_2–Al_2O_3	SiO_2
Bulk density, lb./cu. ft.	58	90
Size analysis, on 100 mesh	2.0	0.5
100–200	41.1	70.0
200–325	43.7	18.0
through 325	13.2	11.5

Equipment and Operation

The equipment and techniques used in the coking tests were similar to those described in earlier work (7) except for modifications described below (Fig. 1).

The reactor, regenerator, risers, standpipes, and cyclones were of stainless steel. The reactor was $3\frac{1}{4}$ in. I.D., 6 ft. high, and was surmounted by a disengaging section 6 in. I.D. and $3\frac{1}{2}$ ft. high. An internal cyclone was mounted at the top of this section, with a dipleg returning solids to the bed. The regenerator, similar in construction, was 9 in. I.D. with a 14 in. I.D. disengaging section containing an internal cyclone. The 9 in. regenerator provided adequate coke burning capacity for regeneration of catalyst with the heavy feed stock. Stripping was accomplished in the standpipes.

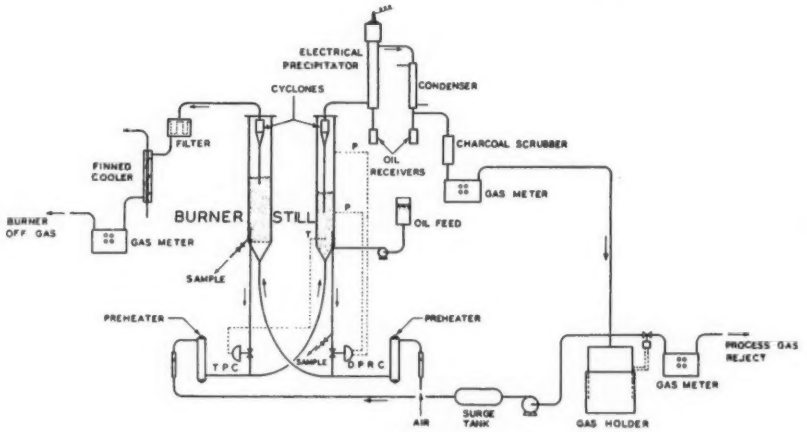

FIG. 1. Pilot plant layout.

Feed rates of about eight pounds per hour were used. Feed was pumped continuously from a heated container mounted on scales so that feed rate could be checked at any time. The oil was fed directly into the side near the base of the reactor bed and recycled process gas carried solids from the regenerator to the reactor as well as agitating the reactor bed. Most of the cracked oil was collected and weighed hourly from an electrical precipitator and a condenser. A light fraction, mainly gasoline, was recovered from the charcoal adsorbers by steam stripping at the end of the run.

The reactor off-gas was metered, and part was recycled as described above. The remainder of the off-gas was rejected after metering and sampling.

The catalyst or sand was continuously circulated to the regenerator where coke was burned. The regenerator off-gas was sampled, metered, and wasted. Materials balances were made on all runs.

Operating data are shown in Table III.

Coking Results

Duration of the runs was about 10 hours. For purposes of yield and product evaluation the first four hours were neglected. Evaluation of silica–alumina catalyst life was not possible with runs of this short duration. However, high sulphur and trace metal content are known to shorten catalyst life.

It had been found in earlier work that coking temperatures between 500° and 525° C. gave satisfactory operating conditions using sand beds. A median temperature of 515° C. was chosen for this coking work with sand. However, with a silica–alumina catalyst bed, this temperature resulted in very severe cracking. Catalytic coking temperature chosen was 475° C. These two operating temperatures were high enough so that the higher boiling constituents in the feed stock did not cause sticking in the fluidized bed. One run was made at 500° C. using a catalyst to study the effect of temperature.

TABLE III

OPERATION

Run No.	92	90	89	84	85	86
Charge Bed	Bitumen inert	Coleville inert	Lloyd. inert	Bitumen catalyst	Coleville catalyst	Lloyd. catalyst
Duration, hr.	10	7	9½	11	10	10
Feed rate (contained oil), lb./hr.	7.05	6.03	9.23	8.22	6.57	6.68
Still(reactor)						
Bed temp., ° C.	512	512	515	475	475	475
Bed depth, in.	34	34	34	34	34	34
Recycle gas, c.f.m.	0.56	0.55	0.63	0.46	0.40	0.42
Bleeds, c.f.m.	0.44	0.50	0.49	0.66	0.66	0.66
Off-gas, c.f.m.	1.14	1.30	1.31	1.56	1.32	1.32
Burner(regenerator)						
Bed temp., ° C.	635	610	600	590	590	590
Bed depth, in.	30	24	24	54	54	54
Air rate, c.f.m.	3.41	3.36	3.52	3.38	3.38	3.38
Bleeds, c.f.m.	0.41	0.41	0.42	0.26	0.31	0.33
Off-gas, c.f.m.	3.75	3.67	3.85	3.19	3.73	3.70

The results are shown in Tables IV and V.

It should be noted that the word "coking" is arbitrarily used to indicate the cracking of a complete crude or reduced crude irrespective of whether the cracking takes place in a catalyst bed or an inert (sand) bed.

Coking wet bitumen and Coleville crude in sand bed yielded 85% by volume coker distillate. The Lloydminster crude yielded 91% by volume. Catalytic coking resulted in lower yields for all three crudes. The lowest yield was with the wet bitumen at 77.6% by volume, while the Lloydminster was 84.7% and

TABLE IV

YIELDS AND INSPECTIONS OF OIL PRODUCTS

Charge Bed	Bitumen inert	Coleville inert	Lloyd. inert	Bitumen catalyst	Coleville catalyst	Lloyd. catalyst
Yield oil, vol. %	85.5	85.0	91.0	77.6	80.0	84.7
Yield oil, wt. %	79.4	80.0	84.2	72.0	73.7	73.7
Oil inspection						
Water, %	Trace	Trace	Nil	Trace	Trace	Trace
Solids, %	Trace	Trace	Nil	Trace	Trace	Trace
Specific gravity, gm./ml.	0.938	0.930	0.912	0.930	0.902	0.888
A.P.I. gravity, deg.	19.3	20.6	23.5	20.6	25.2	27.7
Viscosity 100° F., S.U.S.	76.0	54.9	—	38.2	33.4	33.2
Sulphur total, %	4.0	2.92	—	3.0	2.0	1.6
Conradson carbon, %	7.5	6.0	—	—	3.0	2.4
Distillation, ° F. I.B.P.	122	137	178	113	115	119
10%	308	300	338	208	195	195
20%	440	411	500	303	266	274
30%	528	498	570	387	342	354
50%	620	634	628	515	468	492
70%	662	703	—	631	588	594

TABLE V

YIELDS AND INSPECTIONS OF OTHER PRODUCTS

Run No.	92	90	89	84	85	86
Charge Bed	Bitumen inert	Coleville inert	Lloyd. inert	Bitumen catalyst	Coleville catalyst	Lloyd. catalyst
Process gas, cu. ft./bbl.	—	—	—	1170	755	740
Analysis, %						
Still gas*						
KOH sol.	3.4	4.0	3.8	11.1	6.0	7.6
Unsat.	27.3	26.9	30.6	6.8	17.7	22.2
H_2	14.7	20.1	10.5	43.4	29.8	34.2
CO	0.9	1.4	2.3	3.2	1.1	1.1
Paraffins	53.7	47.6	52.8	31.8	43.6	34.5
Bed material						
Coked solids						
Coke	0.46	0.41	0.32	—	1.2	0.85
Burnt solids						
Coke	0.02	0.01	0.01	—	0.05	0.04

**Corrected to zero N_2.*

the Coleville 80%. The yield of gasoline increased substantially however for all three oils. Figs. 2, 3, and 4 show the distillation curves for the three feed stocks, the three inert coking products, and the three catalytic coking products. Table VI shows the percentage distilling, up to 400° F., 535° F., and 650° F. for these nine oils.

In a catalytic coking run at 500° C. using Lloydminster crude the total oil yield dropped from 84.7% at 475° C. to 77.4% at 500° C., while the gasoline content of the product increased from 36% to 64%.

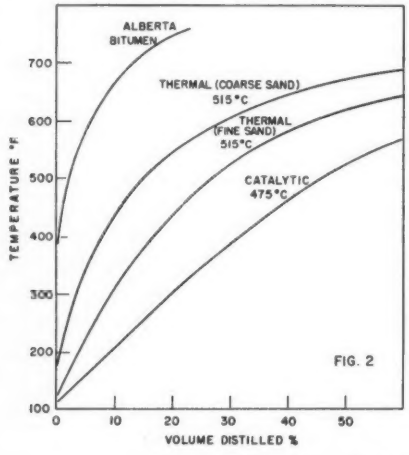

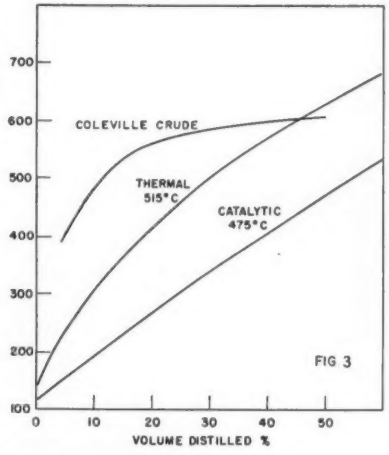

FIG. 2. Distillation curves Alberta bitumen and products.
FIG. 3. Distillation curves Coleville crude and products.

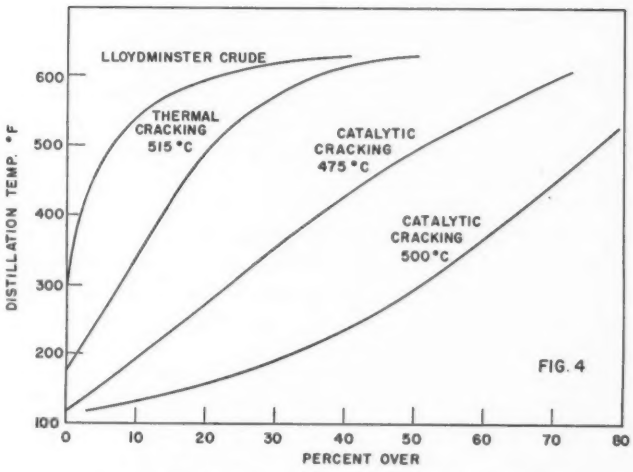

FIG. 4. Distillation curves Lloydminster crude and products.

TABLE VI

COMPARISON OF FEED AND PRODUCTS USING DISTILLATION DATA

Charge source	Cracking		Per cent distilled at:		
	Type	Temp., ° C.	400° F.	535° F.	650° F.
Alberta bitumen	None	—	Zero	3	8
Alberta bitumen	Thermal	515	16	32	62
Alberta bitumen	Catalytic	475	32	52	—
Coleville crude	None	—	5	16	—
Coleville crude	Thermal	515	19	35	53
Coleville crude	Catalytic	475	39	60	—
Lloydminster crude	None	—	2	10	—
Lloydminster crude	Thermal	515	12	25	60+
Lloydminster crude	Catalytic	475	36	58	—
Lloydminster crude	Catalytic	500	64	80	—

A substantial reduction in sulphur content is noted, especially for the catalytic coking product. The sulphur is removed mainly in the form of hydrogen sulphide in the reactor. However, the sulphur is still high and the product would require further expensive treatment, such as hydrogenation, to produce a commercially attractive product.

The Conradson carbon was reduced substantially. In thermal cracking it would appear that there is a surface area effect. On work reported earlier (7) on Alberta bitumen, coarse sand (90% on a 100 mesh Tyler screen) was used, and the gasoline content of the product was 8%. In the present work the same sand was ground more finely to improve the fluidization properties of the bed, and a product containing larger amounts of gasoline was formed.

PART II. A STUDY OF THE GASOLINE CUTS PRODUCED BY COKING

Introduction

In recent years a great deal of effort has gone into studies of the composition of cracking products (1, 2, 6, 8, 10). In the present work a study was made of the products from the thermal and catalytic cracking experiments described above. This was confined to the material boiling in the gasoline range. Careful fractional distillation of the gasoline component of the coker distillates was used, followed by chromatographic analysis to determine the proportions of saturates, unsaturates, and aromatics. This procedure was considered to be a useful method of comparing both the susceptibility of the three crudes to cracking, and the relative effects of inert and catalytic beds on the distribution of hydrocarbon types in the product.

Two other points of interest studied on the gasoline fraction were the distribution of sulphur compounds and the effect of hydrodesulphurization on the distribution of hydrocarbon types. The three feed stocks had high sulphur contents. Coking in a fluidized bed reduced the sulphur content, with the silica–alumina catalyst giving the greater reduction. Since hydrogenation would still be a necessary step to reduce the sulphur content to a commercially attractive level, a knowledge of the types and distribution of sulphur compounds was of interest.

Experimental

Seven gasoline fractions were studied: one thermally cracked sample and one catalytically cracked sample from each of the three crudes and also one thermally cracked sample which had been hydrogenated.

The gasoline samples for study were separated from the rest of the coker distillate by primary distillation, to about 250° C., in a large pot still. These were then carefully fractionated in two Podbielniak Hyper-Cal high temperature fractional distillation columns 25 mm. diameter by 36 in., and 25 mm. by 48 in. long. The 36 in. column was used for the product of sand bed coking and the 48 in. column for the product of catalyst bed coking. The columns contained Heligrid packing and had a multiple metal reflector type radiation shield system in an evacuated jacket.

According to the sample size, the round bottomed flasks used as still pots had a capacity of 3 or 5 liters, and contained a thermometer well. They were attached to the column by means of a 50/30 ball joint. Glass Col Mantles were used for heating the flasks.

Except for the low boiling cuts an automatic fraction collector was used thus allowing continuous operation. Air was displaced from the column by dry nitrogen to prevent reactions of the unsaturated products contained in the samples.

A distillation was started by first flooding the column and then running the still at total reflux for at least six hours before any distillate was taken off. Reflux ratios of 50 to 1 were used to a vapor temperature of 140° C., 100 to 1 between 140° C. and about 180° C., and 150 to 1 between 180° C. and 204° C.

The refractive index was measured of each fraction removed from the fraction

collector and fractions with similar indices were blended together. In this way a very large number of fractions was reduced to about 20 cuts.

The aromatic, olefin, and paraffin plus naphthene content of each cut was determined by chromatography (3) using the standard A.S.T.M. method (D1319–54T). True Bore tubing was used for the analyzer section. Nitrogen pressure was used to force the sample through the silica gel.

Results

Fig. 5 contains a typical distillation curve. It is the gasoline cut of coker distillate produced by cracking Alberta bitumen in a fluidized sand bed at 515° C. Superimposed on the distillation curve is the refractive index curve measured on each of the many fractions. The many fractions were grouped to

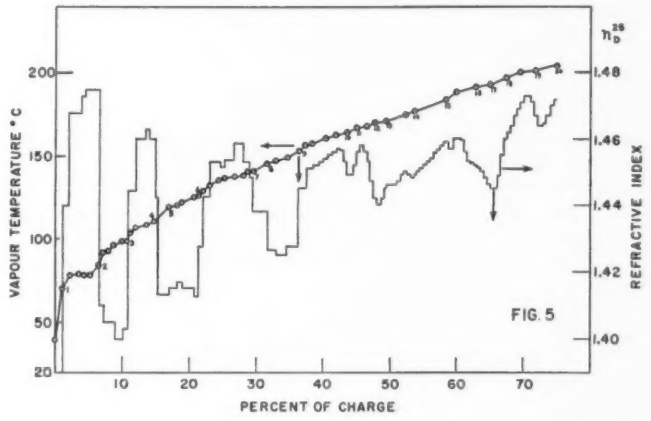

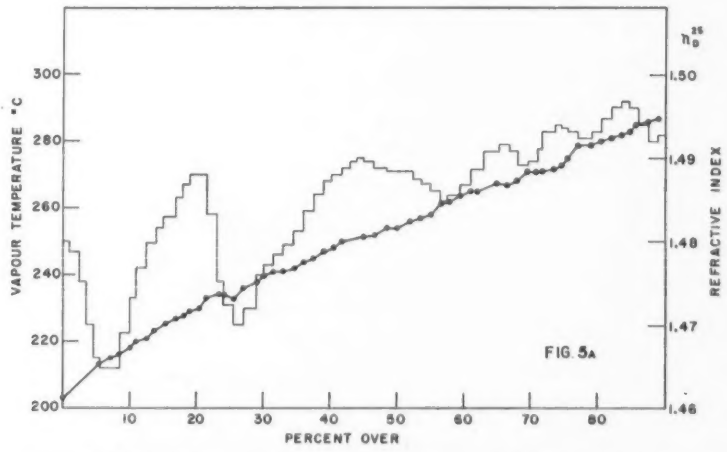

FIG. 5. Fractionation—gasoline cut thermally cracked Alberta bitumen.
FIG. 5A. Fractionation—200°–300° C. cut thermally cracked Alberta bitumen.

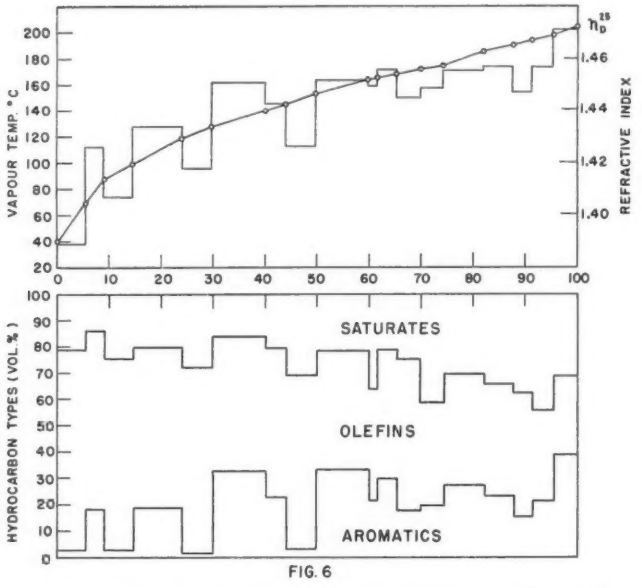

FIG. 6

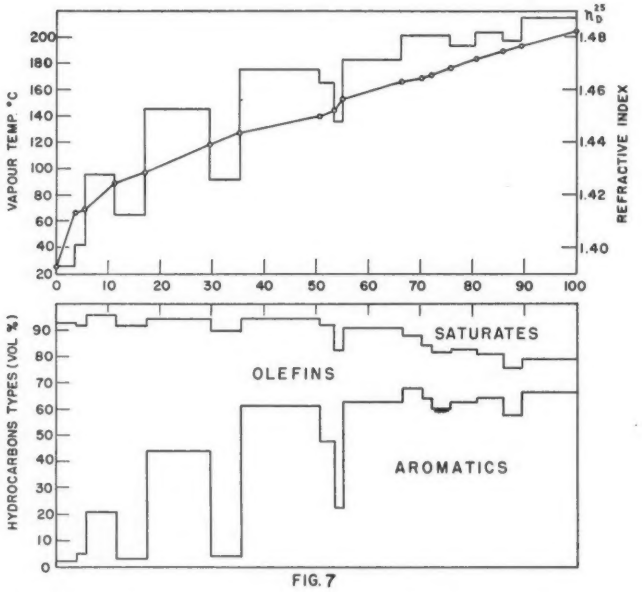

FIG. 7

FIG. 6. Hydrocarbon types—gasoline cut thermally cracked Alberta bitumen.
FIG. 7. Hydrocarbon types—gasoline cut catalytically cracked Alberta bitumen.

yield 20 cuts as indicated by the numbers on the distillation curve. It can be seen that the refractive index served as a guide in the grouping of these fractions. A comparison of the relatively smooth distillation curve with the rapidly fluctuating refractive index curve shows that substantial concentration of hydrocarbon types has been made possible by distillation. The peaks due to benzene, toluene, and xylene plus ethyl benzene are quite prominent. It is interesting to note that even at temperatures above the gasoline range the refractive index curve does not become smooth nor steadily increasing. This is shown in Fig. 5A which gives the data for the fraction boiling in the range 204° to 300° C.

The hydrocarbon type analysis for thermally coked Alberta bitumen is shown in Fig. 6. Also shown are temperatures at which each blended cut was taken for the hydrocarbon type analysis and the refractive index of each blended cut. The olefin content is high, especially in the low boiling range. The saturates content remains relatively constant at about 20% up to 170° C., above which it increases in an irregular fashion. The aromatics curve in the low temperature region is extremely irregular. This is to be expected since there are a limited number of aromatic compounds in this temperature range. Above this the variety of aromatic compounds (i.e. aromatic rings with side chains) becomes sufficient to give a continuous curve with moderate fluctuations.

Fig. 7 shows similar data for gasoline produced from the catalytic coking of Alberta bitumen at 475° C. The results show the marked influence that the catalyst has on the type of product formed. The saturates content is lower than for the thermally cracked bitumen, being less than 10% up to 165° C., increasing to over 20% at 190° C. The aromatic content (plus sulphur compounds) is about doubled except for the 70° to 90° C. blend. There was a decrease in olefin content. The change in composition is more conveniently shown in Fig. 8 and Fig. 9 where per cent olefins and per cent aromatics, respectively, are plotted against vapor temperature for the thermal and catalytic coking. A study of these graphs indicates that the silica–alumina catalyst has a marked influence on the composition of the product. The very substantial increase in aromatic content is mainly at the expense of the olefin content.

In this method of analysis the sulphur compounds (mainly thiophene type) appear with the aromatics.

Figs. 10 to 13 include the distillation data, the refractive index data, and the hydrocarbon type analyses for the gasoline produced from Lloydminster crude and Coleville crude using both sand and catalyst beds. The curves indicate a striking similarity in products. There also appears to be one important difference. There is a much larger amount of material boiling below 70° C. in the Lloydminster and Coleville products than in the Alberta bitumen product. The catalytically cracked gasoline produced from Lloydminster and Coleville crude contains 27% boiling up to 70° C. (mainly C_5 hydrocarbons) whereas Alberta bitumen yielded only 5%. About 90% of this low boiling material consists of olefins.

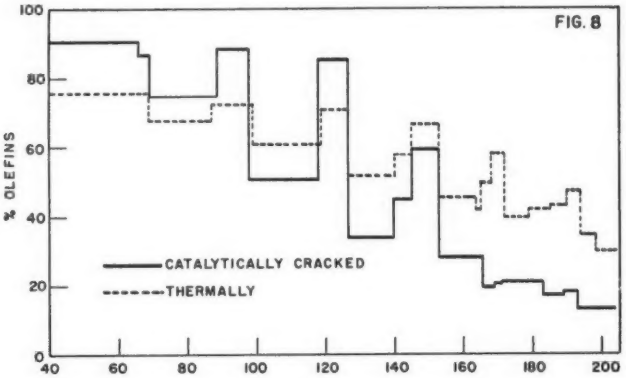

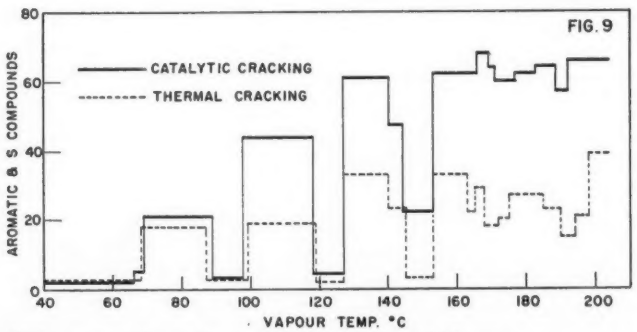

FIG. 8. Olefin content thermally vs. catalytically cracked bitumen.
FIG. 9. Aromatic plus sulphur compound content thermally vs. catalytically cracked bitumen.

The aromatic contents of the three gasolines from catalytic coking are plotted against vapor temperature in Fig. 14. Throughout most of the gasoline range the aromatics content was highest for the Alberta bitumen product and lowest for the Coleville crude product. The difference however is not great, whereas there is a marked similarity in appearance of all three curves.

The compositions of the gasolines studied are given in Table VII. They were

TABLE VII
DISTRIBUTION OF HYDROCARBON TYPES IN GASOLINE*

		% Saturates	% Olefins	% Aromatics and sulphur compounds
Alberta bitumen	Thermal	26.3	53.4	20.3
	Catalytic	11.4	42.0	46.6
	Thermal + hydrogenation	68.6	13.8	17.6
Lloydminster	Thermal	18.1	60.2	21.7
	Catalytic	18.6	51.7	29.7
Coleville	Thermal	26.3	45.0	28.7
	Catalytic	15.2	58.5	26.3

**Calculated mean values over total gasoline range.*

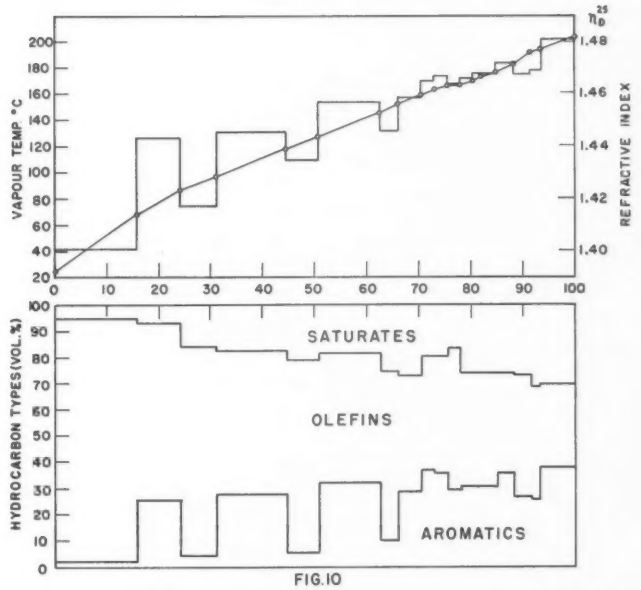

FIG. 10

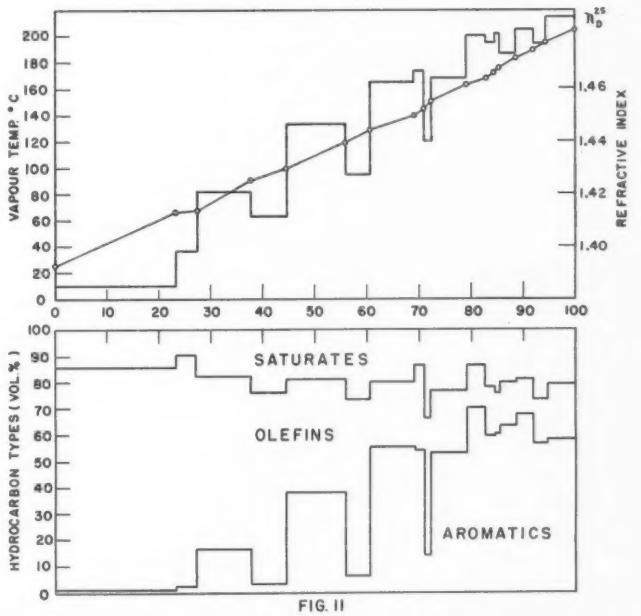

FIG. 11

FIG. 10. Hydrocarbon type—gasoline cut thermally cracked Lloydminster crude.
FIG. 11. Hydrocarbon type—gasoline cut catalytically cracked Lloydminster crude.

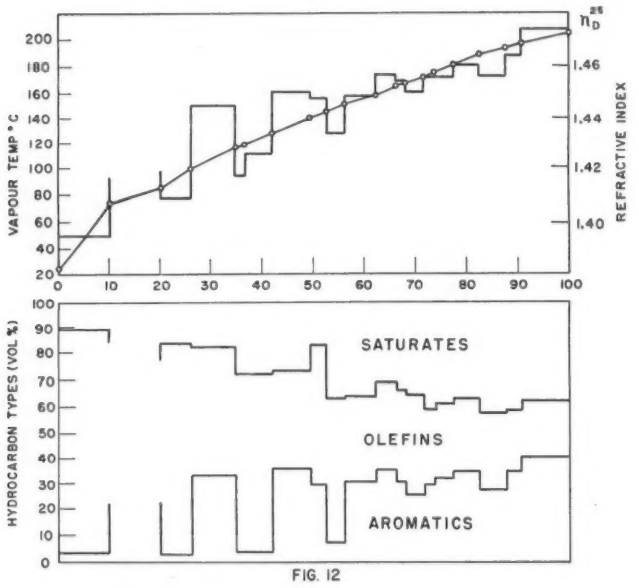

FIG. 12

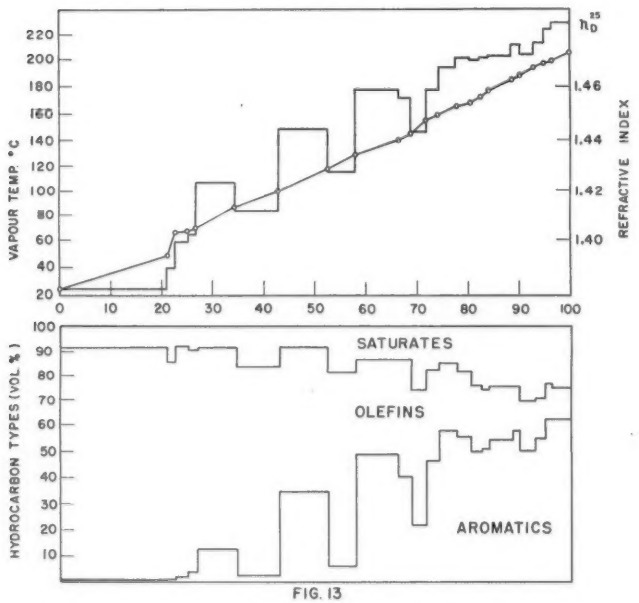

FIG. 13

FIG. 12. Hydrocarbon type—gasoline cut thermally cracked Coleville crude.
FIG. 13. Hydrocarbon type—gasoline cut catalytically cracked Coleville crude.

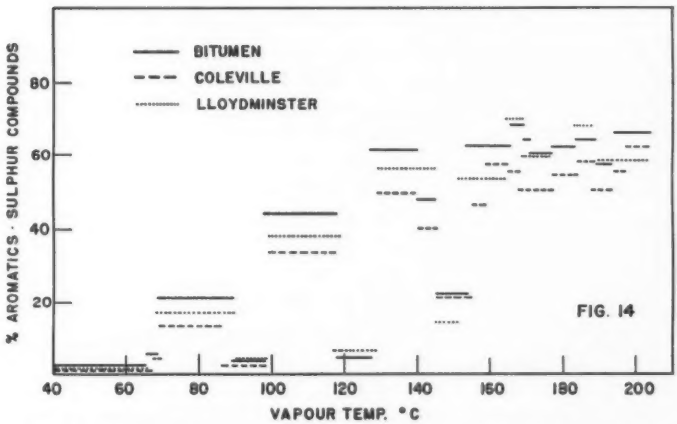

FIG. 14. Aromatic and sulphur compounds effect of feed on catalytically cracked product.

calculated from data used to plot Figs. 6, 7, 10, 11, 12, 13, and 18. The high aromatic content of the catalytically cracked Alberta bitumen is of particular interest when antiknock properties are being considered although it must be remembered that this fraction includes sulphur compounds.

Sulphur Content

The feed stocks were high in sulphur ranging from 3.3% for Lloydminster to 4.8% for Alberta bitumen. Cracking reduces the sulphur content in the product to 4% with inert bed and to 3% with catalyst bed using Alberta bitumen feed stock.

The quantitative separation and identification of sulphur compounds in the gasoline range by conventional methods is extremely difficult possibly because of the high olefin content. Any conclusions at this stage of the work are therefore open to argument.

The blended cuts, Fig. 5, were analyzed for sulphur, and in Fig. 15 the sulphur content is plotted against volume distilled. The position of the peaks in the sulphur curve corresponds to the position of peaks in the aromatics curve.

There is evidence to indicate that the sulphur compounds are thiophenes and in the gasoline boiling range they would be monocyclic compounds. The sulphur content of the blended cut containing benzene was low although the benzene content was 18%. If the sulphur is assumed to occur as thiophene (C_4H_4S) then 0.6% S corresponds to 1.6% thiophene. Following the benzene peak there are four prominent sulphur peaks. The first of these corresponds to the toluene peak and the sulphur compounds boiling in this range are the two methyl thiophenes ($CH_3C_4H_3S$). There is evidence to suggest that these two isomers are the sulphur compounds present.

A small amount of a cut with boiling range 107.5° to 113° C. was separated by chromatographic methods using silica gel. A trace of fluorescent dye was added to the sample prior to chromatography and the sample was then forced

through the column with ethyl alcohol. The saturates came through first and were separated from the following olefins by a yellow fluorescent ring. The olefins were separated from the aromatics by a green ring and the end of the aromatics appeared blue under ultraviolet light. However, on the trailing end of the aromatics there was a reddish colored material with a refractive index somewhat higher than that of toluene (see Fig. 16) indicating a high concentration of sulphur compounds. Five samples were taken during the chromatography: one of the olefin fraction, two of the aromatics fraction, and two of the reddish colored material. The refractive index curve and the sulphur concentration curve are shown in Fig. 16. The end fraction contained 13.5% sulphur. Chemical methods indicated little or no straight chain sulphur compounds in the original cut.

The identity of the sulphur compound or group of compounds has not been firmly established. However, it is believed to be methyl thiophene and if this is true then a thiophene concentration of over 40% was obtained in the end sample.

Using the sulphur concentrations of Fig. 15 and assuming the appropriate thiophene for each aromatic peak, it is possible to calculate the apparent percentage of sulphur compound present. These percentages are shown with the aromatic percentages in Fig. 17.

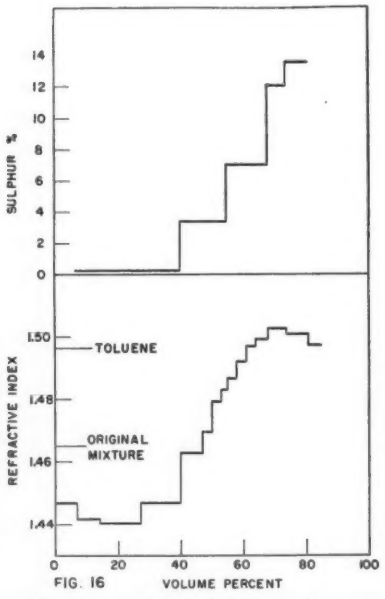

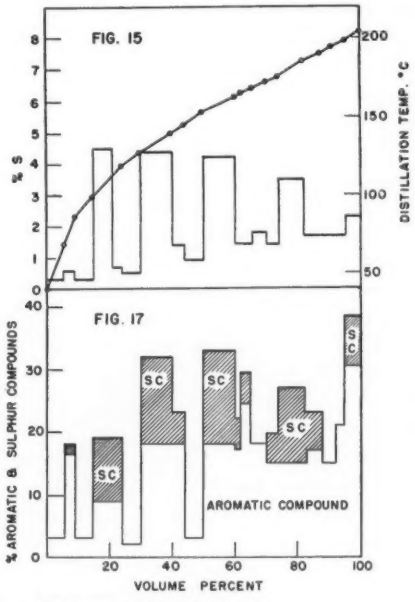

FIG. 15. Sulphur distribution in gasoline cut (bitumen coker distillate).
FIG. 16. Chromatographic concentration of sulphur compounds in the toluene cut.
FIG. 17. Relative concentration of aromatic and sulphur compounds.

Hydrogenated Coker Distillate—Gasoline Cut

The coker distillate produced by the thermal cracking of Alberta bitumen contains a high concentration of olefins, and what is even more objectionable, it has a high sulphur content. No satisfactory economic method of extracting the sulphur compounds is available. Even if there were, the concentration is so high that removal of sulphur compounds would result in severe loss in yield of hydrocarbons.

The most practical approach appears to be hydrogenation. Extensive work has been done by the Mines Branch in Ottawa (12). The top 80% of a coker distillate from Alberta bitumen feed was hydrogenated under the following conditions: pressure 1000 p.s.i., temperature 464° C., and weight hourly space velocity of 4.7. The sulphur content of this hydrogenated material was 0.5%.

A 200 ml. sample which contained the gasoline cut and a small amount of higher boiling material was made available by Dr. D. S. Montgomery of the Mines Branch, Ottawa. This was fractionated in a 12 in. × $\frac{3}{8}$ Stedman column with boil up rates between 100 and 200 ml. per hour and a take off ratio of 1 to 60 up to 150° C., 1 to 75 between 150 and 170° C., and 1 to 150 above 170° C. Refractive indices and chromatographic analysis are shown in Fig. 18.

The olefin content has decreased very substantially; however, it is interesting to note that complete saturation was not achieved. Olefins still represent about 15% of the oil. The aromatic content has been decreased. The hydrogen, to

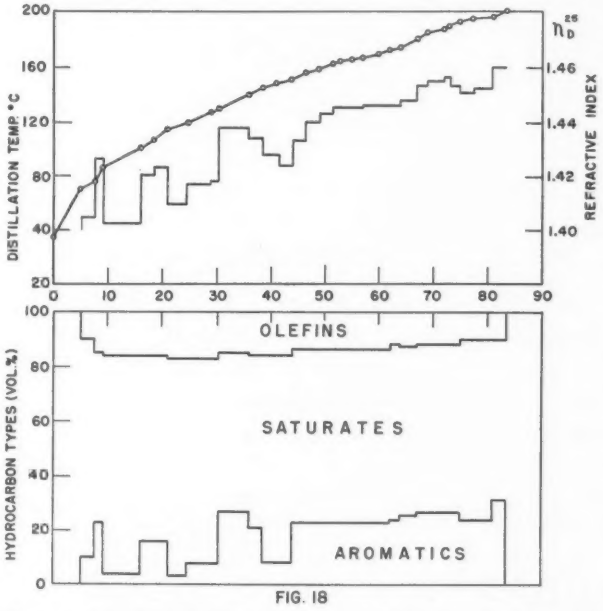

FIG. 18. Hydrocarbon type analysis—gasoline cut thermally cracked and hydrogenated Alberta bitumen.

remove sulphur from the thiophene ring, had to break the ring yielding H_2S and mainly paraffins. The bulk of the hydrogenated product consisted of saturated hydrocarbons.

Conclusions

1. Silica-alumina catalyst proved much more effective in upgrading the three Canadian heavy crude oils studied than did an inert (sand) bed. Coker distillate yields were lower, but the yields of gasoline were substantially higher, the sulphur content and Conradson carbon were lower and there was a very substantial increase in the aromatic content of the gasoline cut.

2. There was a marked similarity in the composition of the gasoline produced from all three feeds except that the Coleville and Lloydminster crude produced substantially more low boiling (C_5) material than did the Alberta bitumen.

REFERENCES

1. ARDERN, D. B., NEWTON, R. H., and BARCUS, G. L. Ind. Eng. Chem. 37: 546. 1945.
2. BATES, J. R., ROSE, F. W., JR., KURTZ, S. S., and MILLS, I. W. Ind. Eng. Chem. 34: 147. 1942.
3. CRITTLE, D. W. and LETOURNEAU, R. L. Anal. Chem. 23: 1620. 1951.
4. DART, J. C., MILLS, G. A., OBLAD, A. G., and PEAVY, C. C. Oil Gas J. May 9: 123. 1955.
5. GISHLER, P. E. Can. J. Research, F, 27: 104. 1949.
6. GLASGOW, A. R., JR., WILLINGHAM, C. B., and ROSSINI, F. D. Ind. Eng. Chem. 41: 2292. 1949.
7. HODGSON, G. W., MATCHEN, B., PETERSON, W. S., and GISHLER, P. E. Ind. Eng. Chem. 44: 1492. 1952.
8. MELPOLDER, F. W., BROWN, R. A., YOUNG, W. S., and HEADINGTON, C. E. Ind. Eng. Chem. 44: 1142. 1952.
9. PETERSON, W. S. and GISHLER, P. E. Petroleum Engr. April: 553. 1951.
10. RAMPTON, H. C. J. Inst. Petroleum, No. 354, 39: 305. 1953.
11. VOORHIES, A., JR., and MARTIN, H. Z. Proc. Am. Petroleum Inst. III, 33: 39. 1953.
12. WARREN, T. E., BOOTH, F. L., CARSON, R. E., and BOWLES, K. W. Proc. Athabasca Oil Sands Conf. Sept. 1951. p. 289.

SOLVENT EXTRACTION OF SASKATCHEWAN LIGNITES

I. SURVEY OF LIGNITES AND SOLVENTS[1]

By R. L. Eager, S. D. Cavers,[2] W. Graham,[3] N. R. Dunne,[4] and W. J. G. Cudmore[5]

ABSTRACT

The results of extracting some Saskatchewan lignites with various solvents are reported. Of the solvents tried, mixtures of benzene and ethanol appeared to be the most satisfactory. For the most part, the extract was a black, shiny, brittle solid with a conchoidal fracture. The yields of extract ranged from 2 to 5% on the moisture-free basis. These yields are lower than those reported for certain German and American lignites. Over the particle size range $-\frac{1}{2}$ in. +4 mesh to −60 mesh the size of the particles extracted did not affect the yield appreciably.

INTRODUCTION

Saskatchewan's mineable lignite reserves have been estimated to lie between 13 and 24 billion tons (8). Up to the present time only a comparatively small amount has been used as fuel, mainly because of the high moisture content of lignite, but also because of its undesirable property of slacking during storage and handling. Evidently the Saskatchewan lignite mining industry would benefit if further uses for its product could be found. In Germany, and more recently in the United States (10, 14), an industry has been built up based on the solvent extraction of a wax present in certain brown coals and lignites. Named *montan wax*, this wax belongs to the broad class of natural waxes, and possesses many valuable properties which make it of commercial value.

Previous work on the extraction of Saskatchewan lignites has not been extensive. In an investigation of Canadian lignites made prior to 1920 by Arthur D. Little Inc. (16) samples from Bienfait and Estevan, Saskatchewan, were examined together with samples from Alberta and British Columbia. No experimental details were presented but the following comment was made:

> "In only one case was Montan wax (benzol extract) found, and that was so small as to be commercially unimportant. When this work had been completed, it was learned that the Standard Oil Co. had made a similar search with similar results."

The present study was undertaken since a more comprehensive survey of the extractable material content of Saskatchewan lignites and the use of solvents other than benzene seemed desirable.

[1]*Manuscript received November 14, 1955.*
Contribution from the Department of Chemistry and Chemical Engineering, University of Saskatchewan, Saskatoon, Sask. Presented in part at the Annual Conference of the Chemical Institute of Canada, Winnipeg, 1951.
[2]*Present address: British Columbia Research Council, Vancouver 8, B.C.*
[3]*Present address: Chemical Engineering Section, National Research Council, Ottawa, Ont.*
[4]*Present address: Shell Oil Co., Calgary, Alta.*
[5]*Present address: Research Department, Standard Oil Company (Indiana), Whiting, Ind., U.S.A.*

EXPERIMENTAL

Coal Samples

Samples of lignite were obtained from the three districts of Saskatchewan with important lignite deposits: the Cypress Hills district, the Wood Mountain district, and the Souris River Valley district (8). The source of each sample of lignite used in the present study is given in Table I. Each sample was taken from a single seam at an exposed face. The samples were made as representative as possible by taking increments from a strip running from the top to the

TABLE I

COAL SAMPLES

Source of sample		Sample number	Air-drying loss, % by weight of the coal as received	Proximate analysis, % by weight, on "air dried" basis				Gross calorific value*, on "air dried" basis, B.T.U./lb.
District	Location in district			Moisture	Volatile matter	Fixed carbon	Ash	
Souris River Valley	Taylorton	1	8.9	26.0	31.9	35.1	7.0	8160
"	Shand	2	9.1	25.0	32.2	36.0	6.8	8210
"	Pinto†	7	10.2	24.3	29.9	38.4	7.4	8300
"	Roche Percee	8	9.6	23.6	32.7	37.4	6.3	8290
"	Estevan	9	12.3	26.9	30.2	36.6	6.3	8130
"	Pinto†	10	11.0	25.4	30.2	39.3	5.1	8300
Wood Mountain–Willowbunch	Stonehenge	3	22.6	19.3	35.5	26.4	18.8	6900
"	St. Victor	4	26.5	19.5	33.1	33.4	14.0	7210
"	Willowbunch	5	27.8	22.4	33.6	33.6	10.4	7240
"	Gye	6	23.8	23.0	32.3	37.5	7.2	7650
"	Wood Mountain	13	21.4	19.7	31.4	32.5	16.4	7360
Cypress Hills	Shaunavon	11	23.5	23.9	33.9	35.4	6.8	7910
"	Eastend	12	19.9	21.7	32.8	34.6	10.9	7850
"	Shaunavon	16	—	24.9	35.5	28.1	11.5	7150
"	Shaunavon	18	—	12.4	37.6	35.6	14.4	8320

**No correction was made for the formation of nitric or of sulphuric acids.*

†Samples 7 and 10 were from adjoining sections of land and represent different seams of lignite.

bottom of the seam. When Sample 18 was taken, the presence of water in the mine prevented the sampling of approximately the bottom 2.5 ft. of a seam approximately 7.5 ft. thick. For Sample 3 the top 3 ft. of a 17 ft. seam could not be sampled. Each sample weighed at least 50 lb. In preparing the samples for the extraction tests, care was taken in each case that the material removed for testing was representative of the larger sample.

Proximate analyses were obtained for all the samples tested. These analyses are given in Table I. Samples 1 to 13 inclusive were shipped to the laboratory in sealed containers. Therefore, for these samples, the information given on the "as received" basis in Table I is applicable, to a close approximation, to the coal as mined. The results given in Table I on the "air dried" basis were obtained with coal dried to constant weight in air at room temperature and atmospheric pressure. The results given on the "dry coal" basis were calculated for coal dried at 105° C. The analytical methods used were those recommended by the A.S.T.M. (1).

Method of Extraction

The procedures used for liquid extraction of coal in the laboratory have not been standardized. However, in two of the more recent investigations the experimental procedures used were similar to one another. These investigations were that of Cawley and King (3) on the extraction of British lignite and peat, and that of Selvig, Ode, Parks, and O'Donnell (14) on the extraction of American lignites. In the present investigation a similar procedure has been followed, thus enabling a reasonably reliable comparison to be made of the extractable material contents of British, American, and Saskatchewan lignites.

Ordinary laboratory glass Soxhlet extractors with 150 ml. boiling-flasks were used for most of the work. The thimble held 20 gm. of ground lignite. Air-dried lignite was used in all the experiments since previous work had shown that drying at 105° C. decreases the yield of extract (6). A small plug of glass wool was placed over the weighed lignite in each thimble to prevent any of the sample from being washed out. The thimble rested on a short length of glass rod placed in the bottom of the extraction chamber. This arrangement allows a more complete siphoning of solution than is obtained with the thimble resting on the bottom of the chamber (9).

Preliminary tests on Saskatchewan lignites indicated that an extraction time of 24 hr. was necessary if essentially complete removal of extractable material was to be obtained from finely ground lignite samples. Unless otherwise specified, extractions were carried out for 24 hr. of continuous operation on lignite ground to pass a 60 mesh Tyler screen. The time of extraction and fineness of grind differed somewhat from the conditions used by Cawley and King (2) and by Selvig *et al.* (14). Cawley and King extracted minus 10 mesh (B.S.) samples of lignite for 16 hr. whereas Selvig *et al.* extracted minus 20 mesh (Tyler) samples for 12.5 hr.

At the conclusion of an extraction the solution was evaporated to dryness. The extract was freed from the last trace of solvent by heating under vacuum and by a final drying to constant weight at 100° C. The flask containing the dried extract was weighed and the per cent yield of extract was calculated. Unless otherwise noted the yield reported is the mean for duplicate determinations.

As a check on the extraction procedure a sample of Arkansas lignite from Dallas County was obtained from W. A. Selvig, U.S. Bureau of Mines. A single determination using a mixture of 80 parts by volume of benzene and 20 parts by volume of 95% ethanol resulted in a yield of 14.7% of extract on the moisture free basis. In Reference 14 this sample was numbered 46107 and the yield reported was 14.2%.

Choice of Solvent

The first step in the survey of Saskatchewan lignites for their content of extractable material was to find a suitable solvent. In Germany benzene alone and benzene–alcohol mixtures seem to have been the most popular (11, 15). The most commonly used mixture was one containing 80 parts by volume of

benzene and 20 parts by volume of ethyl alcohol (15). Whether the ethanol used was absolute or 95% is not stated. In their extraction tests on British lignite Cawley and King (3) used benzene for most of their work. However, for a few of their tests they used a mixture containing 65 parts by volume of benzene and 35 parts by volume of ethanol. In their survey of American lignites Selvig *et al.* (14) used both benzene alone and a mixture of 80 parts of benzene and 20 parts of 95% ethanol by volume (13).

Previous investigations (3, 12, 14) have shown that mixtures of solvents give a higher yield of extract than do single solvents. Furthermore the use of azeotropic mixtures has several advantages as compared to the use of mixtures in general (12). Since the effect of the dissolved extractable material on the composition of azeotropes is slight (12), the composition of the vapor is identical with that of the liquid. Thus there is no change in the composition of the solvent in contact with the coal during an extraction run. Because of the constant boiling point the rate of heat transfer is also constant during the extraction process. As a result of these considerations azeotropic mixtures were used as solvents for most of the present investigation.

A factor which must be considered when using binary azeotropes as solvents for the extraction of lignite is the eventual presence of water as a third component. The air-dried lignite used in the present work still contained appreciable amounts of moisture. Hence the presence of water in the solvent was likely once extraction had begun. It has been shown (12) that the boiling points of azeotropic mixtures of the type used in this investigation are not markedly affected by small quantities of water. In agreement with this the boiling points of the azeotropes used in this investigation were found to remain constant during the extraction runs.

The compositions of the various solvents used are listed in Table II. Where ethanol is specified without the designation "95%", sufficient of the 95% grade was used to give the stated amount of pure ethanol. Graduated cylinders were used in preparing the mixtures. For each of the azeotropes listed the lower boiling constituent was added in an amount slightly in excess (12) of that corresponding to the composition given in Table II. The ratio of benzene to ethanol in the 73: 20 mixture is such that on the addition of the proper amount of water the ternary azeotrope of benzene, ethanol, and water would be formed. In use this binary mixture probably became the ternary azeotrope since water was added through the use of 95% ethanol in preparing the mixture and since more water would probably be gained from the lignite during the extraction operation.

The data given in Table II show the results of extracting lignite Sample 1 with the various solvents. Mixtures of benzene and ethanol (and water) appeared to be the solvents most satisfactory for further use in this research. The yield of extract was comparatively high and the appearance of the product corresponded to that reported for montan wax (14). Furthermore, as pointed out previously, benzene–ethanol mixtures have been used both in industry and in laboratory studies where waxy substances were extracted from lignite.

TABLE II

YIELD OF EXTRACT OBTAINED WITH VARIOUS SOLVENTS

Lignite Sample 1, −60 mesh
Except where otherwise specified 20 gm. samples were extracted
Except where otherwise stated boiling points (5) are at 760 mm. pressure
Except where otherwise stated compositions of azeotropes were calculated from the compositions by weight given in Reference 5

Solvent	Composition, parts by vol.	B.P., °C.	Extr. time, hr.	Appearance of extract	Yield of extract, wt. %, on moisture-free basis
Benzene*	—	80.2	58	Not available*	1.8
Pyridine*	—	115.4	49	"	6.6
95% ethanol*	—	78.3	58	"	3.2
Acetone*	—	56.2	58	"	2.3
Benzene* 95% ethanol	50 50	68.7†	266	"	9.9
Benzene Ethanol	65‡ 35	68.2	24	Black, shiny, brittle, conchoidal fracture	4.5
Benzene Ethanol	73 20	64.9§	24	"	4.6
Chloroform Acetone	68‡ 32	64.5	24	"	3.1
Ethyl acetate Ethanol	65‡ 35	71.8	24	"	3.4
Toluene Ethanol	30‡ 70	76.6	24	"	4.1
Benzene Methanol	58‡ 42	58.3	24	"	4.2
Chloroform Methanol	79‡ 21	53.5	24	"	3.9
Pyridine *n*-Butanol	25‡ 75	118.7	24	"	4.6
Toluene *n*-Butanol	67 33	108‖	24	"	4.5
Benzene Acetic acid	98‡ 2	80.5	24	Dark brown, shiny, brittle, conchoidal fracture	2.3
Skellysolve "C" 95% ethanol	58.8¶ 41.2	66‖	24	Brown, dull, softer, and less brittle than extracts from previous runs, conchoidal fracture less evident	4.2

**The procedure used differed slightly from that described in the text. For example, 5 gm. samples were extracted, extractions were not done in duplicate, and the appearance of the extract was not recorded.*

†*Reference 4.*

‡*Binary azeotrope.*

§*Boiling point of ternary azeotrope of composition: benzene 73.2, ethanol 20.4, water 6.4% by volume.*

‖*Boiling point at approximately 715 mm. mercury pressure determined in the present work.*

¶*This mixture was found to have a constant boiling point.*

Pyridine gave a yield similar to that obtained with benzene–ethanol. However, pyridine was not considered a satisfactory solvent for use in the present investigation since it is known (6) that pyridine readily extracts constituents of coal which are not waxy substances.

Extraction Tests on Saskatchewan Lignites

The 65:35 mixture of benzene and ethanol was used to extract portions of the various lignite samples described in Table I. The results of these experiments are shown in Table III. The yields of extract ranged from 2.2 to 5.3% of the moisture-free coal. The highest yield, 5.3%, was obtained from Sample 11, a sample from Shaunavon. The next highest yield, 4.5%, was obtained from Sample 1, a lignite from Taylorton. Other lignites from the Estevan district gave yields of approximately 3%. The extracts obtained in the tests described in Table III were all of approximately the same appearance, being black, shiny, brittle, and having a conchoidal fracture.

TABLE III

EXTRACTION TESTS ON VARIOUS SASKATCHEWAN LIGNITES
Extraction time: 24 hr.
Screen size: −60 mesh
Solvent: benzene–ethanol 65:35

Lignite sample number	Source of sample		Yield of extract weight %, on moisture-free basis
	District	Location in district	
1	Souris River Valley	Taylorton	4.5
2	"	Shand	2.9
7	"	Pinto*	2.9
8	"	Roche Percee	3.1
9	"	Estevan	2.7
10	"	Pinto*	2.5
3	Wood Mountain–Willowbunch	Stonehenge	2.7
4	"	St. Victor	2.6
5	"	Willowbunch	2.7
6	"	Gye	2.2
13	"	Wood Mountain	2.9
11	Cypress Hills	Shaunavon	5.3
12	"	Eastend	3.7

**Samples 7 and 10 are from adjoining sections of land and represent different seams of lignite.*

Table IV shows the variation in the yield of extract for samples of coal obtained from different locations of the same mining operation. Samples 11, 16, and 18 were all obtained from the Wilkins coal mining lease (No. 19311) located in Legal Subdivision 5 of Section 23, Township 7, Range 19, west of the third meridian. The solvent used was the 73:20 mixture of benzene and ethanol. As mentioned previously, Sample 18 was not a completely representative sample of the seam. The yield of extract varied between 3.4% and 5.9% on the moisture-free basis.

TABLE IV

EXTRACTION OF LIGNITE SAMPLES FROM THE WILKINS LEASE
Extraction time: 24 hr.
Screen size: −60 mesh
Solvent: benzene–ethanol 73: 20

Sample number	Yield of extract weight %, on moisture-free basis
11	5.9
16	4.7
18	3.4*

**The Soxhlet extractors were operated intermittently for a total extraction time of 24 hr.*

Effect of Particle Size

The effect of particle size on the rate of extraction and on the yield of extract for a 24 hr. extraction was investigated. Sample 16 was used in this work. The desired size range of lignite was prepared by first grinding the coal to the approximate size desired and then selecting, by means of Tyler sieves, the material to be extracted. Each size range studied was prepared individually in this way with the exception of the −60 mesh material. This was obtained by grinding a portion of Sample 16 to pass a 60 mesh Tyler sieve.

Rate of extraction studies were made using the following four size ranges: $-\frac{1}{2}$ in. +4 mesh, −4 +10 mesh, −10 +20 mesh, and −20 +35 mesh. The 73: 20 mixture of benzene and ethanol was used as the solvent. The yields at various times were found by removing the solvent from the boiling-flask of the Soxhlet extractor and determining the amount of extract present. Fresh solvent was added to the boiling-flask and the extraction was continued. The cumulative yield is shown as a function of time in Fig. 1.

In yield studies lignite of various size ranges was extracted for 24 hr. with the 73: 20 mixture of benzene and ethanol. The size ranges investigated were the four listed in the discussion of extraction rate, plus the following: −35 +65 mesh, −65 +170 mesh, and −60 mesh. The yields are given in Table V.

The slopes of the lines shown in Fig. 1 indicate that as the particle size of the lignite is decreased from $-\frac{1}{2}$ in. +4 mesh to −10 +20 mesh the initial rate of extraction is increased. However, for a further decrease in size, to −20 +35 mesh, the initial extraction rate appears to decrease. The results given in Table V show a corresponding dependence on particle size of the yield for a 24 hr. extraction. The yield increases as the particles size of the lignite decreases in the range $-\frac{1}{2}$ in. +4 mesh to −10 +20 mesh. For still finer material, however, the yield decreases slightly. Considering individual lignite particles the rate of extraction probably increases for decreased particle size. However, as the particle size is decreased the tendency for uneven packing of the bed is probably increased, with consequent channeling of the solvent. This latter effect results in less efficient extraction as the particle size is decreased below approximately −10 +20 mesh. However for a 24 hr. extraction the effect of particle size on yield is minor for the particle size ranges investigated.

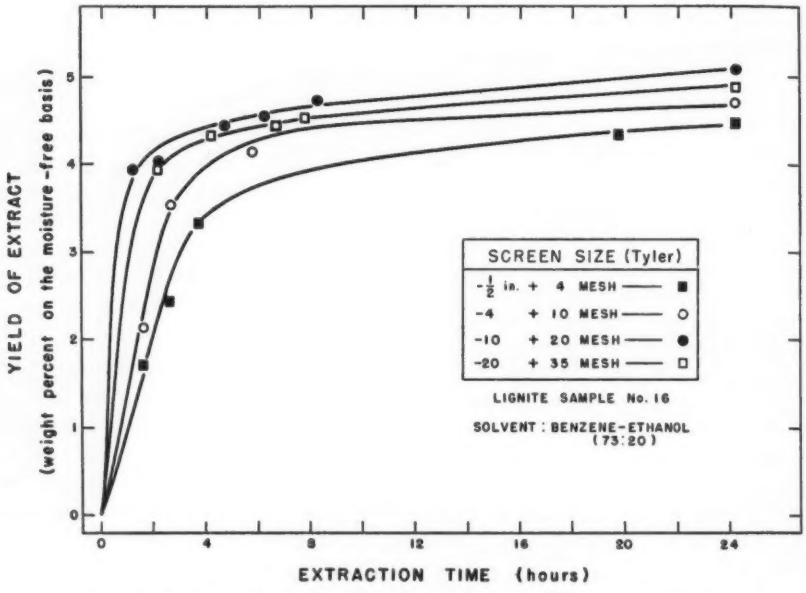

FIG. 1. Effect of lignite particle size and of time on the yield of extract.

TABLE V

EFFECT OF PARTICLE SIZE OF LIGNITE ON YIELD OF EXTRACT

Sample 16
Extraction time: 24 hr.
Solvent: benzene–ethanol 73: 20

Size Tyler screen mesh	Yield of extract weight %, on moisture-free basis
− ½ in. + 4	4.5
− 4 + 10	4.7
−10 + 20	5.1
−20 + 35	4.9
−35 + 65	4.9
−65 +170	4.3
−60	4.7

Extraction of Saskatchewan Leonardite

Leonardite (7) occurs in outcroppings at several points in southern Saskatchewan. In its natural state it contains over 60% moisture. A sample from the Souris River Valley district was obtained prior to the beginning of this investigation, air-dried to 6% water, ground to −20 mesh, and stored in a bottle

having a screw type lid. This sample was extracted with various solvents. Table VI shows the results. Each solvent produced a yellow extract composed of fine granules. The yields were very low.

TABLE VI

EXTRACTION TESTS ON SASKATCHEWAN LEONARDITE

Screen size: −20 mesh
Extraction time: 24 hr.

Solvent	Yield of extract weight %, on moisture-free basis
Benzene–ethanol, 65: 35	1.0
95% ethanol	0.5
Ethyl acetate – ethanol, 65: 35	0.5
Ethyl acetate	0.4

CONCLUSIONS

After several solvents had been investigated, benzene–ethanol mixtures were chosen for use in a survey of Saskatchewan lignites for their content of extractable material. The coal samples investigated contained up to 6% of substances which could be extracted in 24 hr. under the conditions used in the experiments. The three Shaunavon samples investigated contained between 3.4 and 5.9% extract on the moisture free basis, whereas those from the Souris River Valley and from Wood Mountain–Willowbunch contained between 2.2 and 4.5% extract with only two samples out of 11 yielding 3% or higher. Considerable variation was noted in the extract content of samples from a single mining operation. The yields from Saskatchewan lignites are very similar to those reported by Selvig *et al.* (14) for North Dakota lignite and are much lower than the figures of 10 to 23% obtained by the same authors with benzene–ethanol mixtures for California lignites. The percentages of extract in the Saskatchewan samples investigated are also much lower than those of certain German lignites which contained from 10 to 18% wax (14).

For the experimental procedure used the rate of extraction increases with increasing fineness of grind of the lignite until fine sizes are reached. At this point the rate begins to fall off again, probably as a result of channeling in the bed. However, for a 24 hr. extraction under the conditions used in this work the effect of particle size on the yield is small. The yield versus time plot (Fig. 1) is similar to that obtained by Selvig *et al.* (14).

A sample of Saskatchewan leonardite yielded very little extractable material.

The properties of the lignite extracts will be considered in a later paper.

ACKNOWLEDGMENTS

The authors are indebted to the Saskatchewan Research Council for financial assistance. Some of the lignite samples were generously provided by A. J. Williams and W. W. Robertson of the Saskatchewan Department of Natural Resources and Industrial Development. W. A. Selvig of the United States Bureau of Mines kindly provided a sample of Arkansas lignite.

REFERENCES

1. AM. SOC. TESTING MATERIALS, Standards on Coal and Coke. D, 271. 1947.
2. CAWLEY, C. M. and KING, J. G. J. Soc. Chem. Ind. (London), 64: 237. 1945.
3. CAWLEY, C. M. and KING, J. G. Dept. Sci. Ind. Research (Brit.), Fuel Research Tech. Paper, 52. 1946.
4. CHU, J. C., GETTY, R. J., BRENNECK, L. F., and PAUL, R. Distillation equilibrium data. Reinhold Publishing Corporation, New York. 1950.
5. HORSLEY, L. H. Ind. Eng. Chem., Anal. Ed. 19: 508. 1947.
6. KIEBLER, M. W. *In* Chemistry of coal utilization. Vol. 1. *Edited by* H. H. Lowry. John Wiley & Sons, Inc., New York. 1945.
7. LAVINE, I. Lignite: occurrence and properties. Dept. of Chemical Engineering, University of North Dakota, Grand Forks. 1940.
8. MACKAY, B. R. Coal reserves of Canada. Reprint of Chap. 1 and App. A of report of Royal Commission on coal, 1946. King's Printer and Controller of Stationery, Ottawa. 1947.
9. NEUSTADT, M. H. Ind. Eng. Chem., Anal. Ed. 14: 431. 1942.
10. ODE, W. H. and SELVIG, W. A. Ind. Eng. Chem. 42: 131. 1950.
11. PALMER, G., SHILLITOE, G. S., and MACMASTER, A. The German montan wax industry. British Intelligence Objectives Subcommittee Final Rept. 13, Item 22. 1945.
12. REILLY, J., KELLY, D. F., and RYAN, D. V. J. Soc. Chem. Ind. (London), 56: 231. 1937.
13. SELVIG, W. A. Private communication.
14. SELVIG, W. A., ODE, W. H., PARKS, B. C., and O'DONNELL, H. J. American lignites: geological occurrence, petrographic composition, and extractable waxes. Bull. 482, U.S. Bur. Mines. 1950.
15. STEINLE, J. V. Economic study of German synthetic waxes. Office of Military Government for Germany (U.S.), Field Information Agency, Technical, Final Rept. 737. 1946.
16. WEST, C. J. Chem. & Met. Eng. 22: 929. 1920.

LACTOSE CRYSTALLIZATION IN FROZEN MILK[1]

By H. Tessier, Dyson Rose, and C. V. Lusena

ABSTRACT

A dilatometric method for estimating the amount of lactose crystallized from frozen milk is described. Results obtained by this method indicate that crystallization of lactose in frozen solutions is controlled by the same factors that control crystallization from solutions at higher temperatures. The most important of these factors are the activity of suitable nuclei, the temperature, and the degree of supersaturation. Since lactose crystallization is closely related to the precipitation of casein from frozen milk under most conditions these same factors should affect the storage life of frozen milk.

INTRODUCTION

Crystallization of lactose appears to be associated with the precipitation of casein during storage of frozen milk (19, 21). Crystallization of lactose has been extensively studied in relation to "sandiness" in ice cream but the conditions used for freezing ice cream differ greatly from those encountered during quiescent freezing of canned milk. Moreover, most studies on lactose crystallization have depended on either an optical or a polarographic method (2, 19, 20). The optical method is only qualitative, and the polarographic method has several disadvantages, including low sensitivity, and the inability to include β crystals. A dilatometric method is not subject to these errors, and has the added advantage that crystallization can be followed continuously in one sample. A dilatometric method was therefore developed, necessary data on the molal depression of the freezing point in supersaturated lactose solutions were established, and studies of lactose crystallization in frozen milk undertaken. Details of the method, and the results obtained, are presented in this paper.

APPARATUS AND PROCEDURE

The dilatometers consisted of 20 ml. Pyrex glass bulbs fused directly to 125 cm. of 1.5 mm. i.d. calibrated capillary tubing, and mounted vertically on a support graduated in centimeters. The manometer fluid was a hydraulic oil having a relatively small linear coefficient of expansion, a low pour point, and a low viscosity.

For filling, the dilatometer bulb, without manometer, was temporarily fitted with a stopcock and short tube. This apparatus was weighed, then 15 ml. of sample previously deaerated by boiling under vacuum at room temperature for 30 min. was added. The system was evacuated for five minutes, the stopcock closed to retain the vacuum, and the weight of sample determined. Sufficient oil was then introduced through the filling tube, care being taken to exclude air, to completely cover the sample. The vacuum was released, the stopcock detached, and the manometer fused to the bulb. Additional oil was added through the manometer by means of a syringe fitted with 120 cm. of

[1]*Manuscript received December 30, 1955.*
Contribution from the Division of Applied Biology, National Research Laboratories, Ottawa, Canada. Issued as N.R.C. No. 3936.

No. 18 hypodermic needle tubing, and the level adjusted to approximately 20 cm.

The initial volume of all samples was measured at 0° C. after a 24 hr. equilibration. Heat treatments, when required, were given after this period. Freezing was initiated by immersing the lower 2 to 3 mm. of the bulb in an alcohol bath at −20° C., and slowly completed by lowering the bulb into the bath. When the sample was completely frozen, the dilatometer was transferred to a controlled temperature bath in a refrigerated room operating at a slightly lower temperature than the bath. Both bulb and manometer temperatures were thus controlled at temperatures sufficiently alike to make the "stem" correction insignificant.

At the conclusion of a test, but before the dilatometers were removed from the cold room, the oil was collected and its volume measured. The manometer reading was then corrected for contraction of the oil calculated from a coefficient determined experimentally under test conditions.

CALCULATIONS

During the initial freezing of a solution without crystallization of a solute the entire volume increase results from ice formation. The additional increase in volume that accompanies solute crystallization arises from two sources: (*a*) the change in volume occupied by solute, and (*b*) the increase in volume of the water released for freezing by removal of the solute. For the two component lactose–water system the total volume change at temperatures below the eutectic (−0.65° C.) and when crystallization is complete can be calculated from the equation:

[1] $$\Delta Vt = Wc + Lf$$

where ΔVt = total volume change, cc.,
W = weight of water present, gm.,
L = weight of lactose present, gm.,
c = difference in volume, per gm., between water at 0° C. and ice at given temperature,
f = difference in volume per gm., between lactose in solution and as crystals.

When lactose crystallization is incomplete, the difference between the observed volume changed (ΔV_0) and ΔVt can be calculated from a similar equation:

[2] $$\Delta Vt - \Delta V_0 = W^1c + L^1f$$

where W^1 = water not frozen, gm.
and L^1 = lactose not crystallized, gm.

The molal concentration of unfrozen solution at temperature t° C. is $(0-t)/M$ where M is the molal depression of the freezing point by the solute. and therefore

[3] $$W^1 = L^1 \frac{1000\,M}{360(0-t^\circ)}.$$

Substituting [1] and [3] into [2] and rearranging

$$L^1 = \frac{360(0-t)(Wc+Lf-\Delta V_0)}{360f\,(0-t)+1000\,Mc},$$

W and L were determined from the composition of the solution being studied. Values for c were determined at three temperatures (*vide infra*), and intermediate values were determined by linear interpolation. Values for M are given in Table I, and for f in Table II. Since all solutions studied were supersaturated to both α- and β-lactose, either form could crystallize. However, α-lactose hydrate is the more probable crystal (2) so the value of $f = 0.028$ was used for all calculations reported. Formation of β crystals would change only the Lf and not the Wc volume change, introducing a maximum error of about 5% in 2 molal solution (−4.5° C.) and of about 14% in 6.5 molal solution (−19.5° C.). The method thus includes both α and β crystals with fair accuracy.

In solutions of mixed solutes, such as milk, the "apparent" L^1 calculated from this equation will be in error to the extent that other solutes depress the freezing point. However, unless salts also precipitate, this error will be nearly constant throughout a storage period at fixed temperature. The amount of lactose crystallizing (ΔL^1) during storage can therefore be calculated from the difference between ΔV_0^1 at the beginning and ΔV_0^2 at the end of the period of observation.

Thus

$$\Delta L^1 = \frac{360(0-t)(\Delta V_0^2-\Delta V_0^1)}{360f\,(0-t)+1000\,Mc}.$$

The volume change on freezing normally consisted of a rapid increase during the freezing of "free" water, followed by a more or less prolonged period of slow increase. Occasionally a "plateau" interceded between the rapid and slow phases, indicating existence of a "metastable" (20) lactose solution. However, since this "plateau" was often absent the initial readings for milk samples (ΔV_0^1) were arbitrarily taken 24 hr. after freezing.

RESULTS

Volume Change (ΔV) for Water

The over-all volume change (ΔV) between water at 0° C. and ice at −2°, −13°, and −24° C. was determined by the same techniques used for the samples. The average increase in volume at −2° C. was 0.0929 ml./gm.; at −13° C., 0.0910 ml./gm.; and at −24° C., 0.0892 ml./gm. By extrapolation the volume of ice at 0° C. was found to be 0.0932 ml./gm., greater than that of water at 0° C. This value is well within the range reported in the literature (4).

Good duplication of the ΔV for water was not attained in these calibrations. Statistical analysis of 170 observations indicated an over-all error of ±4.2% (coefficient of variation). The coefficient of variation within one filling (i.e. a dilatometer filled once but frozen and thawed several times) was only ±1.4%, and differences between dilatometers were not significant. Reproducibility with solutions was not determined, but appeared to be close to that attained within

single "fillings". Probably trace impurities affected the results with water, but had a negligible effect in solutions where freezing was not complete.

Constants for Lactose

Supersaturated lactose solutions are not sufficiently stable to allow determination of the freezing points by conventional means, but solutions below 3 molal can be cooled and held for short periods without crystallization of lactose. Aliquots of 1, 2, and 3 molal solutions were therefore cooled to a range of temperatures, at 0.2° C. intervals, spanning the estimated freezing point. The size of an added ice crystal was observed over a 30 min. period and the temperature at which the size remained unchanged was recorded as the freezing point.

To determine the freezing point of higher concentrations, lactose solutions were frozen at various temperatures while subjected to a centrifugal force of about 500 *g*'s at the tip. Under these conditions, ice crystals floated on a clear layer of supersaturated solution. After periods of 18 to 72 hr., the tube was broken in the cold, and the concentration of the solution estimated by means of a refractometer. Since the equilibrium temperature within the centrifuge was above that of the refrigerated room in which it was operated, the actual temperature at which the solution formed, i.e. its freezing point, was read from a thermometer suspended in aqueous glycerol in the balancing cup immediately after the centrifuge stopped.

Results obtained by these two methods are given in Table I. The molal depression increased progressively from 2.0° C. at 1 molal to 3.0° C. at 6.4 molal.

TABLE I

MOLAL DEPRESSION OF THE FREEZING POINT BY LACTOSE IN SUPERSATURATED SOLUTION

Method	Concentration of lactose, molal	Freezing point, ° C.	Molal depression (M), ° C.
Change in size of added ice crystal	1	− 2.0	2.0
	2	− 4.5	2.2
	3	− 7.2	2.4
Frozen in centrifuge	1	− 1.9	1.9
	2.5	− 5.5	2.2
	3.6	− 9.3	2.6
	5.1	−14.6	2.9
	6.4	−19.5	3.0

The volumes occupied by known weights of lactose when it was in solution and when suspended in toluene were determined by use of a picnometer, and are given on a 1 gm. basis in Table II. To include the possible volume change of the water of crystallization, α-lactose was considered as the hydrated form throughout, the volume change shown being that of 0.05 gm. of solvent water plus 0.95 gm. lactose crystallizing to 1 gm. lactose hydrate. The volume in solution is that of the equilibrium mixture calculated as α-hydrate or as β-anhydride as required.

TABLE II

VOLUME CHANGE UPON CRYSTALLIZATION OF LACTOSE
(Averages of triplicate estimations at 20° C.)

Sample	Apparent specific volume, ml./gm.		Volume change (f), ml./gm.
	In sol'n.	As crystals	
α-Lactose hydrate	0.628	0.656*	0.028
β-Lactose	0.609	0.627†	0.018

**Density calculated from this value = 1.525, value from International Critical Tables, $d_4^{20} = 1.525$.*
†Calculated density, 1.593.

Percentage of Water Frozen

Average data (triplicate dilatometers) on the percentage of water initially frozen in milk and whey at various temperatures are given in Table III. To reduce the probability of lactose crystallization during the time required for the determination, values at the lowest temperature were determined first. The temperature was then raised by 4° C. steps, and volume readings were taken after the volume was equilibrated 24 hr. at each temperature. Calculated data for lactose solutions are also tabulated (Table III).

TABLE III

PERCENTAGE OF WATER FROZEN IN MILK, WHEY, AND LACTOSE SOLUTION AT VARIOUS TEMPERATURES

Temperature, ° C.	Water frozen, %					
	Skim milk		Whey		Lactose solution†	
	T.S.* 9.3%	T.S. 26.0%	T.S. 6.5%	T.S. 20.3%	5%	15%
−24	96.0	88.0	97.0	90.0	98.1	94.5
−20	95.5	86.0	96.5	88.0	97.9	93.7
−16	95.0	84.5	96.0	86.0	97.6	92.7
−12	94.5	81.0	95.5	83.0	97.0	91.0
− 8	92.5	74.0	95.0	77.0	95.8	87.4
− 4	87.5	53.0	91.0	58.0	91.2	73.7
− 2	75.0	20.0	73.0	30.0	84.7	54.2

**T.S. Total solids by oven method.*
†Values calculated from the molal depression of the freezing point (Table I).

The data for skim milk are in close agreement with the calorimetric data of Tumerman *et al.* (19). About half of the total unfrozen water appears to be retained by lactose, one-third by soluble whey constituents other than lactose, and one-sixth by the casein–phosphate curd.

Rate of Lactose Crystallization

Data on the rate of lactose crystallization from pure solution and from solution in an artificial "serum"* at −12.5° C. are given in Fig. 1. For each

**Composition of serum: 24.8 ml. M $CaCl_2$, 33.9 ml. M K_2HPO_4, 28.2 ml. M Na_3 citrate, 15.9 ml. M $MgCl_2$, HCl to dissolve, NaOH to pH 6.7, made to 1 liter (13).*

test, nine dilatometers were filled with 15% lactose solution. Three were frozen without heat treatment, three were immersed in a 66° C. bath, and three in an 82° C. bath, for 30 min., then cooled and frozen.

Crystallization from water occurred very rapidly, especially in the unheated samples. Heating to either 66° or 82° C. delayed the onset of crystallization, but did not affect the rate at which crystallization occurred once it was well established. Crystallization of lactose from artificial serum occurred much more slowly in all samples, but the effect of heat treatment was similar to that observed in pure solution.

The rate of lactose crystallization at −12.5° C. from skim milk concentrated to 24.1% total solids is shown in Fig. 2. Crystallization occurred very rapidly

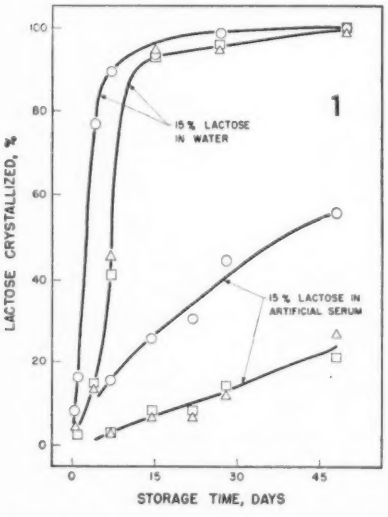

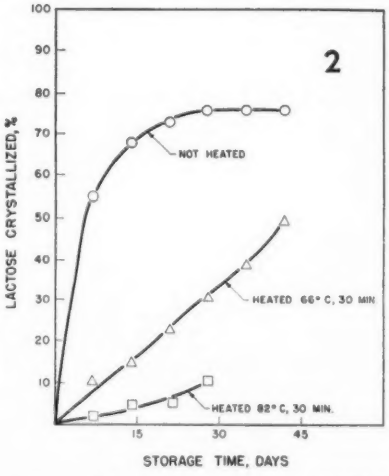

FIG. 1. Rate of lactose crystallization from water and from salt solution at −12.5° C. ○——○ not heated; △——△heated at 66° C. for 30 min.; □——□ heated at 82° C. for 30 min.

FIG. 2. Rate of lactose crystallization from concentrated milk at −12.5° C.

from the unheated sample, but appeared to level off at 76%. This low value may indicate that considerable lactose had crystallized before the initial ΔV_0^1 was determined. Crystallization was much slower with the heated samples, and was not approaching completion in 40 days. Heating to 82° C. appeared to delay crystallization even more than heating to 66° C., though these two temperatures had a similar effect on lactose solutions.

The rate of crystallization from the unheated sample of milk was greater than that from artificial serum, even though the degree of supersaturation should have been slightly less (Table III). This indicates that better nucleation was provided in the milk, as milk solids do not decrease lactose solubility (9).

Data on the effect of storage temperatures on the rate of crystallization of

lactose from an unheated concentrated skim milk (21.5% total solids) (Fig. 3) indicated that lactose crystallization occurred more slowly at lower temperatures. At −24° C. (−10° F.), a temperature at which milk is known to have good stability (1, 3), only 40% of the lactose crystallized in 20 weeks.

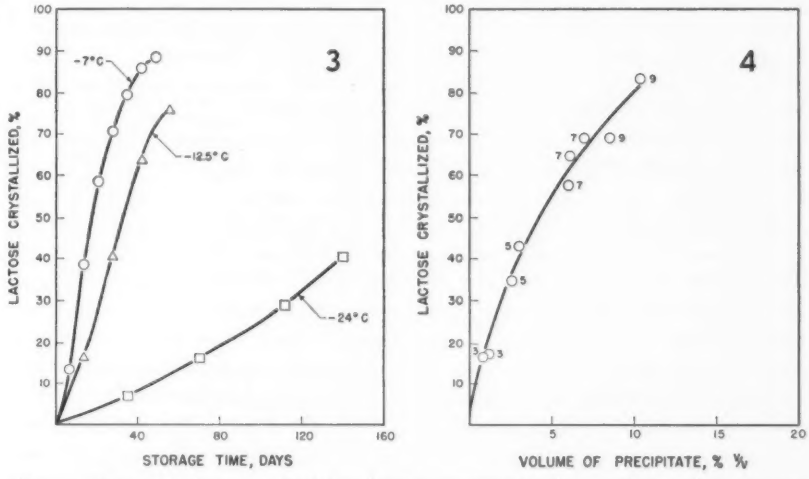

FIG. 3. Rate of lactose crystallization from concentrated milk stored at various temperatures.

FIG. 4. Relation between lactose crystallization and volume of precipitate in concentrated milk. Numbers beside points indicate storage time in weeks.

Relation of Volume of Precipitate to Lactose Crystallization

Tumerman *et al.* (19) showed a relation between lactose crystallization determined polarographically, and the volume of precipitate formed in frozen milk at +15° F. A similar relation was apparent from the volume of precipitates found at the conclusion of the above dilatometric tests. To study this relation throughout a storage period, nine dilatometers were filled from one lot of concentrated skim milk (23.3% total solids). Individual dilatometers were opened at intervals during a nine week storage period at −12.5° C., and the volume of precipitate determined after dilution to normal solids content (12). The results obtained (Fig. 4) indicate a close relation between the volume of precipitate and the percentage of lactose crystallized within the one test. A similar relation was observed when the amount of lactose crystallized was influenced by storage temperature or by sample treatment as well as by storage time, although the volume of precipitate for a given percentage of lactose crystallized varied considerably between milk samples. Samples heated to 82° C. for 30 min. were exceptional in that casein was fully precipitated before 10% of the lactose had crystallized.

DISCUSSION

Crystallization of a solute from solution involves nucleation followed by growth of crystals. Nucleation occurs spontaneously at high degrees of super-

saturation, but is frequently induced at lower degrees of supersaturation by suitable nuclei (5, 10, 17). These nuclei may be partially destroyed by heat (8). Nucleation is suppressed at very low temperatures (15), while rate of crystal growth is influenced by crystallization pressure (degree of supercooling or supersaturation), temperature, and the presence of other solutes (11, 16).

The influence of these variables on crystallization of lactose from solution at temperatures above −0.65° C. has been studied by Herrington (6), but no method was available for studying frozen solutions. However, the dilatometric method devised for the present work made it possible to follow lactose crystallization from frozen solutions. Results obtained by this method indicate that nuclei, degree of supersaturation, and temperature influence the rate of lactose crystallization from frozen milk. Thus, heating samples to 66° or 82° C. delayed nucleation but did not alter the rate at which crystallization occurred once nucleation had taken place (curves for lactose in water, Fig. 2). This indicates that heat sensitive nuclei were involved in the early stages of crystallization. The influence of degree of supersaturation is indicated by the slower crystallization of lactose from artificial serum than from water. Inorganic salts lower the degree of supersaturation by retaining more water unfrozen, and possibly by increasing the solubility of lactose (7). Inorganic salts may also interfere directly with crystallization (11). On the other hand, low temperatures increase the degree of supersaturation, but reduce the rate of crystallization (Fig. 3). Probably both nucleation and rate of crystal growth were retarded by low temperatures to a greater extent than they were promoted by the increased supersaturation.

These observations on lactose crystallization provide an explanation for the effect of some processing treatments on the stability of frozen milk. This aspect of the problem is discussed in the following papers (13, 14, 18).

REFERENCES

1. Bell, R. W. and Mucha, T. J. J. Dairy Sci. 35: 1. 1952.
2. Decker, C. W. and Reid, W. H. E. Univ. Missouri Coll. Agr. Research Bull. 373. 1943.
3. Doan, F. J. Food Technol. 6: 402. 1952.
4. Dorsey, N. E. Properties of the ordinary water substance. (Am. Chem. Soc. Monograph No. 81). Reinhold Publishing Corporation, New York. 1940.
5. Dorsey, N. E. Trans. Am. Phil. Soc. 38: 245. 1948.
6. Herrington, B. L. J. Dairy Sci. 17: 501. 1934.
7. Herrington, B. L. J. Dairy Sci. 17: 805. 1934.
8. Hinshelwood, C. N. and Hartley, H. Phil. Mag. 43: 78. 1922.
9. Hunziker, O. F. and Nissen, B. H. J. Dairy Sci. 9: 517. 1926.
10. La Mer, V. K. Ind. Eng. Chem. 44: 1269. 1952.
11. Lusena, C. V. Arch. Biochem. and Biophys. 57: 277. 1955.
12. Rose, D. Can. J. Technol. 32: 78. 1954.
13. Rose, D. Can. J. Technol. 34: 145. 1956.
14. Rose, D. and Tessier, H. Can. J. Technol. 34: 139. 1956.
15. Tammann, G. The states of aggregation. D. Van Nostrand Company, Inc., New York., 1925.
16. Tammann, G. and Büchner, A. Z. anorg. u. allgem. Chem. 22: 371. 1935.
17. Telkes, M. Ind. Eng. Chem. 44: 1308. 1952.
18. Tessier, R. and Rose, D. Can. J. Technol. 34: 211. 1956.
19. Tumerman, L., Fram, H., and Cornely, K. W. J. Dairy Sci. 37: 830. 1954.
20. Whittaker, R. J. Dairy Sci. 16: 177. 1933.
21. Wildasin, H. L. and Doan, F. J. J. Dairy Sci. 34: 438. 1951.

EFFECT OF HEAT AND OF PREFREEZING STORAGE ON THE STABILITY OF FROZEN MILK[1]

By Dyson Rose and H. Tessier

ABSTRACT

Moderate heat treatment (up to 150° F. for 30 min.) tended to increase the storage life of frozen milk and frozen concentrated milk. Severe heat treatment (180° F. for 30 min.) greatly decreased storage life. Storage at 35° F. before freezing decreased the storage life of pasteurized and of concentrated milk. This effect was completely prevented by moderate heat treatment either immediately after concentration or after prefreezing storage. Data are presented to show that the stabilizing action of moderate heat treatments and the destabilizing effect of prefreezing storage are related to the effect of these treatments on the rate of crystallization of lactose. The destabilizing action of severe heat treatment is related to the presence of heat denatured serum protein.

INTRODUCTION

The effects of various factors on the quality of frozen milk and frozen concentrated milk have been studied extensively (1, 3, 6, 19, 21). The rate of casein precipitation from frozen milk is affected by heat treatments (4, 9, 23), delays between concentrating and freezing (8, 24), and crystallization of lactose (20, 22). It has been reported (6) that heat treatment up to 180° F. for 15 min. lessened "the tendency for the formation of irreversibly coagulated protein" during storage at 0° F., and also that (24) pasteurization at 160° F. for 30 min. increased the stability of skim milk separated at 50° F., but decreased that of skim milk separated at 120° F. However, most workers (4, 7, 10) agree that processing temperatures above 180° F. for 15 min. decrease casein stability. Since most workers concentrated the milk at about 140° F., the effect of lower temperatures has not been studied.

Addition of lactose crystals or sand to milk hastened protein precipitation (24), while enzymic hydrolysis of lactose increased protein stability (22). These observations suggest a relation between lactose crystallization and protein precipitation, and a quantitative relation has been observed under some conditions (20, 22). However, this relation does not hold for severely heated milk (20).

Tentative explanations for some of these effects have been offered (22, 24), but a fuller understanding of them would assist in efforts to develop a stable frozen milk. Studies on lactose crystallization (20) suggested that a moderate heat treatment should stabilize milk by destroying nuclei for lactose crystallization. It also appeared possible that prefreezing storage might affect lactose crystallization rather than directly affecting protein stability. Results of studies designed to test these hypotheses and to explain the effect of severe heat treatments are reported in this paper.

[1]*Manuscript received December 30, 1955.*
Contribution from the Division of Applied Biology, National Research Laboratories, Ottawa, Canada. Issued as N.R.C. No. 3927.

MATERIALS AND METHODS

Raw whole milk, or freshly separated pasteurized skim milk (pasteurized at 143° F., 30 min., separated at 50° F.), was obtained from the Central Experimental Farm, Ottawa. Concentration was effected in a Mojonnier "Lo-Temp" evaporator operating at a milk temperature of 70° F., and producing 4 liters of distillate per hour. Canning, sampling, and test procedures were described previously (16). Except where otherwise stated, heat treatments are recorded as the time of immersion of 100 ml. samples in 2-2/16 × 2-14/16 in. cans in water baths maintained at the desired temperature. Following immersion, the cans were cooled in running water at about 40° F. The canned milks were stored at +10° and 0° F. Triplicate cans were analyzed at each sampling date.

For tests with resuspended casein, the casein – colloidal phosphate complex was obtained by centrifuging skim milk in a Spinco preparatory centrifuge, No. 30 head, at 28,000 r.p.m. (av. R.C.F. = 66,000) for 55 min. The supernatant serum containing a small amount of casein (about 7%) was decanted, and the casein – calcium phosphate was macerated to a paste with a few milliliters of the desired suspending fluid. The suspension was then transferred to a volumetric flask and made to volume with suspending fluid. Casein from approximately 250 ml. of milk was made to a volume of 200 ml. Fifteen milliliter aliquots were frozen in glass vials at +10° F. Duplicate vials were analyzed at each sampling date.

For convenience, the time required to develop 4% precipitate by volume and the time to lose 1 mgm. of nitrogen per milliliter of decantate were averaged, and are reported as the "storage life" (16).

EXPERIMENTAL AND RESULTS

Effect of Heat Treatments and Holding Periods

Samples of skim milk and of concentrated whole milk were canned, and heated for 30 min. at 100°, 125°, 150°, and 180° F. The results (Table I) showed that samples heated to 150° F. were consistently the most stable while samples heated to 180° F. were severely destabilized. Differences between samples heated to 100°, 125°, and 150° F. were generally small. The storage life of all moderately heated samples of concentrated milk was 50 to 80% greater than that of the unheated controls. Moderate heating of skim milk was slightly beneficial even though the milk had been previously heated for pasteurization.

The effect of a 24 hr. prefreezing storage period at 35° F. was tested with raw, pasteurized, and concentrated whole and skim milk (Table II). Prefreezing storage reduced the storage life of unheated whole and skim samples by as much as 30%, and of the unheated concentrated samples by 50 to 65%. However, heated samples were not affected by subsequent prefreezing storage. It was also observed (data not shown) that heating after the prefreezing storage period but before freezing cancelled the destabilizing effect of prefreezing storage.

TABLE I

STORAGE LIFE OF MILK AND CONCENTRATE HEATED TO VARIOUS TEMPERATURES IMMEDIATELY BEFORE FREEZING

(Pasteurized milk was used throughout)

Sample	Heat treatment, ° F.	Storage temp., ° F.	Storage life, days
Skim milk, T.S. 8.3%	Nil	10	75
	150	"	87
	180	"	55
Skim milk T.S. 8.3%	Nil	0	84
	150	"	92
	180	"	61
Concentrated skim, T.S. 20.8%	Nil	0	61
	100	"	97
	125	"	97
	150	"	113
	180	"	10
Concentrated whole, T.S. 29.9%	Nil	10	36
	100	"	55
	125	"	55
	150	"	55
	180	"	8

TABLE II

EFFECT OF STORAGE BEFORE FREEZING ON THE STABILITY OF FROZEN MILK

Sample	Storage 35° F. before freezing	Temperature of frozen storage, ° F.	Storage life, days	Decrease, days
Raw whole	None	10	51	16
	24 hr.	"	35	
Pasteurized whole	None	10	46	16
	24 hr.	"	30	
Concentrated whole (T.S. 30.5%)	None	10	26	13
	24 hr.	"	13	
Raw skim	None	0	121	40
	24 hr.	"	81	
Pasteurized skim	None	0	63	12
	24 hr.	"	51	
Concentrated skim (T.S. 25.2%)	None	0	37	24
	24 hr.	"	13	
Concentrated skim heated to 150° F. for 30 min.	None	10	31	0
	24 hr.	"	31	
Concentrated skim heated to 180° F. for 30 min.	None	10	14	0
	24 hr.	"	14	

Tests with Centrifuged Casein

In an attempt to learn how milk was destabilized by heating to 180° F. several tests were made with casein separated from the whey components by centrifugation. In one test, casein from raw skim milk was resuspended in (*a*) serum of raw milk, (*b*) serum from milk heated to 180° F. for 30 min., (*c*) raw milk serum heated to 180° F. after separation from the casein, and (*d*) serum as for (*c*), but recentrifuged after heating. The results (Expt. A, Table III) indicated that stability was not reduced by use of a serum from

TABLE III

EFFECT OF SEVERE HEAT TREATMENTS* ON THE STABILITY OF RESUSPENDED CASEIN

Source of casein	Source of serum	Storage life, days
Experiment A		
Raw milk	Raw milk	63
Raw milk	Heated milk	66
Raw milk	Raw milk, serum heated	50
Raw milk	Raw milk, serum heated, recentrifuged	61
Experiment B		
Raw milk	Artificial†	20
Heated milk	Artificial†	13
Raw milk, casein heated	Artificial†	18
Experiment C		
Pasteurized	Pasteurized	49
Pasteurized	Heated	52
Heated	Pasteurized	37
Heated	Heated	44

**180° F. for 30 min.*
†For composition of serum refer to (17).

heated milk, but was reduced by use of a serum heated after separation from the casein. Removal of coagulated serum protein by centrifugation after heating improved the storage life of the casein suspension.

In a second test, casein from raw milk and from milk heated to 180° F. for 30 min. was resuspended in water. An aliquot of the raw casein suspension was then heated to 180° F. for 30 min. All suspensions were recentrifuged and the casein was suspended in a lactose and salt solution approximating the composition of normal serum. The double centrifuging and the use of artificial serum seriously reduced the storage life of all samples (Expt. B, Table III), but nevertheless, the results show that casein heated in milk was destabilized to a greater extent than that heated in water.

In a third test, the casein and serum obtained by centrifuging pasteurized and heated (180° F., 30 min.) milks were interchanged. The most stable product resulted from the suspension of casein from pasteurized milk in serum from heated milk, while the least stable product was obtained with casein from heated milk in serum from pasteurized milk. Casein from heated milk also showed low stability when suspended in serum from heated milk.

DISCUSSION AND CONCLUSIONS

The effect of heat on the stability of milk proteins in frozen storage varied with the severity of heat treatment. Two distinct effects were observed: (*a*) a stabilizing action of heat treatments at 100° to 150° F. for 30 min. (inclusive of heating time), and (*b*) a destabilizing effect at 180° F. for 30 min. This destabilizing effect has been observed by other workers (4, 7, 10).

Since crystallization of lactose destabilizes the proteins in frozen milk (20, 22), the stabilizing effect of moderate heat treatments probably resulted from a destruction of nuclei that promote lactose crystallization (20). The conditions under which milk was concentrated for these studies may promote formation of "seed" crystals of lactose, which would be readily destroyed by heat, but the stabilizing effect of heat on pasteurized milk must depend upon destruction of heterogeneous nuclei.

Since calcium concentration affects stability of frozen milk (5, 10, 12), it is possible that the decrease in soluble calcium brought about by heat treatments (11, 13, 15) could affect storage life. However, relatively severe heating is required to induce significant changes in free calcium (170 to 176° F. for 30 min. (2, 14)), and a relatively high proportion of calcium must be removed to significantly affect storage life (30 hr. dialysis against water (5), 10–15% (13, 24)). It is therefore unlikely that heating to 150° F. for 30 min. would decrease soluble calcium sufficiently to influence storage life.

Crystallization of lactose is probably initiated during prefreezing holding periods with 3:1 concentrate, as visible lactose crystals have been reported after prolonged holding at 40° F. (18). The deleterious effect of holding raw or pasteurized milk is more difficult to explain, but may result from an increased contamination with heterogeneous nuclei. Heating erased the effect of a holding period, and holding heated milk under conditions that prevented recontamination with heterogeneous nuclei did not reduce its stability during subsequent frozen storage. It thus appears probable that crystallization of lactose is the only factor involved.

The destabilizing effect of severe heat treatments appears to be directly related to the presence of heat denatured serum protein. Raw casein suspended in serum from heated milk was as stable as the control, but raw casein resuspended in serum heated after removal of the original casein was considerably less stable. Centrifuging the heated serum, so as to remove coagulated whey protein, improved stability. Casein heated in aqueous suspension was not significantly destabilized. Casein from pasteurized milk was more stable than that from heated milk regardless of whether it was resuspended in serum from pasteurized or heated milk. However the source of the serum also had a considerable effect on casein stability, and it would appear that serum from heated milk had less destabilizing effect than that from pasteurized milk. Probably more of the denatured protein sedimented with the casein from the severely heated milk, so that this serum actually contained less denatured protein than that from pasteurized milk. The stability of casein from either raw or pasteurized skim milk resuspended in serum from 180° F. milk indicates that loss of native serum protein does not decrease casein stability.

ACKNOWLEDGMENTS

The authors wish to acknowledge with sincere thanks the cooperation of staff of the Dairy Division, Central Experimental Farms, Ottawa, who supplied milk for these tests.

REFERENCES

1. BABCOCK, C. J., STABILE, J. N., WINDHAM, E. S., EVANS, L. B., and RANDALL, R. J. Dairy Sci. 31: 811. 1948.
2. BELL, R. W. J. Biol. Chem. 64: 391. 1925.
3. BELL, R. W. J. Dairy Sci. 22: 89. 1939.
4. BELL, R. W. and MUCHA, T. J. J. Dairy Sci. 34: 432. 1951.
5. CHRISTIANSON, G., COULTER, S. T., and JENNESS, R. J. Dairy Sci. 35: 481. 1952.
6. CORLEY, R. T. and DEAN, F. J. Food Research, 5: 369. 1940.
7. CROWE, L. K. and WINN, H. H. J. Dairy Sci. 23: 1187. 1940.
8. DOAN, F. J. Food Technol. 6: 402. 1952.
9. DOAN, F. J. and LEEDER, J. G. Food Inds. 16: 532. 1944.
10. DOAN, F. J. and WARREN, F. G. J. Dairy Sci. 30: 837. 1947.
11. GEHRKE, C. W., AFFSPRUNG, H. E., and BAKER, J. M. J. Dairy Sci. 36: 560. 1953.
12. HALLER, H. S. and BELL, R. W. Milk Dealer, 40: 98. 1950. Dairy Sci. Abstr. 14: 369. 1952.
13. HILGEMAN, M. and JENNESS, R. J. Dairy Sci. 34: 483. 1951.
14. HORST, M. F. ter. Ned. Melk. Zuiveltijdschr. 4: 247. 1950.
15. MAGEE, H. E. and HARVEY, D. Biochem. J. 20: 873. 1926.
16. ROSE, D. Can. J. Technol. 32: 78. 1954.
17. ROSE, D. Can. J. Technol. 34: 145. 1956.
18. ROSE, D. and MCDONALD, I. J. Can. Dairy Ice Cream J. (2), 32: 38–39. 1953.
19. ROSE, D. and TESSIER, H. Can. J. Technol. 32: 85. 1954.
20. TESSIER, H., ROSE, D., and LUSENA, C. V. Can. J. Technol. 34: 131. 1956.
21. TRACY, P. H., HETRICK, J., and KRIENKE, W. S. J. Dairy Sci. 33: 832. 1950.
22. TUMERMAN, L., FRAM, H., and CORNELY, K. W. J. Dairy Sci. 37: 830. 1954.
23. WEBB, B. H. Can. Dairy Ice Cream J. (5), 30: 31. 1951.
24. WILDASIN, H. L. and DOAN, F. J. J. Dairy Sci. 34: 438. 1951.

INFLUENCE OF SUGARS AND GLYCEROL ON CASEIN PRECIPITATION IN FROZEN MILK[1]

By Dyson Rose

With the technical assistance of J. M. Belec

ABSTRACT

Casein – calcium phosphate complex separated from skim milk by high speed centrifugation and resuspended in salt solution resembling milk serum was used to study the effect of sugars and glycerol on the stability of casein in frozen milk. All sugars stabilized casein while they are in solution, but lactose crystallizes from solution at temperatures below −0.65° C., and its stabilizing action was therefore transient. Sugars probably exert their stabilizing action by retaining water in the unfrozen state, thus diluting the salts and lessening the pH shift, and by increasing the viscosity of the liquid phase.

INTRODUCTION

Crystallization of lactose in frozen milk has been associated with the precipitation of casein during storage (13, 14, 17). Since casein precipitation was promoted by addition of fine sand, Wildasin and Doan (17) suggested that both lactose crystals and the added sand acted as nuclei for the formation of "casein structures". However, the added sand may have promoted lactose crystallization, and there is no proof for the existence of the "casein structures". More recent workers (14) have suggested that casein is protected by soluble lactose and that this protection is withdrawn as the lactose crystallizes. This suggestion is supported by studies of the factors affecting lactose crystallization in frozen solution (13) and the stability of frozen milk (11). It has also been observed (2, 17) that added sucrose tends to stabilize frozen milk.

All solutes retain some water in the unfrozen state at temperatures above their eutectic, and may temporarily retain unfrozen water at temperatures below their eutectic. Retention of unfrozen water by neutral solutes such as sugars and glycerol reduces the salt concentration in the unfrozen portion of frozen solution. From studies on the freezing of living cells (6), it has been suggested that these neutral solutes thus protect cells from damage caused by high salt concentrations. A similar phenomenon may contribute to the storage life of frozen milk, lactose retaining sufficient unfrozen water to delay development of salt concentrations that precipitate casein. This hypothesis was tested by addition of solutes to milk, and by substitution of other solutes for lactose in suspensions of centrifuged casein. The results are presented in this paper.

METHODS

Storage life of skim milk and 3: 1 concentrated skim milk was estimated by the same methods and techniques reported earlier (9, 10). Casein suspensions were handled by these same methods except that samples were frozen in 15 ml.

[1]*Manuscript received December 30, 1955.*
Contribution from the Division of Applied Biology, National Research Laboratories, Ottawa, Canada. Issued as N.R.C. No. 3932.

vials, and duplicate samples were analyzed as required. For convenience, the time required to develop 4% precipitate by volume and the time to lose 1 mgm. nitrogen per ml. (10) were averaged, and are reported as the "storage life".

Artificial serum was prepared by mixing suitable quantities of molar stock solutions of calcium chloride, dipotassium phosphate, trisodium citrate, and magnesium chloride to give the following composition (mgm./ml.); calcium 0.33, phosphate 0.35, citrate 1.80, magnesium 0.13, potassium 0.88. The required amounts of 0.1*M* stock solutions were diluted almost to volume, and the precipitate dissolved by addition of hydrochloric acid. The solution was then adjusted to pH 6.7 with sodium hydroxide. (Final chloride content approximately 1.1 mgm./ml., and sodium approximately 1.0 mgm./ml.) For tests on suspensions simulating concentrated milk, these concentrations were increased threefold.

Casein – calcium phosphate complex was obtained by centrifuging fresh skim milk for 55 min. at 28,000 r.p.m. in a No. 30 head on a "Spinco" preparatory centrifuge. The firmly packed sediments, which contained about 93% of the total casein, were macerated to a paste in a minimum quantity of artificial serum containing no added sugar or glycerol. To ensure equal casein content in the test solutions, this paste was diluted to approximately 45% of the original milk volume with this same serum, and aliquots were then mixed with equal volumes of artificial serum containing double the desired levels of sugar or glycerol. The reduced total volume (90% of original) partially compensated for casein losses during these manipulations. For the tests simulating concentrated milk, this volume was reduced to 30%.

Lactose was determined by copper reduction (15) in copper hydroxide clarified (18) filtrates. Calcium was determined by the method of Marier and Boulet (7), phosphorus by the method of Polley (8) after dry ashing at 600° C. for six hours.

RESULTS

In some preliminary experiments, solutes were added directly to skim milk. Addition of 3% lactose to skim milk before concentrating caused a marked decrease in the storage life of the frozen 3: 1 concentrate, regardless of whether it was heated after concentration or not (Table I). On the other hand, addition

TABLE I

EFFECT OF ADDED LACTOSE ON THE STABILITY OF CONCENTRATED FROZEN MILK

Treatment	Lactose added	Storage life at 10° F., days
Not heated	0	20
" "	8.0*	4
Heated 150° F., 30 min.	0	>35
" " "	8.0*	7

**3% lactose added before concentration.*

of glycerol to concentrated skim milk increased the storage life at +10° F., but the extent of the increase depended upon the treatment of the concentrate (Table II). In unheated samples, added glycerol had only a slight effect. In samples heated to reduce the tendency for lactose crystallization (13) even 0.5% glycerol increased storage life by one third, and higher concentrations increased it still further. These results are difficult to interpret in terms of the mechanism of stabilization.

Casein suspensions in artificial sera of controlled solute content were a more satisfactory test material than skim milk. Analyses of typical casein suspensions (Table III) indicate considerable variability in casein content, depending upon the extent of losses during transfer from centrifuge tubes. Non-casein nitrogen and lactose were reduced to low levels. Calcium and phosphorus tended to be

TABLE II

EFFECT OF GLYCEROL ON THE STABILITY OF 3:1 CONCENTRATED FROZEN MILK

Treatment	Glycerol added, %	Storage life at 10° F., days	Increase, days
Not heated	0	29	
	0.5	34	5
	1.0	34	5
	2.0	40	11
Heated 150° F., 30 min.	0	62	
	0.5	84	22
	2.0	101	39
	5.0	112	50

TABLE III

ANALYSES OF TYPICAL CASEIN SUSPENSIONS IN LACTOSE-FREE SYNTHETIC SERUM

Component, mgm./ml.	Example I		Example II	
	Original milk	Casein suspension	Original milk	Casein suspension
Total nitrogen	5.3	3.8	5.2	4.6
Non-casein N	1.1	0.2	1.3	0.2
Casein N	4.2	3.5	3.9	4.4
Lactose	47.0	3.2	48.4	4.8
Calcium	1.1	1.0	1.2	1.2
Phosphorus	1.0	0.8	0.9	0.9

low, but varied with the loss of casein – calcium phosphate complex during transfer. Comparisons of the storage stability of the original skim milk with that of resuspensions of casein in its own serum, and in the artificial serum containing 4% lactose, are given in Table IV. Resuspended casein tended to be less stable but the difference was not constant. Casein resuspended as soon as possible after centrifugation appeared to give slightly more stable sus-

TABLE IV

EFFECT OF CENTRIFUGATION AND RESUSPENSION ON THE STABILITY OF CASEIN IN FROZEN STORAGE

Storage temp., ° F.	Storage life at 10° F., days		
	Original skim milk	Casein resuspended in	
		Serum	Artificial serum
10	42	35	37
10	41	41	34
10	67	43	48
0	86	72	57
0	94	79	—
0	116	101	—

pensions. Slight differences in the ease of suspension of caseins from different lots of milk were also observed.

Varying the lactose content of artificial serum from 0 to 12% affected stability of the casein suspensions as shown in Fig. 1. At both +10° and 0° F. stability of the resuspended casein was very low in the absence of added lactose. Maximum stability was obtained with 2 to 4% lactose in the serum. Higher amounts led to a decided decrease in stability. A threefold increase in casein and salt content, so as to approximate the composition of a 3:1 milk, made suspensions in higher lactose concentrations more stable.

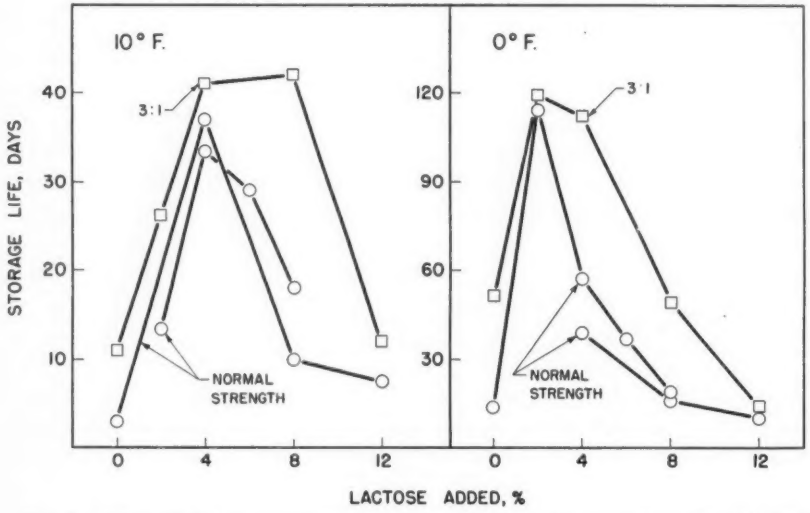

FIG. 1. Effect of lactose concentration on stability of casein suspensions. Straight lines join points of individual tests.

Five tests were made by resuspending casein in artificial serum containing increasing concentration of glycerol (Table V). Regardless of storage temperature or casein concentration, storage life of the resuspended casein increased rapidly with increasing glycerol concentration. Concentrations of 3% and over gave suspensions whose stability exceeded the duration of the tests, and there was no evidence of an optimum level as found with lactose.

TABLE V

EFFECT OF GLYCEROL ON THE STABILITY OF RESUSPENDED CASEIN IN FROZEN STORAGE

Storage temp., ° F.	Casein, mgm. N/ml.	Storage life at 10° F., days					
		Glycerol concentration, %					
		0	1	2	3	4	8
10	3.2	6	8	14	> 60	—	—
	3.1	—	7	19	> 84	> 84	> 84
	10.3	<14	—	<14	—	47	>140
0	3.0	—	14	53	>150	>150	>150
	11.1	—	—	69	—	84	>140

Since the amount of water retained in an unfrozen condition by a solute is, at temperatures above its eutectic, a direct function of molal concentration it was of interest to compare the effect of solutes of different molecular weights. Casein suspensions were therefore prepared with artificial sera containing glycerol, dextrose, or sucrose, and their stability determined (Table VI).

Although the eutectic temperature of sucrose (−6.0° C.) was exceeded, there was no evidence of crystallization. On a molar basis, glycerol appeared to have about one-half the stabilizing effect of dextrose, and one-third that of sucrose.

TABLE VI

STABILITY OF FROZEN CASEIN SUSPENSIONS PREPARED WITH GLYCEROL, DEXTROSE, AND SUCROSE

(Casein concentration 3.25 mgm. N/ml.)

Solute	Temp., ° F.	Storage life at 10° F., days		
		Solute concentration, molar		
		0.11	0.22	0.33
Sucrose	+10	73	> 84	> 84
Dextrose	"	15	> 84	—
Glycerol	"	7	19	> 84
Sucrose	0	>147	>147	>147
Dextrose	"	74	>147	—
Glycerol	"	14	53	>147

A few other solutes were tested. Within the accuracy of the tests, maltose had the same stabilizing effect as sucrose, indicating that the reducing group was not involved. Soluble starch had a negligible stabilizing effect while soluble dextrin (B.D.H., corn) appeared to decrease storage life of skim milk considerably.

DISCUSSION

Published data on the stability of frozen milk show that added sucrose (2, 17), or conversion of part of the lactose to glucose and galactose (14), increased storage life. A direct relation between the amount of lactose crystallized from solution and the volume of precipitate has been observed (13, 14), and it has been shown that various processing treatments affect stability of frozen milk indirectly by influencing the rate of lactose crystallization (11). The importance of the solute has thus been demonstrated. Data presented in the present paper support these observations, and provide an explanation for the stabilizing action of sugars on casein sols.

All casein suspensions prepared without sugar or glycerol in the artificial serum were very quickly precipitated in frozen storage. Sugars and glycerol had a marked stabilizing action provided they remained in solution. Thus lactose, with a high eutectic point ($-0.65°$ C.) and low solubility, was the least effective. The greater stabilizing effect of 2 to 4% lactose solutions, as compared to higher concentrations, indicates that the more concentrated lactose solutions, being more highly supersaturated throughout the cooling range, nucleated before the temperature decreased sufficiently to retard nucleation (5, 16). The increase in stability at higher lactose levels when casein and salt concentration was increased threefold reflects the influence of serum salts on the rate of lactose crystallization (13).

Increasing the concentration of milk or milk serum causes precipitation of calcium phosphate, with a concomitant shift in the $H_3PO_4 \leftrightharpoons H_2PO_4^- \leftrightharpoons HPO_4^= \leftrightharpoons PO_4^{\equiv}$ equilibrium and a release of hydrogen ions. Concentrating milk 3:1 lowers its pH by about 0.2 units, and pH values below 6.0 have been recorded in partially frozen milk (12). At the temperatures studied, sugars and glycerol retain considerable water at least temporarily in the unfrozen state. They thus lessen the concentrating effect of freezing, delay the pH shift throughout the cooling range, and reduce the maximum acidity developed for a fixed storage temperature.

However, if the protective action of these solutes depended entirely upon their depression of the freezing point they would behave similarly on a molar basis. The finding that they are not similar on a molar basis indicates that some other factor is at least equally as important as the salt dilution and pH restricting effects. Tentatively it can be suggested that viscosity of the unfrozen portion plays an important role in controlling the rate of casein coagulation. Diffusion or re-orientation phenomena are almost certainly involved in the developing of insoluble casein precipitates, and high viscosities retard diffusion. At equimolar concentrations sucrose solutions are much more viscous than glycerol solutions, thus sucrose had a greater stabilizing effect.

In rough figures, freezing casein suspensions to −12.5° C. would develop serum salt concentrations sufficient to give approximately a 4° C. depression of the freezing point, and a sugar or glycerol concentration of about 3 *M* (13). This represents approximately a 30-fold increase in concentrations of 0.11 molar solutions (1% glycerol, 4% sucrose). However, to compensate for the lower viscosity and obtain equal storage stability it was necessary to start with about 3% glycerol. The increase in concentration was then approximately ninefold, and the depression caused by inorganic salts became about 1.2° C. Thus a one-third reduction in salt concentration approximately compensated for the viscosity difference between 3.0 *M* sucrose and glycerol.

This relation between salt dilution and viscosity will vary with the temperature of storage. At very low temperatures, frozen milk has a long storage life (3, 4), and it can therefore be assumed that viscosity has become the dominant factor. Factors affecting the crystallization of lactose from solutions at subeutectic temperatures will also affect the over-all storage stability. The ideal stabilizing agent for use in frozen milk should therefore be one that greatly increases the viscosity of the unfrozen portion and tends to stabilize the lactose against crystallization. Several stabilizers that have been tested (1) might be expected to have these effects, but sugars and glycerol appear to be the only ones that retain their desirable properties under the conditions developed in frozen milk.

REFERENCES

1. Babcock, C. J., Stabile, J. N., Windham, E. S., and Randall, R. J. Dairy Sci. 32: 175. 1949.
2. Babcock, C. J., Strobel, D. R., Yager, R. A., and Windham, E. S. J. Dairy Sci. 35: 195. 1952.
3. Bell, R. W. and Mucha, T. J. J. Dairy Sci. 35: 1. 1952.
4. Doan, F. J. Food Technol. 6: 402. 1952.
5. Herrington, B. L. J. Dairy Sci. 17: 501. 1934.
6. Lovelock, J. E. Biochim. et Biophys. Acta, 11: 28. 1953.
7. Marier, J. R. and Boulet, M. In press.
8. Polley, J. R. Can. J. Research, E, 27: 265. 1949.
9. Rose, D. Can. J. Technol. 32: 78. 1954.
10. Rose, D. and Tessier, H. Can. J. Technol. 32: 85. 1954.
11. Rose, D. and Tessier, H. Can. J. Technol. 34: 139. 1956.
12. Tessier, H. and Rose, D. Can. J. Technol. 34: 211. 1956.
13. Tessier, H., Rose, D., and Lusena, C. V. Can. J. Technol. 34: 131. 1956.
14. Tumerman, L., Fram, H., and Cornely, K. W. J. Dairy Sci. 37: 830. 1954.
15. Underkoffler, L. A., Guymon, J. P., Rayman, M. M., and Fulmer, E. I. Iowa State Coll. J. Sci. 17: 251. 1943.
16. Whittaker, R. J. Dairy Sci. 16: 177. 1933.
17. Wildasin, H. L. and Doan, F. J. J. Dairy Sci. 34: 438. 1951.
18. Woodman, A. G. Food analysis. 4th ed. McGraw-Hill Book Company, Inc., New York. 1941. p. 134.

THERMODYNAMIC PROPERTIES OF ACETIC ACID – WATER[1]

By A. C. Plewes, R. M. Butler, and K. Pugi

ABSTRACT

The integral latent heats of vaporization of acetic acid – water mixtures were determined at 760 mm. With these data an enthalpy concentration chart was prepared for liquid and vapor samples ranging from 0 to 100% acid. Heats of mixing in the vapor phase were estimated and the results indicate that the enthalpy change of mixing is caused by the reaction of acid monomer to dimer and tetramer coupled with the association of acid monomer with the water vapor.

INTRODUCTION

The value of enthalpy–composition data in the solution of many problems in chemical industry has been known for some time. Unfortunately, few investigators have bothered with such research projects, and data, accurate or otherwise, are difficult to find.

Studies of this kind have been begun at Queen's University and continuing efforts will be made to obtain and correlate various thermodynamic properties of aqueous mixtures. The present work is concerned with the measurements of the integral latent heats of vaporization of acetic acid – water mixtures at atmospheric pressure.

EXPERIMENTAL EQUIPMENT AND PROCEDURE

The apparatus shown in Fig. 1 is a modification of a unit conceived by Dana (1) and improved by Plewes (9). In brief, the calorimeter vaporizes liquid feed at constant composition with a known wattage. The present design permits the study of corrosive liquid mixtures, and improvements in current and voltage control permit an evaluation of wattage with small error.

The calorimeter (Fig. 1) is made up of a heater, C, and a silvered Dewar vessel, B, surrounded by a larger glass unit, S. Liquid from a constant head device which enters S at Y is boiled at constant pressure. It then enters, through a capillary, D, inserted in the base of the Dewar B, the vaporization chamber where unit C boils the liquid away as quickly as it enters. Vapors are withdrawn through unit N to a condenser and collection system where the sample is retained for future weighing. Vessel B is evacuated during a run through Z. The vacuum coupled with silver Dewar prevents heat loss from the inside to the outside of the unit. Vessel S acts as a preheater for the liquid feed and ensures an adiabatic state for the inner unit B.

Heat energy for vaporization is provided by the immersion heater, C. This is made of an electrical resistance element covered with Silicone Oil and jacketed by Pyrex glass tubing. Such an arrangement makes it possible to deal with highly corrosive mixtures which normally attack naked heater

[1]*Manuscript received December 5, 1955.*
Contribution from the Department of Chemical Engineering, Queen's University, Kingston, Ontario.

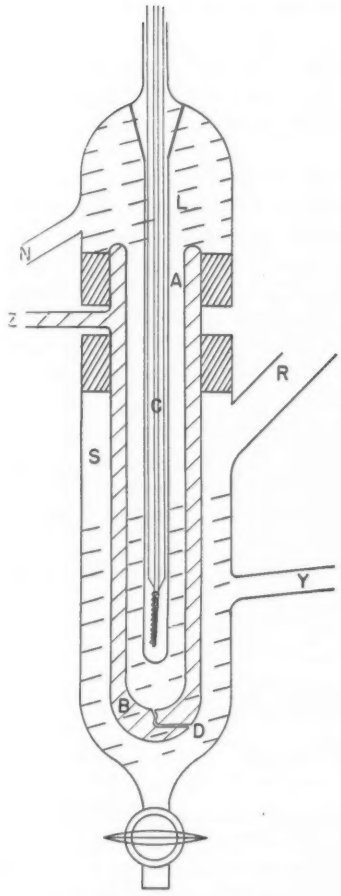

FIG. 1. Calorimeter.

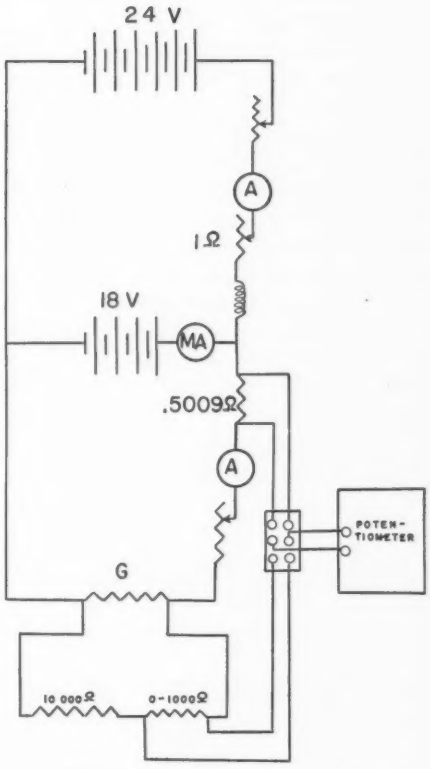

FIG. 2. Electrical wiring diagram.

elements. A glass cap, L, externally heated with nichrome wire covers the top of units B and C.

A 24-volt battery served as a power source and was connected in parallel with an 18-volt cell as ballast. (See Fig. 2.) The least fluctuation in current was obtained with an acid density of 1.175. It was found that the discharge curve of voltage versus time was flat in this region and so permitted withdrawal of energy in the most desirable manner.

Current measurements were made by the determination of the potential drop across a standard resistance of 0.500 ohms located in series with the heater coil. Voltage was determined by the use of a 10,000 ohm standard resistance coupled with a 0–1000 ohm resistance box shunted across the heating

element. Such units made it possible to evaluate the wattage delivered to the calorimeter within ±0.2%.

It was discovered that losses due to conduction were much more important than the electrical resistance (I^2R) losses. For this reason 24-gauge copper wire served well as inlet leads to the heater since it favored the least over-all loss for accurate work.

Runs were continued for a period of two to three hours to ensure equilibrium conditions. Product removal of 3–5 cc. per minute was desirable to prevent entrainment and to make a determination possible in a reasonable time.

Acetic acid of 99.5% purity was obtained from the Shawinigan Chemicals Limited and was distilled in a column packed with ¼ in. glass helices; this unit contained 20 theoretical plates and had a reflux ratio of 20/1. The middle two-thirds of the distillate indicated a boiling point of 118.2° C. at 760 mm. and a density of 1.0439 at 20° C. This fraction was used for the determination of the latent heats of various acid–water mixtures.

City water was once distilled and used without further treatment.

The samples of condensate were analyzed by the use of 0.1 *N* barium hydroxide solution, protected so that the carbon dioxide of the air could not contact the liquid reagent. Phenolphthalein was used as an indicator during this work.

The apparatus was originally tested with pure acid and water and satisfactory results were obtained as shown in Table I.

TABLE I

HEATS OF VAPORIZATION OF PURIFIED REAGENT AT 760 MM.

Compound	Author's data, joules/gm.	Literature, joules/gm.
Water	2257	2256 (5)
Acetic acid (100%)	404 (Direct measurement)	
	403 (By extrapolation to 100%)	405 (6)

The latent heat of 100% acetic acid was estimated also by extrapolation measurements made from 95 to 99.8%. It will be noted that the two values obtained differed by only 0.2%, a divergence of the same order of magnitude as the probable error of the given measurements.

EXPERIMENTAL RESULTS

The results of this study are shown in Table II. The data on integral heat of vaporization were used to prepare the enthalpy concentration chart shown in Fig. 3, and the following information was used in the correlation:

(1) The enthalpy of each pure component in the liquid state is zero at 0° C.

(2) The specific heats of mixtures and pure materials (7) and the latent heats of the pure components are available (5, 6).

(3) The integral heats of vaporization at 760 mm. are reported herein.

TABLE II

INTEGRAL HEATS OF VAPORIZATION OF ACETIC ACID – WATER MIXTURES AT 760 MM.

Wt. % acetic acid	Integral heat of vaporization, joules per gm.	Integral heat of vaporization, joules per mole
0.79	2242	
3.00		40,650
7.00		39,600
10.40	2074	
11.40		38,650
16.80		37,920
20.40	1887	
24.00		36,900
30.50	1695	
31.60		35,500
40.40	1512	
42.10		33,760
51.60	1310	
54.90		31,500
61.20	1131	
70.80	945	
71.80		28,750
80.10	765	
87.90		26,200
89.60	597	
93.60	513	
95.80	474	
97.80	440	
99.19	416	
99.77	406	

(4) The integral heats of solution of mixtures at a given temperature are available (8).

(5) Boiling point – composition data are known for the mixtures at 760 mm. (4).

In this work it is assumed that the enthalpy of pure acetic acid and water is zero at 0° C. Above 0° C. the enthalpies of either component can be calculated from specific heat data.

Liquid isotherms were estimated at 10-degree temperature intervals from 0° C. to 110° C., using the heats of solution and the heat content of the pure components. Above and below 40° C. heats of solution were calculated from the data shown in Table III, which were experimentally determined by Payn and Perman (8). The liquid boiling line at 760 mm. was then drawn so that it intersected liquid isotherms at prescribed compositions and temperatures.

The addition of the integral heat of vaporization of a given acid–water mixture to the boiling liquid enthalpy then gave a point on the vapor line. Data for liquid and vapor lines are listed in Table IV. It is interesting to note in Fig. 3 that the vapor and boiling liquid lines are straight over the complete range of concentration studied.

Once this phase of work was completed it was planned to estimate integral heats of mixing in the vapor state to provide additional data concerning the structure of the vapors.

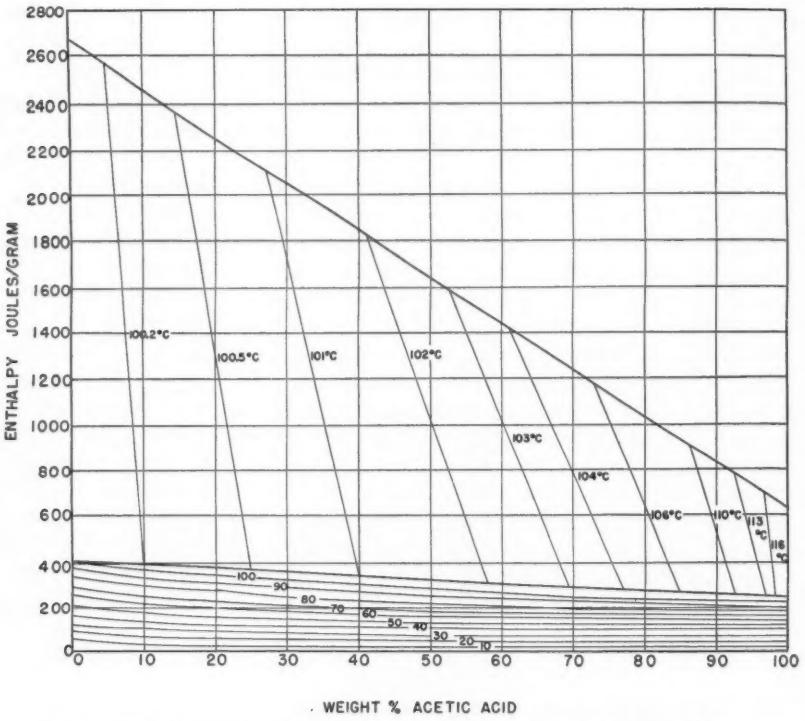

FIG. 3. Enthalpy–concentration data for acetic acid – water mixtures at 760 mm.

TABLE III

INTEGRAL HEAT OF SOLUTION OF ACETIC ACID – WATER MIXTURES AT 40° C. (8)

Mole % acetic acid	Heat of solution, joules/mole
0	
10	5
20	124
30	199
40	280
50	329
60	403
70	396
80	367
90	271

To obtain the heats of mixing the enthalpy of pure acetic acid and water vapor was calculated at zero pressure for a given temperature. It is reasonable to assume that the condition of both starting materials will approach the ideal

TABLE IV

ENTHALPIES OF ACETIC ACID – WATER MIXTURES AT 760 MM. IN JOULES PER GM.

Wt. % acetic acid	Saturated vapor	Boiling liquid
0	2674	418
10	2476	400
20	2283	390
30	2088	378
40	1893	360
50	1678	340
60	1470	320
70	1265	305
80	1057	290
90	859	278
100	659	256

state at zero pressure, and that the enthalpies of the mixtures then could be estimated by the simple equation:

$$H = H_A X_A + H_B(1-X_A)$$

where H = enthalpy of mixture,
H_A = enthalpy of pure A,
H_B = enthalpy of pure B,
X_A = mole fraction of A.

The difference between the experimentally determined and the ideal enthalpies would, then, amount to the heat of mixing.

The variation of enthalpy with pressure from atmospheric to 0.04 atmospheres was determined by the following thermodynamic relationship (2):

[1] $$\Delta H = H_2 - H_1 = \int_{0.04}^{P} \left[V - T\left(\frac{\partial V}{\partial t}\right)_p \right] dp$$

where H = enthalpy variation with pressure,
H_2 = enthalpy of acetic acid vapor at pressure p which is vapor pressure at dew point temperature of mixture,
H_1 = enthalpy of acetic acid vapor at 0.04 atmospheres,
V = specific volume of acid vapor.

P–V–T data for acetic acid were taken from International Critical Tables (3).

The integral was evaluated graphically after determining $(\partial V/\partial t)_p$ by graphical differentiation. From 0.04 atmospheres to zero pressure it was assumed that the acid vapor was composed of monomer and dimer and that any change in enthalpy with pressure was due to association or dissociation reactions. Then,

$$\Delta H_2 = H_1 - H^\circ = \alpha \Delta H_R,$$

where ΔH_2 = variation of enthalpy with pressure from 0.04 to zero atmospheres,
H_1 = enthalpy at 0.04 atmospheres,
H° = enthalpy at zero atmospheres,
ΔH_R = molar heat of association of monomer to dimer,
α = degree of association of monomer to dimer at equilibrium for the reaction

$$\text{AcOH} \rightleftarrows \tfrac{1}{2}(\text{AcOH})_2 \text{ and } K_p = \frac{(p \text{ dimer})^{\frac{1}{2}}}{p \text{ monomer}}.$$

Therefore

$$K_p^2 = \frac{p \text{ dimer}}{(p \text{ monomer})^2} \text{ and } \alpha = 1 \pm \sqrt{\frac{1}{4PK_p^2+1}}.$$

Therefore

[2] $$\Delta H_2 = H_1 - H^\circ = \alpha \Delta H_R = 1 \pm \sqrt{\frac{1}{4PK_p^2+1}}\, \Delta H_R.$$

The total enthalpy change with pressure was, then, the sum of equations [1] and [2].

In the case of water vapor the enthalpy at zero pressure at a given temperature was taken from the steam tables (5). The data collected are shown in Table V. From Table VI it can be seen that in all cases heat was evolved on mixing or that some association of acid or acid and water was evident. This was simply tested as follows: Let it be supposed that any heat of mixing in the vapor is due to the association of monomer to dimer only.

Let N_1 represent moles of acid monomer,
N_2 represent moles of acid dimer,
N_3 represent moles of water,
and Y_L represent mole fraction acid as determined by titration and calculated as monomer.

TABLE V

ENTHALPIES OF ACETIC ACID – WATER VAPOR MIXTURES AT ZERO PRESSURE AND STATED TEMPERATURE IN JOULES PER GM.

Wt. % acetic acid	Temp., ° C.	Enthalpy		
		Water vapor	Acid vapor	Vapor mixture
0	100	2683.0		2683
10	100.3	2683.3	978.9	2514
20	100.6	2684.0	978.8	2343
30	101.2	2684.4	979.0	2173
40	101.8	2685.1	980.0	2003
50	102.6	2687.5	980.0	1834
60	103.6	2689.1	982.0	1665
70	104.6	2691.4	984.0	1496
80	106.4	2695.8	986.3	1328
90	114.5	2703.0	991.8	1162
100	118.0	2714.4	1002.0	1002

TABLE VI

HEATS OF MIXING OF ACETIC ACID – WATER MIXTURES AT 760 MM. IN JOULES PER GM.

Wt. % acid	Heat of mixing	
	H actual – heat zero pressure	Based on acid dimerization only
0		
10	38	15
20	60	43
30	85	70
40	110	100
50	156	141
60	195	190
70	231	238
80	275	285
90	304	335
100	340	374

Then

[3] $$Y_L = \frac{N_1+2N_2}{N_1+2N_2+N_3}$$

for equilibrium conditions

$$p_2 = K_p^2 p_1^2$$

where p_1 = partial pressure of monomer,
p_2 = partial pressure of dimer,
K_p = equilibrium constant at a given temperature (10).

If Dalton's law is assumed,

[4] $$N_2 = \frac{K_p^2 N_1^2 P}{N_1+N_2+N_3}$$

where P is total pressure in atmospheres. Let Y_1 be true mole fraction of monomeric acid in vapor phase; then

[5] $$Y_1 = \frac{N_1}{N_1+N_2+N_3}.$$

Combining equation [4] with equation [5] we get

[6] $$N_2 = K_p^2 P N_1 Y_1.$$

Therefore

[7] $$Y_1 = \frac{N_1+2K_p^2 P N_1 Y_1}{(N_1/Y_1)+K_p^2 P N_1 Y_1}$$

and rearranging

[8] $$\frac{Y_1^2(2K_p^2 P - K_p^2 P Y_L)}{Y_L} + \frac{Y_1}{Y_L} - 1 = 0.$$

Y_1 can be calculated knowing Y_L, P, and K_p at a given temperature. The

amount of dimer is easily calculated and the resulting heat of dimerization follows (10).

Fig. 4 shows that the heat of dimerization is smaller in weak acid mixtures than the enthalpy difference between actual vapors and those calculated at zero pressure. It is suggested that the additional heat change may be explained by the association of water and monomeric acetic acid.

Between 50 and 70% the enthalpy differences agree closely. However, above 79% the actual heat changes are less than those calculated on the basis of dimerization only. Ritter and Simons (10) showed the presence of tetrameric acid in the vapor at 760 mm. and showed that the heat of formation of tetramer is less than the heat of formation of dimer. The presence of tetramer in concentrated acid mixtures could thus explain the difference shown.

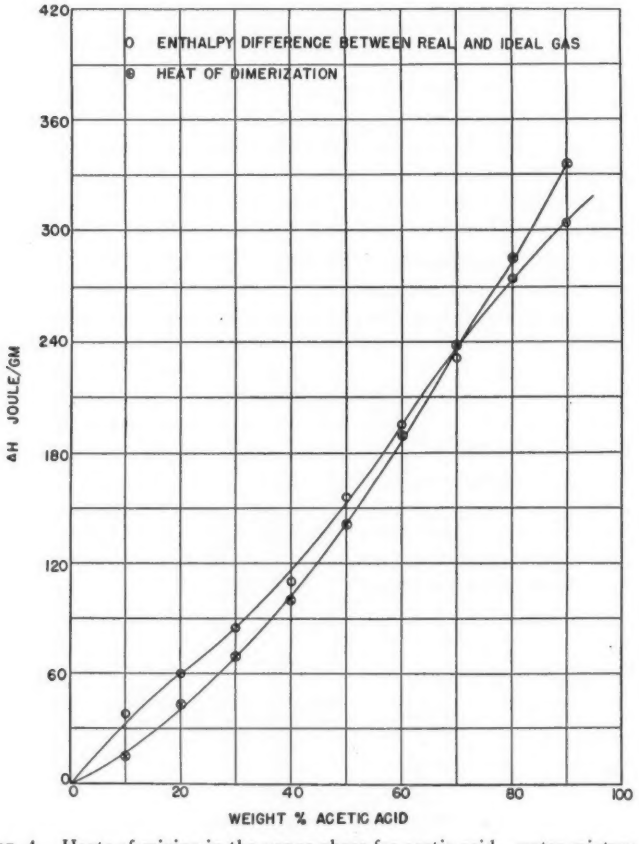

FIG. 4. Heats of mixing in the vapor phase for acetic acid – water mixture.

ACKNOWLEDGMENT

The authors wish to acknowledge the gift donated by the Dye and Chemical Company which made this study possible.

REFERENCES

1. DANA, L. I. Proc. Am. Acad. Arts Sci. 60: 241. 1925.
2. HOUGEN, O. A. and WATSON, K. M. Chemical process principles. Pt. II. John Wiley & Sons, Inc., New York. 1947.
3. INTERNATIONAL CRITICAL TABLES. Vol. III. McGraw-Hill Book Company, Inc., New York. 1927.
4. INTERNATIONAL CRITICAL TABLES. Vol. V. McGraw-Hill Book Company, Inc., New York. 1927.
5. KEENAN, J. H. and KEYES, F. G. Thermodynamic properties of steam. John Wiley & Sons, Inc., New York. 1936.
6. KLOTZ, I. M. Chemical thermodynamics. Prentice-Hall, Inc., New York. 1950.
7. NEUMANN, M. B. Z. physik. Chem., A, 258. 1932.
8. PAYN, R. C. and PERMAN, E. P. Trans. Faraday Soc. 25: 599. 1925.
9. PLEWES, A. C., JARDINE, O. A., and BUTLER, R. M. Can. J. Technol. 32: 133. 1954.
10. RITTER, H. L. and SIMONS, J. H. J. Am. Chem. Soc. 67: 757. 1945.

CORROSION STUDIES OF CARBON STEEL IN ALKALINE PULPING LIQUORS BY THE POTENTIAL–TIME AND POLARIZATION CURVE METHODS

I. THEORY, METHODS, AND SELECTED RESULTS[1]

By W. A. Mueller

ABSTRACT

Potential–time curves and corrosion rates indicate that carbon steel immersed in strong white liquor near room temperature displays two stable states which differ in potential and corrosion rate. Chemical or electrochemical pretreatment of the steel samples controls the range of the initial potential and consequently the establishment of either the active state at −1.05 to −1.1 volt, or the passive state at −0.65 to −0.8 volt against the calomel cell. Theoretical principles were derived for the measurement of reproducible polarization curves and their analysis to determine the electrochemical reactions involved. These principles were realized in an experimental method for recording continuous polarization curves. By this method the potentials recorded during conversion from the active to the passive state were proved to form an S-shaped curve, not a break as hitherto assumed. As a supplement, a multipoint-curve method was developed measuring corrosion rate and current density as a function of the potential even under conditions of changing concentration or temperature. With this method a visible demonstration of the corrosion-potential curve was carried out. This demonstration is based on the formation of a dark brown film which shifts downward from the corroding steel sample. By this means a narrow potential range of high corrosion rate, limited by corrosion-free ranges of either cathodic or anodic protection, is indicated.

A. THE PROBLEMS UNDER STUDY

Recent investigations in the field (2, 13, 17) and in the laboratory (4, 15) of the complex corrosion problem exhibited by carbon steel in contact with alkaline pulping liquors have convincingly indicated that the chemical composition of the liquors is the most significant factor in the corrosion in alkaline pulping digesters. This relation is clearly demonstrated by the graph of Christiansen (2), Fig. 1, which plots the average of the digester corrosion rates in milli-inches per 2000 cooks (MP2TC) against the "corrosiveness". Corrosiveness, as defined, is the value of a corrosion rate which is calculated by means of an equation derived from laboratory corrosion rates. However, this relation between mill corrosion rates and laboratory corrosion rates is still somewhat questionable as the actual regression line (*a*) deviates considerably from the "ideal" regression line (*b*) which presumes equal mill and laboratory corrosion rates and passes through the origin. Thus Fig. 1 poses the question: What causes this deviation of mill corrosion rates from laboratory corrosion rates?

A more striking problem was pointed out in two independent studies of Hassler (4) and of Ruus and Stockman (15). In the two studies it was found

[1]*Manuscript received October 28, 1955.*
Contribution from the Pulp and Paper Research Institute of Canada, Montreal, Que. Presented at the Corrosion Symposium jointly sponsored by the National Research Council, the Chemical Institute of Canada, and the National Association of Corrosion Engineers, Montreal, Que., Sept. 15, 1955.

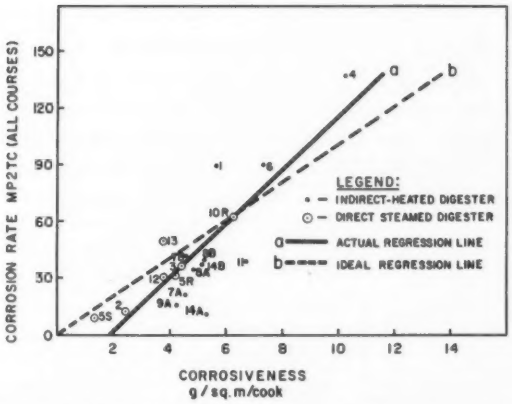

FIG. 1. Corrosion rates observed in Canadian mills against corrosiveness of liquors used (2).

that the corrosion rates were not always reproducible and that under certain presumably identical conditions, the variations were considerable, e.g. in white liquor with a sulphur addition of 3 gm./liter the rates oscillate between negligibly small values of 10 to 20 to the enormous value of 650 to 750 MP2TC. The latter is a rate which would destroy a digester of average wall thickness within a year. Mean values of rates which vary with a range of 1 to 50 are not reliable. On the other hand, they suggest that minor changes of the corrosion conditions may establish low corrosion rates. Hassler attributes this lack of reproducibility to the properties of the initial state of the steel sample at the moment of immersion in the liquor. He distinguishes between the active state of an acid-cleaned sample and the inert state of a sample covered by a film of dried black liquor. However, he is not satisfied with his results and proposes a more intensive study.

Another problem (15) is offered by the observation that, during the heating period of the kraft cook, the corrosion rate is high and falls unexpectedly in the temperature range near the boiling point of the liquor. At this point the changing liquor-composition and temperature come into play.

The problems mentioned are only a few of the most impressive. In order to cast some light on these questions, the conditions on the border line between the active and the passive range have to be studied carefully. The direct and normal method of carrying out a corrosion study by measuring the loss of weight or steel thickness only, as done by other investigators, apparently is unsatisfactory for the investigation of the problems outlined. However, electrochemical methods measuring potential–time curves and current density – potential curves (also called polarization curves) are expected to provide some basic information on the conditions of the active and the passive states. The first object of this study is to find the means of analyzing electrochemically the corrosion reactions in order to single out quantitatively their different components.

B. POTENTIAL–TIME CURVES AND CORROSION RATES

I. *Experimental Method of Measuring Potential–Time Curves*

A very simple electrochemical method is the potential–time curve technique. It is frequently applied to determine whether a metal is in the active or the passive state (19). The unit in which the tests were carried out (Fig. 2) consisted of a polythene beaker (B) containing the liquor, a calomel cell (C), and the steel samples (S). A multipoint switch (S_{10}) connected the steel samples in

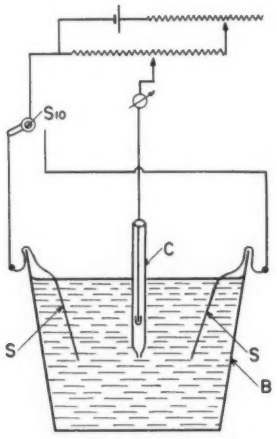

FIG. 2. Potentiometer circuit used for measuring potential–time curves.

turn with a potentiometer circuit to check their potential against the calomel cell without drawing current. The high electrical conductivity of the solution guaranteed a uniform potential in the bulk of the liquid. Therefore the potential of all samples which were placed in the beaker could be measured by employing one stationary calomel cell.

Generally the beaker was open to the air in order to simulate mill conditions, as mill liquor is usually prepared in open tanks and finds intimate contact with the air content of the chips in the digester. To reproduce the corrosion conditions of the kraft cook, strong white liquor composed of 100 gm./liter NaOH and 35 gm./liter Na_2S was employed. The carbon steel sheet from which the samples for the study of potential–time curves were cut had, according to the analysis carried out in the Department of Mines and Technical Surveys in Ottawa, the composition shown below:

	C	Mn	Si	P	S
%	0.18	0.54	0.245	0.015	0.035

The dimensions of the samples approximated 0.02 in. thickness, 0.1 in. width, and 3 in. length.

II. *Typical Potential–Time Curves*

Four examples may demonstrate typical effects of the pretreatment on the potential:

(1) Fig. 3 shows how slightly passivated samples may become reactivated by washing with tap water. The samples, kept for a few days in the open and at room temperature, were cleaned with dilute hydrochloric acid for a few

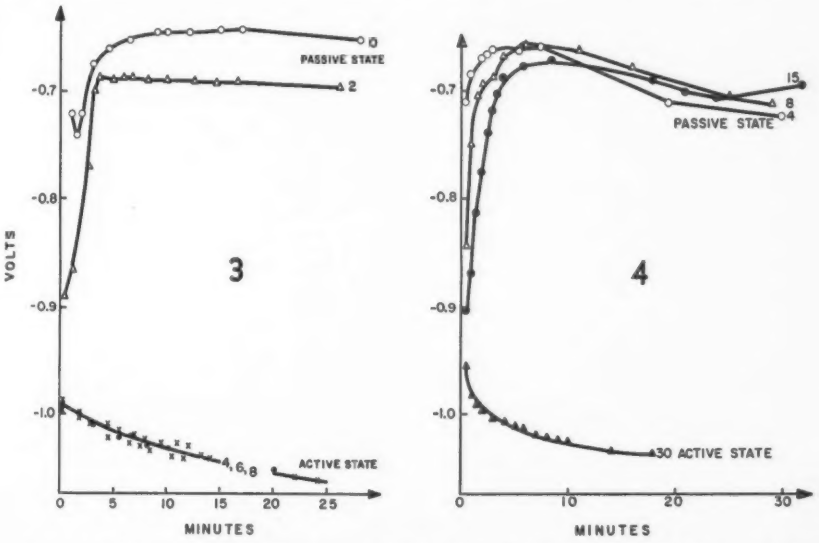

FIG. 3. First graph of potential–time curves showing the activating effect on slightly passivated steel samples when they were rinsed with tap water for an increasing number of minutes.

FIG. 4. Second graph of potential–time curves showing the activating effect on strongly (anodically) passivated steel samples when they were rinsed with tap water for an increasing number of minutes.

seconds in order to activate them, rinsed with water to remove the acid, wiped dry with a paper towel, and kept in air at room temperature for 20 min. to passivate them slightly.

After this pretreatment, sample 0, immersed in white liquor, assumed a potential of −0.72 v. against calomel and maintained a potential close to the original value. Sample 2, after the same pretreatment as sample 0, was rinsed with tap water for two minutes before immersion in the liquor. Owing to this minor alteration of the pretreatment, the initial potential decreased to −0.89 v. But during five minutes' immersion in liquor, the potential shifted back to −0.7 v. against calomel. However, the other samples, rinsed with water for four, six, or eight minutes, acquired the same initial potential of −0.99 v. when immersed in the liquor but their potential shifted slowly to −1.05 v. Thus two groups were finally singled out, one with the potential of −1.05 v. in the active state including all samples of an original potential lower than

−0.9, and the other of a potential near −0.7 v. in the passive state accumulating the samples of a potential higher than −0.9 v.

(2) The second experiment was carried out to show the effect of the strongly passivating pretreatment, which consisted of the steel samples being used as anodes in dilute sodium hydroxide for three hours. This strongly passivating pretreatment required some additional minutes of tap water rinsing to shift the original potential from the passive to the active state (Fig. 4). Sample No. 15, after 15 min. washing, was still in the passive range. However 30 min. rinsing was sufficient to activate a pretreated sample.

(3) The third experiment shows another effect of a strongly passivating pretreatment. This group of samples was kept in an oven for about six weeks at 130° C. and then activated by immersion in dilute hydrochloric acid for 10 sec. After they were rinsed with tap water for 10 sec., the samples were dried with a paper towel and kept at room temperature for 20 min. in air. Again the potential shifted to more negative values when the samples were rinsed with tap water. After six minutes' rinsing, Sample 6, immersed in liquor, was still passive but Sample 8, immersed in liquor, became active after eight minutes' rinsing (Fig. 5).

(4) The fourth experiment was designed to reveal the activating effect of the cathodic treatment. The steel samples, immersed in 25 gm./liter sodium hydroxide, were put in a circuit as cathodes at 0.44 amp. for 15 min. After the samples were rinsed for a minute and dried with paper towels, they were placed in a desiccator for an increasing number (0, 4, 8, 12, and 20) of minutes.

After this pretreatment, potential–time curves were taken (Fig. 6). The dry air of the desiccator apparently shifts the initial potential from the active to the passive state. However, the stable range of the passive state is still closely confined. Hence potential oscillations exceeding the limit of this range result in rapid activation of the samples.

The four examples may sufficiently demonstrate the general behavior but many more experiments still have to be made to give a complete survey of all possible arrangements. All the samples with any type of pretreatment finally reached either the passive state at a potential of −0.65 to −0.8 v. or the active state at −1.0 to −1.15 v.

III. *Corrosion Rate as Influenced by the Active or Passive State*

The importance of the described potential measurements can be underlined by the proof that the corrosion rate in the active state is much greater than in the passive state. Therefore, a few measurements of corrosion rates are added.

(1) Four steel samples were cleaned with dilute hydrochloric acid to remove the mill scale, rinsed with water, and dried in an oven at 130° C. Samples 1 and 2 were immersed in liquor immediately and proved to be passive. After samples 3 and 4 were rinsed for six minutes their potential value showed that they were still passive. Therefore, they were rinsed with water for another six minutes, checked again, and it was found that samples 3 and 4 had changed to the active state. They were then immersed in liquor at room temperature

for one day, and all samples kept their state (Nos. 1 and 2, −0.75 to −0.77 v., Nos. 3 and 4, −1.08 v.). Before the experiments the weights were taken after the samples were dried. Following the experiment the samples were washed with dilute hydrochloric acid (1 acid: 20 water) for about 5–10 sec. to remove the deposit of ferrous sulphide or ferric sulphide, then rinsed with tap water

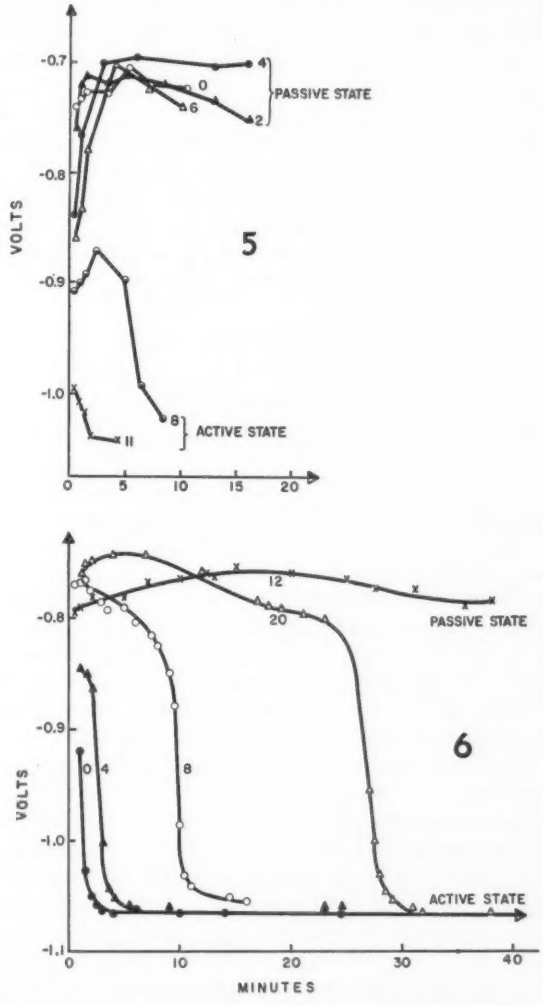

FIG. 5. Third graph of potential–time curves showing the activating effect on steel samples which were passivated in air and then rinsed with tap water for an increasing number of minutes.

FIG. 6. Fourth graph of potential–time curves showing the passivating effect on strongly (cathodically) activated steel samples when they were exposed to air for an increasing number of minutes.

for 10 sec., dried with a paper towel, heated in the oven, and the weight taken again.

(2) In the second experiment the procedure was the same as in the first except that samples 1 and 2 were treated in the same way as samples 3 and 4 in the previous experiment, and samples 3 and 4 as samples 1 and 2 previously.

(3) The third experiment was carried out just like the first, but the duration of the treatment was extended to 4.67 days. The results are tabulated in Table I.

TABLE I

		Sample No.			
		1	2	3	4
1st expt., 1 day	Loss of mgm. weight	2.5	1.9	7.2	10.3
	Corrosion rate MPY	2.0	1.7	6.0	7.9
		Passive		Active	
2nd expt., 1 day	Loss of mgm. weight	14.0	7.5	2.2	2.8
	Corrosion rate MPY	11.2	6.6	1.8	2.1
		Active		Passive	
3rd expt., 4.67 days	Loss of mgm. weight	2.0	1.9	46.6	58.4
	Corrosion rate MPY	0.3	0.4	8.4	9.6
		Passive		Active	

MPY = milli-inches per year.

That the corrosion rates are surprisingly low will be explained later by comparison with the corrosion–potential curve. However, in the passive state (Nos. 1 and 2 of the first experiment, Nos. 3 and 4 of the second experiment, and Nos. 1 and 2 of the third experiment) the sample always had a much lower corrosion rate than in the active state (Nos. 3 and 4 of the first experiment, Nos. 1 and 3 of the second experiment, and Nos. 3 and 4 of the third experiment). This result demonstrates that the corrosion rate of steel in the active state, as checked by the potential measurement, is many times greater than the corrosion rate in the passive state. The accurate value of this ratio is much higher than the ratio of the above values, as the small loss of weight experienced when the samples are cleaned accounts for nearly all of the small loss in the passive state. This statement can be proved by comparing the loss of weight in the passive state after 4.67 and 1 day; it thus becomes evident that the actual loss in the passive state is below the limit of accuracy. Minor differences in the pretreatment of the samples are responsible for this remarkable difference. In the experiments described, this difference consisted in rinsing two steel samples in tap water for 12 min. in order to render them active before experiments were carried out. The other two samples which were not rinsed remained passive.

IV. *Scientific Significance of the Hypothesis of Two Stable States*

Uhlig and Haring (18) present an example of potential–time curves which indicate the behavior of iron of unspecified pretreatment immersed in solutions of different composition. At first sight their curves resemble the curves of Figs. 3 to 6. However, the title of the curve reveals that the variation of the potential–time curves of Uhlig and Haring is affected by the varied composition of the solutions, not by a varied pretreatment of the steel sample as is the case of the curves of Figs. 3 to 6. In all these diagrams the initial potential after immersion lies somewhere between the active and the passive state, but the final state is clearly active or passive. These points of agreement and disagreement elucidate the situation. Apparently the white liquor under study represents an "ideal solution on the borderline between the corroding and passivating classes" which Evans (3) defines and describes in his textbook. Measuring potential–time curves when endeavoring to study the effect of the pretreatment seems much simpler and clearer than the method tried by Mears and Evans (11) who checked the probability of water drops yielding rust.

C. THE POLARIZATION CURVE

I. *Principle*

The usual concept of the electrochemical nature of corrosion implies the possibility, at least theoretically, of separating anodic and cathodic areas on the corroding surface. If all couples on a corroding surface are statistically equivalent to a single couple, the current of which follows Faraday's law, the electrochemical nature of the corrosion under study is accepted as proved. This principle may be successfully applied to explain the polarization curves of electrodes which are actually cells, for instance, consisting of two electrochemically different metals or of differently-aerated areas of the same metal. The studies of polarization curves carried out on this continent and in England (3, 5, 16, 18, 19) are based on this condition.

However, it seems justifiable to widen the definition of an electrochemical process so as to include all those corrosion phenomena which consist of two groups of reactions occurring simultaneously at the same electrode as revealed by some European investigations. These may be oppositely directed reactions of the same metal (10), e.g. (*a*) formation of ions from metal and (*b*) plating out the same metal. In addition reactions of a completely different nature (12) may be involved as (*a*) depolarizing (oxidizing) reactions of dissolved substances (e.g. O_2) removing negative charges from the electrode so as to allow a continuous corrosion process; (*b*) reducing reactions of dissolved substances removing positive charges may also take part, particularly within the anodic potential range (9).

All these reactions are associated with an exchange of electrical charges between electrode and liquid and therefore deserve the designation 'electrochemical'. They form single polarization curves and, by superimposing, actual polarization curves. (The comparison with polarographic curve suggests itself, but it is postponed until comparable measurements are at hand.)

To single out the different reactions appears an important step towards investigation of the mechanism of corrosion. To this end a few studies of very simple known reactions in the active range only were carried out (1, 12, 20). For instance, Bonhoeffer (1) studied the conditions for iron to dissolve in sulphuric acid and proved that the polarization curve is quantitatively composed of the curves related to the two reactions:

$$\begin{aligned} Fe &\rightarrow Fe^{++}+2e, \\ 2H^{+}+2e &\rightarrow H_2. \end{aligned}$$

In the first reaction, iron dissolves in the form of ferrous iron; in the second reaction, hydrogen is plated out on the steel. The dissolution of iron and the formation of hydrogen is quantitatively attended by the exchange of electrical charges according to Faraday's law. Hence the current can be calculated:

[1] $$I = I_{Fe} - I_{H},$$

where I = measurable current density,
I_{Fe} = partial current density originating from dissolving iron,
I_{H} = partial current density originating from developing hydrogen.

The equivalent of Fe^{++} formed or of H^{+} reduced can be calculated according to Faraday's law:

[2] $$\frac{I}{F} = \frac{d((Fe^{++}) - (H^{+}))}{dt},$$

where F = Faraday's constant,
(Fe^{++}) = equivalent Fe^{++} formed,
(H^{+}) = equivalent H^{+} reduced.

Since there are no known exceptions to Faraday's law, Eqs. 1 and 2 can be extended to include any reaction at a metal electrode. All substances which are reduced by reaction with the electrode remove negative charges from the electrode, while all substances which are oxidized at the electrode add negative charges to the electrode. Hence Eqs. 1 and 2 can be generalized to:

[3] $$I = I_{Me} - I_{R} + I_{O},$$

where I_{Me} = partial current density originating from dissolving metal,
I_{R} = partial current density originating from substance being reduced at the electrode,
I_{O} = partial current originating with the substance being oxidized at the electrode.

[4] $$\frac{I}{F} = \frac{d((Me^{n+}) - (R) + (O))}{dt},$$

where (Me^{n+}) = equivalent metal ions formed,
(R) = equivalent of substance reduced,
(O) = equivalent of substance oxidized.

(As iron is not plated out under the given conditions, this reaction is not allowed for in Eqs. 3 and 4.) The current, measured in faradays, equals the

equivalent of metal ions formed minus the equivalent of reduced substance plus the equivalent of oxidized substance, both per time interval. It is possible to measure the current–time integral $1/F \int_0^t I\,dt$ and the loss of metal in equivalents (Me^{n+}). Their difference equals the equivalent of the amount of oxidized substance minus the amount of reduced substance:

$$[5] \qquad (Me^{n+}) - \int_0^t \frac{I\,dt}{F} = \Delta(R) - \Delta(O).$$

The reduction is more pronounced in the cathodic range and the oxidation in the anodic range. This fact simplifies the application of Eq. 5, since in the cathodic potential range, which is of primary interest for this corrosion study, only depolarizing (reducing) substances are usually of influence. Because the loss of metal and the integral of the current can be measured as functions of the potential, the amount of reduced substance as a function of the potential can be calculated. Thus the polarization curve is broken down into the two or three basic groups of reactions to allow their independent study. The object of this method is the elaboration of all the individual reactions which contribute to current density and corrosion rate.

II. *An Experimental Method for Recording Continuous Polarization Curves*

Polarization curves which are to be analyzed for the reactions involved have to be reproducible and unequivocal, i.e., supplying nearly identical values when measured by either increasing or decreasing potential. Any break in the potential in the course of the polarization curve reveals conditions the analysis of which is open to question. In addition it seems wise to make arrangements, if feasible, for registering the curves of several steel samples simultaneously, so as to have a basis for the formation of average values.

(*a*) *Criticism of the Existing Experimental Method*

Reference to the pertinent literature and textbooks on chemical passivity reveals that a break in the polarization curve, from the active to the passive range, is usual (8). In this paper, Fig. 42 given by Kittelberger (7) is considered to plot typical polarization curves which were measured at steel immersed in air saturated $N/10$ K_2SO_4 solution at pH = 6.0. The curves established by measurement with increasing or decreasing potential are closely adjacent only in the potential range from -1.5 to -0.5 v. However, from -0.5 to $+1.6$ v. the curves differ significantly and each of them includes a completely unstable range. Unstable curves of this type provide no reliable basis for any conclusions as to the chemical reactions occurring under equilibrium conditions. Thus arises the question whether this instability is an inherent property of the metal–liquid system under study or whether it is only the result of an unsuitable experimental arrangement.

The typical features of the arrangement are the cell with the steel samples and the calomel electrode C used for checking the potential between sample and liquid. There is a large calomel cell CC used as a counterelectrode. The

voltage is drawn from the rheostat R with slide wires. If the current i in the circuit becomes zero, the potential drop ΔE in the resistors vanishes. According to Ohm's law, ΔE is given by

$$\Delta E = i.R. \qquad [6]$$

When a lead of an electrical circuit breaks, the whole potential difference shifts from the resistors where it becomes zero to the point of rupture. Accordingly, when the electrode becomes passive, ΔE shifts to the surface of the electrode, because in the considered range of the passive state, increasing potential difference does not cause an increased current. A similar potential shift at the counterelectrode adds to the shift in the potential under study owing to the immediate cessation of current flow. This explanation can very easily be proved. By diminishing the product iR (R = the whole resistance of the circuit), ΔE should be decreased proportionally. Hence to avoid the break in the polarization curve, the experimental arrangement was designed to guarantee a ΔE kept below a maximum of a few millivolts. Therefore a sample of surface area 0.085 sq. cm., small enough to reach the maximum current density with a current of a few milliamperes, was used. Moreover, the electrical circuit was designed to reach a sufficiently low internal resistance.

(*b*) *The Experimental Arrangement*

The principles outlined govern the design of the measuring circuit (Fig. 7). A two-volt battery B1 feeds two ring rheostats (R_1, R_2) and a helipot potentiometer H. A mechanical device shifts the sliding contact inside the 10 ohm helipot potentiometer in three, six, or nine hours from one end to the other, and a switch at the end reverses the direction of the potential changes. The current, which enters the liquor through the steel electrodes S, is drawn from the helipot potentiometer and is recorded on a 12-point recording potentiom-

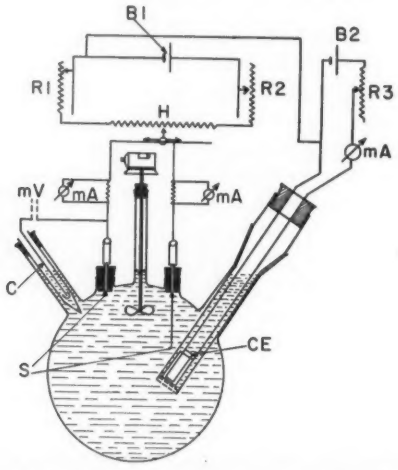

FIG. 7. Experimental arrangement for recording continuous polarization curves.

eter (Speedomax) by means of shunts. The voltage difference against saturated calomel is simultaneously measured by a potentiometer.

The counterelectrode CE is supposed to maintain an almost constant potential. However, drawing any current normally changes the potential to some extent. To secure a counterelectrode of sufficiently constant potential a stainless steel cathode is used, consisting of a small piece of pipe. A stainless steel anode is placed inside this cathode. The current of 100 to 300 ma. in the counterelectrode circuit is drawn from the battery B2 and regulated by a rheostat R.

This arrangement, although much simpler than the electronic device otherwise used (14), gives satisfactory results. It was chosen in order to avoid a change in ΔE greater than about 10 mv. when i is shifting to zero. By introducing steel samples of free surface area of 0.085 sq. cm., the current is held sufficiently low without interfering with the current density requirements, which depend only on the corrosion conditions.

A basic problem of small area electrodes is the establishment of a well-defined surface area with clear boundaries. The samples used in this study were cut from steel sheets, and then about half their length was turned down on the lathe to form a cylinder of 0.33 cm. diameter. The other half length of the sample showed the original thickness of the steel sheet. Thus the type of steel could easily be identified. The turned-up end was pushed through a hole in a rubber stopper to expose only the end to the attacking liquor. The use of wax (7) for limiting the attacked area was discarded, as under certain conditions, e.g. high content of polysulphides, the samples often have to be cleaned mechanically by a paper towel.

(*c*) *Typical Polarization Curves Displaying a Corrosion Maximum*

As outlined above, the experimental arrangement was designed to record reproducible polarization curves close to the steady state. Fig. 8 shows a

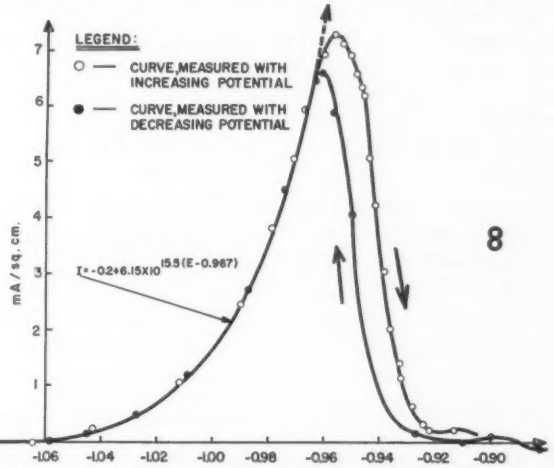

FIG. 8. Continuous polarization curves of iron immersed in white liquor at 30° C. measured at "slowly" (107 mv./hr.) increasing or decreasing potential.

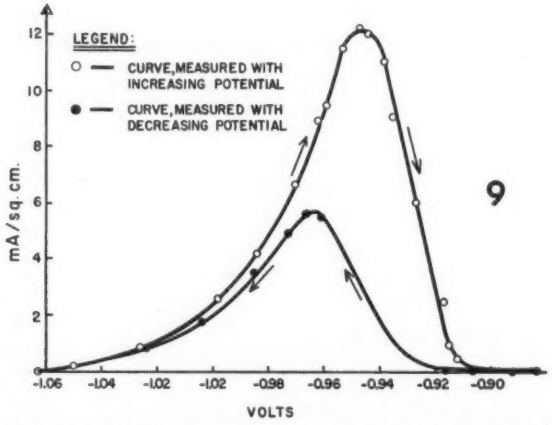

FIG. 9. Continuous polarization curves of iron immersed in white liquor at 30° C. measured at "rapidly" (157 mv./hr.) changing potential.

polarization curve of carbon steel (p. 168) immersed in "white liquor" (100 gm./liter NaOH+35 gm./liter Na_2S) as recorded by the Speedomax at 30° C. Generally the potential drawn from the helipot is changed uniformly with time by means of a mechanical device; however, the potential difference between steel samples and liquor is still, to a minor degree, influenced by the change of the current density. Thus, at the "break" in the curve, the potential changes faster than otherwise. On the other hand, the rate of potential change is slowed down as far as necessary to record curves close to the steady state. The curves taken at increasing and decreasing potentials are almost identical. Characteristic features are the exponential increase of the current density with increasing potential and the S-shaped "break". In order to derive reproducible curves, the steel samples must not be exposed to a very different potential before the experiment begins, and they have to be kept immersed in the liquor at the starting potential for at least 15 minutes. Thus the current density at the beginning of the experiment is brought close to the steady state value. The rate of potential change with time has to be kept below a certain value; otherwise curves which deviate considerably from the steady state (Fig. 9) may be recorded.

Often the problem of the formation of a sulphide layer is encountered. It can shift the boundary between active and passive potential to more negative values. The sulphide layer is easily removed by rubbing the electrodes with a paper towel. A peculiar feature of this process is that after cleaning, the current density of the sample does not immediately return to the current density of an uncovered sample, but takes a few minutes (Fig. 10). Therefore only maximum points of the curve taken after cleaning were used for the synthesis of the polarization curve.

III. *Second Experiment Method. The Multipoint Curve*

A continuous polarization curve furnishes the most complete information

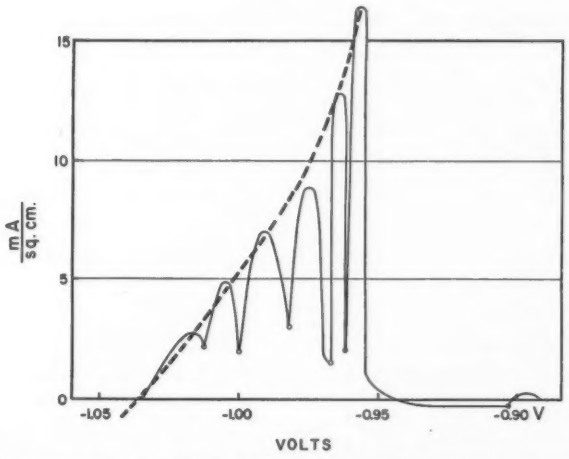

FIG. 10. Polarization curve displaying the influence of formation and removal of iron sulphide on iron electrode immersed in white liquor at 60° C.

as it comprises all the possible waves of the curve. However, the continuously-measuring method displays a definite disadvantage. It is unsuited for a study of the polarization curve as a function of changing concentration or temperature (e.g. during a cook), since it takes some hours to check the curve at one concentration and temperature. Also, the oxidizing and reducing reactions in the counterelectrode cell, even though occurring in a separated cell, may produce substances of high enough concentration to influence the polarization curve.

These problems are solved or diminished (as to the change in concentration) by the multipoint-curve technique, introduced here to complete the measurements made by the continuous method.

(*a*) *Principle of the Multipoint-curve Technique*

Ten steel samples, immersed in the liquor under study, were kept at a series of nearly constant potentials, each differing from the previous one by 50 to 100 mv. Current density and potential were checked for each electrode. Thus, 10 points on the polarization curve were checked at steady state conditions simultaneously. In addition, the corrosion rate as a function of the potential can be checked to establish the corrosion–potential curve. Hence this technique allows the study of the influence of changing concentration and temperature on the polarization and the corrosion–potential curves and presents itself as the ideal method for measuring the changing conditions during cooks.

(*b*) *Experimental Arrangement for Checking the Multipoint Polarization and the Corrosion–Potential Curve*

The experimental arrangement for measuring the 10-point polarization and corrosion–potential curve is outlined in Fig. 11. To establish the potential

stages required, a current of about 100 ma. is drawn from a two-volt battery B and regulated by a rheostat R_1. The established voltage difference is measured by the voltmeter V. During the measuring period switch S2 is in the lower position. Ten milliammeters (mA, mV) of 1 ohm resistance are switched in the circuit in series to be used as resistors for forming the potential stages and to serve as milliamp- and millivolt-meters. Each of them indicates the potential difference between two electrodes E. In addition, the difference of the

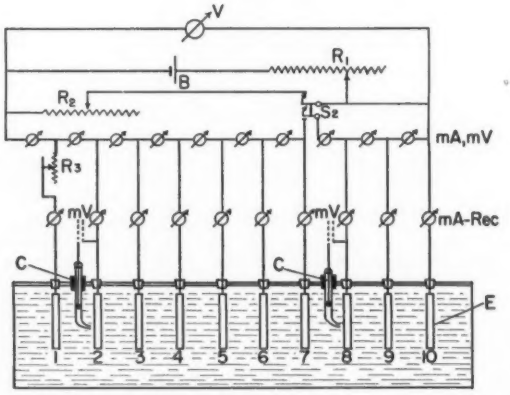

FIG. 11. Experimental arrangement for measuring the 10-point polarization and corrosion-potential curves.

milliampere readings of two succeeding instruments is equal to the current which leaves or enters the steel sample at the junction between the milliammeters. In order to reach fairly constant current-density values, the samples have to be in the final state immediately at the beginning of the experiment. Double pole switch S2 in the upper position interrupts the circuit, for instance between the samples 7 and 8, and switches in the resistor R2. This design allows the application of a variable potential difference between the left group (samples 1 to 7) and the right group (samples 8 to 10). Thus the left group can be activated and the right group passivated at the beginning of each experiment.

The arrangement described is the portable arrangement mentioned above. To establish a more accurate current–time integral, the current is recorded simultaneously in 10 channels of the 12-point recording potentiometer (Speedomax) (mA-Rec) by means of 10 shunts. Two calomel cells (C), joined with a potentiometer (mV), measure the potential difference between electrodes E and the solution. At the most cathodic electrode (sample 1), where polarization alters during the evolution of hydrogen, the current can be regulated by the rheostat R_3. In addition, sample 1 can be pretreated by developing hydrogen till the potential becomes fairly constant. Thus a shift of the potential at the other electrodes can be avoided.

(*c*) *Disproof of Basic Objection to the Principle of the Multipoint-curve Technique*

The question arises as to whether the current measured is the whole current, or whether some current enters a steel electrode on the more positive side and leaves the electrode on the more negative side. The amount of current entering or leaving the steel sample from the liquid is a function of the potential difference between the liquid and the steel sample. Therefore the current density in the liquid influences the current density at the electrode only in so far as it causes a potential slope in the liquid. This potential slope can be kept reasonably small in liquors of high electrical conductivity by suitable arrangement of the steel samples, by placement of the samples at proper distances round a circle. The potential slope in the liquor can easily be checked as the potential difference of two identical calomel electrodes, put in the liquor at the spots of interest. The course of the polarization curve (Fig. 12) indicates that a few millivolts of potential difference between the liquid at the two sides of a steel sheet do not essentially influence the average value of the current density.

(*d*) *Preliminary Experimental Results*

Measurements of corrosion rate and current density were carried out on carbon steel (analysis, p. 168) immersed in concentrated white liquor. The portable arrangement was used to carry out the first series of tests. This method checks the current leaving the steel samples without a recording instrument as the difference of two readings. In addition, more elaborate and exact measurements, based on recording current density – time curves, were carried out.

Fig. 12 shows the polarization curve (current density against potential) and the corrosion–potential curve (corrosion rate as a function of the potential) which were measured at 10 sq. cm. steel samples during two and one-half hours. The calculation of the corrosion rate as current density according to Faraday's law is possible if the reaction occurring is known (see above). Plotting Fig. 12 was based on the assumption that the dissolution of iron in the active state takes three valences per atom.* It will need further study to measure the exact value of n and to elucidate the reactions involved and the ionic state of iron under these conditions.

Fig. 12 demonstrates that in the white liquor investigated, corrosion rates at a current density of zero in the active and passive states are very low compared with the maximum corrosion rate. This fact explains the low corrosion rates which were found experimentally (Table I). Moreover Fig. 12 shows the depolarization curve which is computed as the difference in polarization-curve values minus corrosion–potential curve values.

The most suitable attack appears to be to measure the exact curve of the maximum corrosion range by the continuous polarization-curve method and to add the corrosion–potential curve and some points of the anodic and of the cathodic ranges to the polarization curve measured by the multipoint method.

**Probably iron forms ferrous ions and simultaneously S^{--} is oxidized to elementary sulphur respectively polysulphide.*

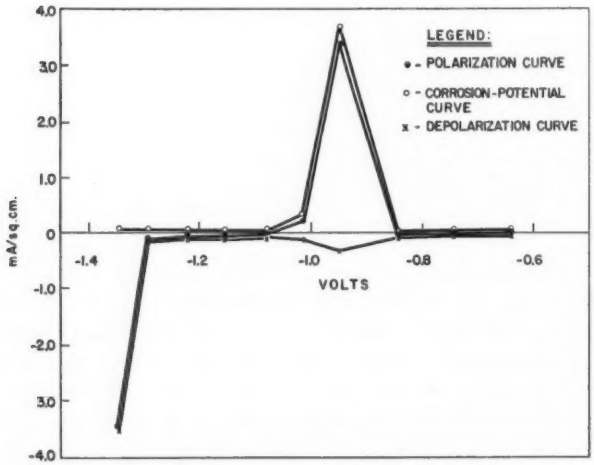

FIG. 12. Polarization curve, corrosion–potential curve, and depolarization curve measured with the 10-point curve technique.

Fig. 13 shows a polarization curve which is based on measurements taken by either method. It may be noticed that the small value of negative current density is found in the passive range, only if enough depolarizing substances (O_2) are present. This negative current density is an indispensable condition of a stable passive state.

A side phenomenon of the multipoint method is the formation of dark brown films which slide down the corroding samples as a visible demonstration of

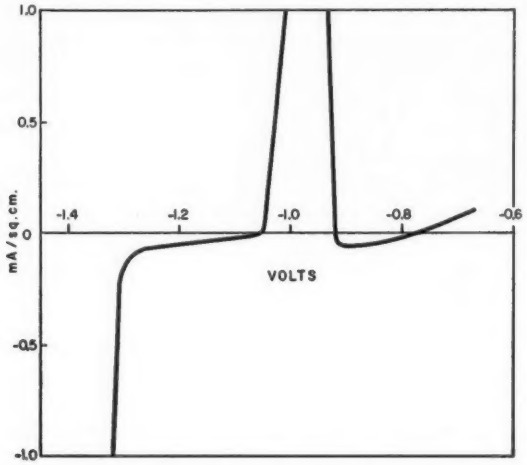

FIG. 13. Polarization curve combined from measurements performed with either method.

the corrosion taking place. Fig. 14 shows a photo of 10 steel samples during the corrosion experiment. Potential differences were applied between the steel samples and the liquor in stages of about 80 mv., increasing from the sample furthest left to its adjacent one, etc. Two of the samples, kept in the potential range of high corrosion rate, display the dark (brown) film which indicates a high corrosion rate; the surrounding ones are free of corrosion because of

FIG. 14. Photo of steel samples taken during 10-point curve measurement. The two corroding samples form a dark film of corrosion products.

either cathodic or anodic protection. Thus the photo demonstrates the possibility of anodic or cathodic protection and it represents a visible proof of the corrosion–potential curve of Fig. 12.

D. DISCUSSION

I. *Stability of the Active and Passive States*

The potential–time curves plotted in Figs. 3–6 indicate the existence of two stable potential ranges. One range is in the active state and the other is in the

passive state under conditions which are identical except for the chemical pretreatment of the steel. The explanation of this surprising finding can be based on a discussion of the form of the polarization curve (Fig. 13).

The equilibrium condition of the potential can be expressed with reference to the definition of a mechanical equilibrium as follows: the equilibrium potential is reached if the current density is zero at a constant potential. The equilibrium is stable if the potential, after receiving a small displacement, tends to return towards its original value. The criterion of stability on the polarization curve is a positive value of the gradient current density versus potential because this means a current of positive charges leaves the steel electrode in order to restore the original potential, when the potential is increased. The equilibrium is unstable if the potential, after receiving a small displacement, tends to move further away. The criterion of unstable equilibrium is a negative gradient of the polarization curve when the curve passes through the current density zero. The equilibrium is neutral if neither one nor the other reaction follows the potential displacement.

According to this principle, two stable potentials, one in the active and the other in the passive state, are indicated by the potential–time curves. The potential shifts to those stable values and the polarization curve shows a positive gradient at current density zero (Fig. 13). In addition, there is a typical unstable equilibrium near the potential -0.90 v. in the unstable potential range between those stable potentials. In the range < -0.90 v. the potential shifts to the more negative stable potential in the active state (-1.05 to -1.10 v.), and in the range > 0.90 v. the potential shifts to the more positive values. At -0.90 v. the polarization curve passes through the current density zero with a negative gradient and this proves the instability of the equilibrium.

This hypothesis readily explains the manner in which oxidizing reactions stabilize the passive state. Oxidizing components of the liquid remove negative charges from metal electrodes, lower the polarization curve to more negative values of current density, and shift the equilibrium potential to more positive values.

The final stable range of the potential in the potential–time curves being explained, the initial, unstable range is easily elucidated. The initial potential depends, in a significant manner, on the chemical or electrochemical pretreatment. Oxidizing pretreatment causes a shift of the initial potential to more positive values, while reducing pretreatment causes a shift to more negative values. Thus the initial potential can be regarded as a criterion of the pretreatment.

II. *Establishment of the Steady State Polarization Curve*

In order to derive the steady state polarization curve, two curves are actually registered (Fig. 8). One is registered with increasing potential current densities (at or above equilibrium values) and the other with decreasing potential current densities (at or below equilibrium values). Therefore the arithmetical mean between the two curves, both of which are relatively near together, is close to the actual steady state values.

III. *Practical Aspects*

The objects of this first report are to elucidate the theoretical explanation of the polarization curve, to describe the methods developed, and to prove that they suit the problems. Hence some experimental results are here included as examples. In addition, it may be mentioned that the polarization curve of black liquor deviates very significantly from the curves of white liquor. Thus the change of the polarization curve during the cook promises to explain the variation of the liquor corrosiveness. However, practical conclusions, for instance, in terms of anodic or cathodic protection, pretreatment of liquor etc., may be drawn later on in the following part of this report when the bulk of experimental results will be at hand.

REFERENCES

1. BONHOEFFER, K. F. Z. Elektrochem. 55: 151. 1951.
2. CHRISTIANSEN, C. B. and LATHROP, J. B. Pulp & Paper Mag. Can. 55: 113. 1954.
3. EVANS, U. R. Metallic corrosion, passivity and protection. 2nd ed. Edward Arnold & Company, London. 1946.
4. HASSLER, J. W. Tappi, 38: 265. 1955.
5. HOLLER, H. D. J. Electrochem. Soc. 97: 453. 1950.
6. HOPPER, E. W. and MORRISON, J. B. Tappi, 38: 8. 1955.
7. KITTELBERGER, W. W. and ELM, A. C. Corrosion, 5: 101, 155. 1949.
8. KORTÜM, G. and BOCKRIS, J. O'M. Textbook of electrochemistry. Elsevier Publishing Company, New York. 1951.
9. LANGE, E. and NAGEL, K. Z. Elektrochem. 53: 21. 1949.
10. MASING, G. Werkstoffe u. Korrosion, 1: 433. 1950.
11. MEARS, R. B. and EVANS, U. R. Trans. Faraday Soc. 31: 530. 1935.
12. POURBAIX, M. J. Electrochem. Soc. 101: 217*c*. 1954.
13. ROALD, B. Norsk Skogind. 7: 382. 1953; Paper Ind. 36: 412. 1954.
14. ROBERTS, M. H. Brit. J. Appl. Phys. 351. 1954.
15. RUUS, L. and STOCKMAN, L. Svensk Papperstidn. 56: 857. 1953; Paper Ind. 35: 1242. 1954.
16. SCHWERDTFEGER, W. J. and MCDORMAN, O. N. J. Electrochem. Soc. 99: 407. 1952.
17. SHOUMATOFF, N. and TEEPLE, H. O. Tappi, 38: 202. 1955.
18. SPELLER, F. N. Corrosion causes and prevention. McGraw-Hill Book Company, Inc., New York. 1951.
19. UHLIG, H. H. The corrosion handbook. John Wiley & Sons, Inc., New York. 1948.
20. WAGNER, C. and TRAND, W. Z. Elektrochem. 44: 391. 1938.

HYDRAULIC STABILITY IN THE SIMPLE SURGE TANK[1]

By A. W. Marris[2]

ABSTRACT

The hydraulic oscillations occurring in a simple surge tank operating under the condition of constant hydraulic power input to the turbine are investigated experimentally by means of a model. Results are obtained for the several critical conditions, the perpetuation of oscillations of constant amplitude, dead-beat transition of water level, drainage, etc. The criteria for the successive amplitudes of stable oscillations to exhibit given decrements are investigated, and the variation of the frequency of these oscillations with the degree of damping. The over-all experimental results are compared with the relevant conditions predicted by the approximate theory based on the integral of the linear portion of the differential equation describing the motion.

SUMMARY OF PRINCIPAL NOMENCLATURE

H = total elevation of water level in reservoir above tail-water level.
V = velocity of flow in pipe between reservoir and surge tank.
H_0 = elevation of steady water level in surge tank above tail-water level for steady flow V_0 in pipe and penstock.
$h_{f_0} = H - H_0$ = friction head-loss in pipe between reservoir and surge tank for steady pipe flow velocity V_0.
h_f = friction head-loss in pipe for flow velocity V.
c, p = constants in pipe friction law $h_f = cV^p$.
t = time.
y = elevation of water level in surge tank above water level in reservoir.
w = elevation of water level in surge tank above steady flow level $w = y + h_{f_0}$.
r = transient velocity of flow in penstock between surge tank and turbine; $V_0 = r_0$.
L = length of pipe between reservoir and surge tank.
A = cross-sectional area of pipe penstock and inlet to surge tank.
F = cross-sectional area of surge tank.

$X = h_{f_0} \Big/ \sqrt{\frac{L}{g}\frac{A}{F}}\, V_0$
$Y = h_{f_0}/H$
} dimensionless parameters for representing stability characteristics.

k = one half of coefficient of dw/dt in differential equation giving w as a function of time.
m^2 = coefficient of w in equation.
$n^2 = gA/LF$.
θ = phase angle of oscillations of water level in surge tank.
R = theoretical amplitude of oscillations of water level in surge tank.

[1]*Manuscript received January 16, 1956.*
Contribution from the Department of Civil Engineering, University of British Columbia, Vancouver, British Columbia.
[2]*Instructor in the Department.*

R' = magnitude of experimentally observed first downward surge of water level in surge tank.
$Z_{th} = h_{f_0}/RX$.
$Z_{obs} = h_{f_0}/R'X$.

INTRODUCTION

The early theoretical investigations (2, 3) of the water level pendulations to be expected in the simple surge tank operating in conjunction with turbine governors maintaining constant hydraulic power through the turbines lead to an equation of the form

$$\frac{d^2w}{dt^2}+2k\frac{dw}{dt}+m^2w = 0, \qquad [1]$$

where w is the instantaneous elevation of the water level in the surge tank above its level for steady flow and k and m are constants determined from plant dimensions. Equation [1] represents sinusoidal oscillations of exponentially decreasing or increasing amplitudes according as $k > 0$ or $k < 0$, the condition $k > 0$ (or, in terms of plant parameters, $F/A > L/2cgH_0$) being the Thoma condition (3) giving the minimum value of the ratio of surge tank cross-section to pipe cross-section necessary for stability.

An equation of the form [1] is the linear part of a general non-linear equation representing the motion, and it has been stated (1) that for surges resulting from large changes in flow demand, results based on it are not sufficiently accurate and that the complete equation must be attacked by graphical or numerical methods or by means of electronic analogue computers. Aside from the labor involved, such procedures have the disadvantage of yielding only particular results for particular cases. The alternative is to accept the original Thoma condition and impose a 50% or so safety factor upon it, a procedure which may be uneconomical.

It is the purpose of this work to derive as accurate as possible stability criteria on the limited basis of the linear equation, and to see just how well and for what range they predict the behavior of a surge tank model. In the model the condition of constant hydraulic power demand is met by means of a specially designed valve.

In deriving the differential equation to yield the surge tank oscillations the hydraulic "head-loss" h_f in the pipe between reservoir and surge tank is expressed in terms of the mean flow velocity by the equation

$$h_f = cV^p, \qquad [2]$$

where the exponent p is not necessarily 2 and is chosen to give the best agreement with the experimental data for small displacements for which the linear equation may be expected to hold. Whereas for Reynolds numbers above 10^5 such as are obtained in most prototypes the index p will be 2, the same will not be true at the lower Reynolds numbers obtained in the model.

It was also considered that some of the effect of the neglected non-linear terms in the equation could be "counteracted" by a suitable "fictitious" choice of the exponent p.

It was found that the coefficients in the differential equation and therefore the criteria obtained from them are simplified by the introduction of the dimensionless parameters

$$X = h_{f_0} \Big/ \sqrt{\frac{L}{g}\frac{A}{F}}\, V_0, \qquad [3]$$

$$Y = h_{f_0}/H, \qquad [4]$$

and that the stability criteria can be expressed as a single curve in the XY plane.

THEORY

In order to simplify the resulting algebra, the pipe, penstock, and inlet to surge tank will all be taken as having the same cross-sectional area A. When areas are different the same result will hold provided A is taken as area of pipe.

Referring to Fig. 1 representing the water in a general displaced position, the equation of motion of the water in pipe PQ, the equation asserting hydraulic

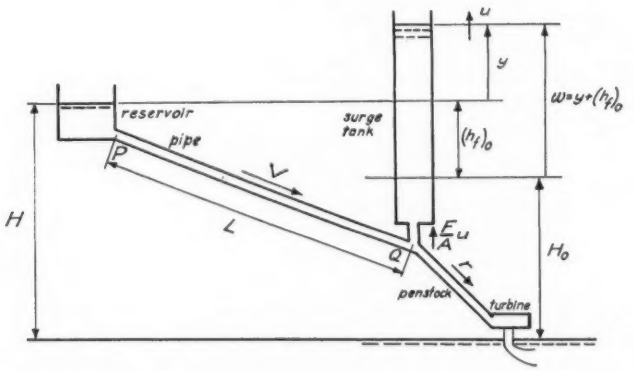

FIG. 1. Schematic drawing of surge tank for definition of variables.

continuity at Q, and the condition for constant hydraulic power input to the turbine are respectively

$$-y-\epsilon c V^p = -w+c(V_0{}^p-\epsilon V^p) = \frac{L}{g}\frac{dV}{dt}, \qquad [5]$$

$\epsilon = +1$ for $V > 0$,

$\epsilon = -1$ for $V < 0$,

$$V = r+\frac{F}{A}u = r+\frac{F}{A}\frac{dw}{dt}, \qquad [6]$$

and

$$(H_0+w)r = H_0\, r_0 = H_0\, V_0, \qquad [7]$$

since $r = r_0 = V_0$ when $w = 0$ at $t = 0$. By [5], [6], and [7], eliminating V and r,

$$[8] \qquad \frac{L}{g}\left(\frac{F}{A}\frac{d^2w}{dt^2}-\frac{V_0H_0}{(H_0+w)^2}\frac{dw}{dt}\right)+w-cV_0^{\,p}+\epsilon\, c\left(\frac{V_0H_0}{H_0+w}+\frac{F}{A}\frac{dw}{dt}\right)^p=0.$$

Equation [8] is the general non-linear differential equation whose solution for the appropriate boundary conditions will describe the oscillations of the water level in the surge tank, p being a non-integral index. The equation as it stands is intractable mathematically; however as long as $w < H_0$ the binomial terms may be expanded to give, as the linear portion of equation [9],

$$[9] \qquad \frac{d^2w}{dt^2}+\frac{gA}{LF}\left(\epsilon\, pc\frac{F}{A}-\frac{L}{gH_0}\right)V_0\frac{dw}{dt}+\frac{gA}{LF}\left(1-\epsilon\frac{pc}{H_0}\,V_0^{\,p}\right)w=0.$$

Equation [9] may be further transformed by introducing the dimensionless parameters

$$[3] \qquad X = h_{f_0}\Big/\sqrt{\frac{L}{g}\frac{A}{F}}\,V_0$$

and

$$[4] \qquad Y = h_{f_0}/H.$$

X will be identified below as the pipe friction loss for steady state velocity V_0 divided by the amplitude of the oscillation occurring when the load causing this final velocity is suddenly accepted under the critical condition, for which the oscillations perpetuate at constant amplitude.

Writing $n^2 = gA/LF$, it follows that

$$\frac{gA}{LF}\left(1-\epsilon\frac{pcV_0^{\,2}}{H_0}\right) = n^2\left(1-\epsilon p\frac{h_f}{H-h_f}\right)$$
$$= n^2\left(\frac{1-(1+\epsilon p)Y}{1-Y}\right)$$

and

$$\frac{gA}{LF}\left(\epsilon pc\frac{F}{A}-\frac{L}{gH_0}\right)V_0 = \frac{A}{F}\frac{V_0}{h_{f_0}}\left(\frac{\epsilon p h_{f_0}^{\,2}}{(LA/gF)V_0^{\,p}}-\frac{h_{f_0}}{H_0}\right)$$
$$= \frac{n}{X}\left(\epsilon p\left(\frac{X}{V_0^{\frac{1}{2}p-1}}\right)^2-\frac{Y}{1-Y}\right),$$

so that equation [9] becomes

$$[10] \qquad \frac{d^2w}{dt^2}+\frac{n}{X}\left(\epsilon p\left(\frac{X}{V_0^{\frac{1}{2}p-1}}\right)^2-\frac{Y}{1-Y}\right)\frac{dw}{dt}+n^2\left(\frac{1-(1+\epsilon p)Y}{1-Y}\right)w=0.$$

Assume now that V is always positive, i.e. that the case of flow from surge tank back into the reservoir is discounted. Then $\epsilon = +1$ and equation [10] becomes

$$[11] \qquad \frac{d^2w}{dt^2}+\frac{n}{X}\left(p\left(\frac{X}{V_0^{\frac{1}{2}p-1}}\right)^2-\frac{Y}{1-Y}\right)\frac{dw}{dt}+n^2\left(\frac{1-(1+p)Y}{1-Y}\right)w=0.$$

For the case $p = 2$, equation [11] simplifies to

$$[12] \qquad \frac{d^2w}{dt^2}+\frac{n}{X}\left(2X^2-\frac{Y}{1-Y}\right)\frac{dw}{dt}+n^2\left(1-\frac{2Y}{1-Y}\right)w = 0,$$

an equation whose coefficients are independent of V_0 and whose critical lines can be represented exactly in the (XY) plane.

For this to be true of equation [11] also, it is necessary to make the approximation of taking $V_0^{\frac{1}{2}p-1}$ as unity in the first term of the coefficient of dw/dt. Equation [11] then becomes

$$[13] \qquad \frac{d^2w}{dt^2}+\frac{n}{X}\left(pX^2-\frac{Y}{1-Y}\right)\frac{dw}{dt}+n^2\left(\frac{1-(1+p)Y}{1-Y}\right)w = 0.$$

Equation [13] represents damped or undamped harmonic oscillations according as $pX^2-Y/(1-Y) >$ or < 0, i.e. according as

$$[14] \qquad X > \text{or} < \sqrt{\frac{Y}{p(1-Y)}}.$$

For $p = 2$, equation [14] expresses the Thoma condition that the oscillations will be damped or undamped according as

$$[15] \qquad F/A > \text{or} < L/2cgH_0.$$

For $p \neq 2$ equation [9] with $\epsilon = +1$ gives the unapproximated modified Thoma condition as

$$[16] \qquad F/A > \text{or} < L/pcgH_0$$

for damped or undamped oscillations. A comparison of equations [15] and [16] shows that if p is in fact less than 2, then an F/A calculated on the basis of the normal Thoma condition will, for the same value of c, result in unstable oscillations. In other words the classical Thoma condition may well yield increasing oscillations instead of oscillations of constant amplitude for plants and models in which the pipe from the reservoir is such that the Reynolds number is low (less than 10^5).

Writing now equation [13] as

$$[17] \qquad \frac{d^2w}{dt^2}+2k\frac{dw}{dt}+m^2w = 0,$$

where

$$[18] \qquad 2k = \frac{n}{X}\left(px^2-\frac{Y}{1-Y}\right)$$

and

$$[19] \qquad m^2 = n^2\left(\frac{1-(1+p)Y}{1-Y}\right),$$

one obtains for the position function of the water level in the surge tank an expression

$$[20] \qquad w = Re^{-kt}\cos(\sqrt{m^2-k^2}\,t-\theta) \text{ for } m > k,$$

and it is seen that the ratio of elevations at times t and $t+s\tau$, where

$$\tau = 2\pi/\sqrt{m^2-k^2},$$

is given by

$$\frac{w_t}{w_{t+s\tau}} = e^{ks\tau} = d^s, \tag{21}$$

where d is the logarithmic decrement of the oscillation, the ratio of corresponding elevations in successive waves.

It follows that

$$k = \frac{1}{\tau}\log_e d = \frac{\sqrt{m^2-k^2}}{2\pi}\log_e d = \frac{n}{2\pi}\log_e d \tag{22}$$

for small damping.

From equations [18] and [22] one obtains

$$pX^2 - \frac{Y}{1-Y} = \frac{X}{\pi}\log_e d. \tag{23}$$

By varying d in equation [23] one obtains a family of characteristics between the parameters X and Y upon each of which the oscillations will have a particular damping factor, the critical characteristic for oscillations of constant amplitude ($d = 1$) being given by

$$pX^2 - \frac{Y}{1-Y} = 0. \tag{24}$$

It must be emphasized that equation [23] is an approximation and that for large damping factors a more accurate form of the equation would be

$$pX^2 - \frac{Y}{1-Y} = \frac{X}{\pi}(1-\rho)\log_e d, \tag{25}$$

where $\rho(<1)$ is a positive function of d, p, and Y. Thus for abscissa X and ordinate Y the characteristics given by equation [23] are too far to the right for large values of d.

Referring to equation [20] it is seen that when $k^2 > m^2$ the expression for w may be written in the form

$$\begin{aligned} w &= e^{-kt}(A\exp\sqrt{k^2-m^2}\,t + B\exp(-\sqrt{k^2-m^2}\,t)) \\ &= A\exp[-(k-\sqrt{k^2-m^2})t] + B\exp[-(k+\sqrt{k^2-m^2})t], \end{aligned} \tag{26}$$

where $A+B = R\cos\theta$, so that the transition from $w = R\cos\theta$ at $t = 0$ to $w = 0$ at $t = \infty$ is non-oscillatory or dead-beat.

In terms of the parameters X and Y the condition for dead-beat transition is, by equations [18], [19],

$$\frac{1}{X^2}\left(pX^2 - \frac{Y}{1-Y}\right)^2 \geq 4\left(1-\frac{pY}{1-Y}\right),$$

or

$$p^2U^2 - 2\left(2-p\frac{Y}{1-Y}\right)U + \left(\frac{Y}{1-Y}\right)^2 \geq 0, \tag{27}$$

where $U = X^2$.

The condition for inequality [27] to hold is that U does not lie between U_1 and U_2 where U_1 and U_2 are the roots of the equation

$$p^2U^2-2\left(2-p\frac{Y}{1-Y}\right)U+\left(\frac{Y}{1-Y}\right)^2=0. \tag{28}$$

The greater root, U_1 say, of equation [28] is given by

$$U_1=\left[\left(2-p\frac{Y}{1-Y}\right)+\sqrt{\left(2-p\frac{Y}{1-Y}\right)^2-p^2\left(\frac{Y}{1-Y}\right)^2}\right]\Big/p^2$$

$$=\frac{4}{p^2}\left(1-\frac{P}{2}\frac{Y}{1-Y}\right)+O\left(\frac{Y}{1-Y}\right)^2.$$

It follows that the condition for a dead-beat transition of the water level is that

$$X\geqslant\frac{2}{p}\left(1-\frac{P}{4}\frac{Y}{1-Y}\right). \tag{29}$$

Again, from equation [26] it is seen that when

$$m^2=n^2\left(1-\frac{pY}{1-Y}\right)\leqslant 0 \tag{30}$$

the solution of equation [17] contains a term of the form $e^{\lambda t}$ where $\lambda > 0$, so that w must increase indefinitely with time. This is the sufficient condition for the surge tank to drain. The original equation will now represent a motion caused by a displacing force proportional to the displacement, instead of that caused by a restoring force proportional to the displacement.

From equation [30] the sufficient condition for drainage of the surge tank is

$$Y\geqslant\frac{1}{1+p} \tag{31}$$

for all values of X.

The question arises as to whether this condition is also necessary, or whether, for certain values of X, the surge tank will drain before Y reaches the value $1/(1+p)$. This question must be held over until the form of the integral [20] has been considered under appropriate boundary conditions.

Consider the case of suddenly opening the turbine gates. Assuming that the full flow to the turbine is accepted instantaneously from the surge tank, one has, at $t = 0$, the boundary conditions

$$w=h_{f_0} \tag{32}$$

and

$$\frac{dw}{dt}=-\frac{A}{F}V_0. \tag{33}$$

It follows that

$$h_{f_0}=R\cos(-\theta)=R\cos\theta \tag{34}$$

and

$$-\frac{A}{F}V_0=-kR\cos\theta+\sqrt{m^2-k^2}\,R\sin\theta. \tag{35}$$

Thus

$$\frac{R}{h_{f_0}} \cos\theta = 1, \tag{36}$$

$$\frac{R}{h_{f_0}} \sin\theta = \left(-\frac{A}{F}\frac{V_0}{h_{f_0}}+k\right) \Big/ \sqrt{m^2-k^2} = \left(-\frac{A}{F}\frac{V_0}{mh_{f_0}}+\frac{k}{m}\right) \Big/ \sqrt{1-\frac{k^2}{m^2}}. \tag{37}$$

If one approximates now by setting $m = n$ so that

$$\frac{A}{F}\frac{V_0}{mh_{f_0}} = \frac{1}{X},$$

one obtains

$$\frac{R}{h_{f_0}} \sin\theta = \left(-\frac{1}{X}+\frac{\log_e d}{2\pi}\right) \Big/ \sqrt{1-\left(\frac{\log_e d}{2\pi}\right)^2},$$

whence, squaring and adding and neglecting $O(\log_e d/2\pi)^3$, say, one has

$$\frac{h_{f_0}}{RX} = \sqrt{\frac{L}{g}\frac{A}{F}}\, V_0 \Big/ R = Z_{th} = (1-X^2)-(1-X^2)\left(\frac{\log_e d}{2\pi}\right)^2+2X\left(\frac{\log_e d}{2\pi}\right)\left(1-\left(\frac{\log_e d}{2\pi}\right)^2\right). \tag{38}$$

It follows from equation [38] that R increases with increase in pipe resistance, i.e. as the oscillations become more damped. (This will be apparent in the experimentally determined oscillation traces shown in Fig. 4—see below: "Experimental Procedure".)

For small X and d only a small fraction greater than 1 one has

$$Z_{th} = h_{f_0}/RX = 1, \tag{39}$$

so that the parameter X is the ratio of the friction head loss to the amplitude of the free oscillations.

It follows by equation [34] that the phase angle θ is given by $\cos\theta = X$, or

$$\theta = \arctan\frac{\sqrt{1-X^2}}{X}. \tag{40}$$

Returning now to consider the condition for drainage of the surge tank. While it would seem to the author that no better necessary condition than the sufficient one given by the inequality [31] is obviously available from the coefficients of the differential equation [17], it was an undoubted fact that in the oscillatory regions the surge tank drained for values of Y far less than $1/(1+p)$. The following "deduction" of a more stringent sufficient condition is therefore submitted.

The condition [31] has been shown to hold for all X. Therefore it holds for

$$X \geqslant \frac{2}{p}\left(1-\frac{P}{4}\frac{Y}{1-Y}\right). \qquad [29]$$

That is, it holds for dead-beat displacements of the water level in the surge tank. In such a dead-beat oscillation the kinetic energy of the liquid in the surge tank is very small as it approaches its final position. One may assert that if the final position is such that $Y \geqslant 1/(1+p)$, then independently of the size of the surge tank, the distribution of relative water levels in reservoir and surge tank is such that the system is statically unstable and that any further slight downward displacement of the water level in the surge tank will result in the displacement being continued, causing drainage.

If this is the case, then it cannot make any difference whether this "point of no return" is reached as the near-end-point of a dead-beat displacement or as a point passed in the oscillatory motion. In the oscillatory motion the point will be passed with a greater downward velocity and therefore the drainage would be all the more assured.

For the oscillatory motion, damped or undamped, the amplitude of the first downward surge has been given by equation [39]:

$$R = h_{f_0}/X.$$

It follows that the "point of no return" will have been passed if

$$R/H \geqslant 1/(1+p),$$

i.e. if

$$\frac{h_{f_0}}{HX} = \frac{Y}{X} \geqslant \frac{1}{1+p},$$

$$Y \geqslant X/(1+p). \qquad [41]$$

The inequality [41] thus appears to give a better sufficient condition for drainage at the lower values of X. However, because of the above-mentioned downward velocity of the water level aiding the propensity of the surge tank to drain, drainage may occur at still lower values of Y.

The condition [41] holds for all $X < (2/p)[1-\frac{1}{4}pY/(1-Y)]$ and so in particular for the region in which the oscillations are of increasing amplitude. It must be taken as implying drainage on the first downward surge.

It is emphasized that conditions [29] and [31] for dead-beat transitions and drainage involved consideration of the coefficient of w in the linear part of the equation of motion, that is, an equation in which terms involving w^2, w^3, etc. have been neglected. These terms will become increasingly important for the large values of X and Y. Thus discrepancies between theory and experiment must be expected in the regions described by conditions [29], [31], and in the upper regions of condition [41].

DESCRIPTION OF THE SURGE TANK MODEL

The general layout of the model is shown schematically in Fig. 2. Total heads H up to 3 ft. were obtained by employing the laboratory flume as the reservoir.

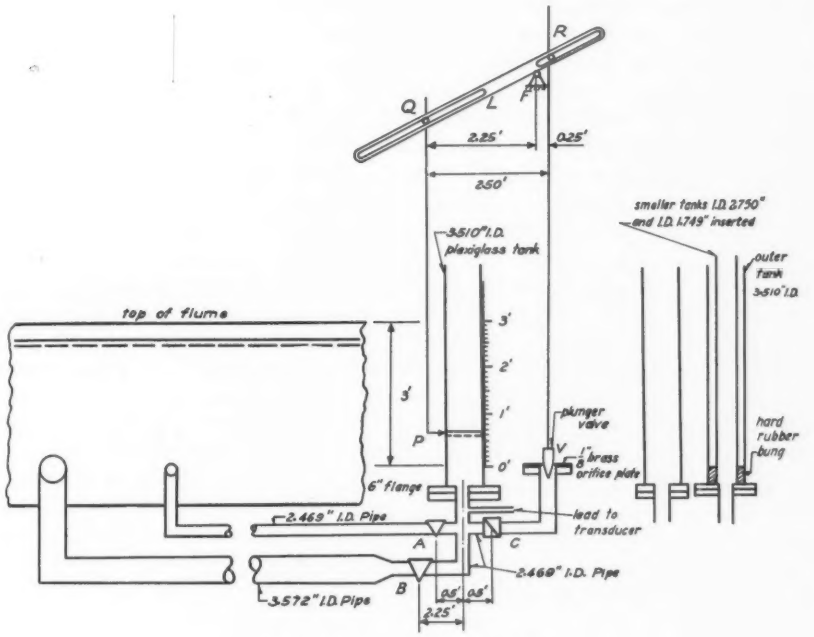

FIG. 2. The surge tank model.

Two galvanized iron pipes led from the reservoir to the plexiglass surge tank, the smaller, of measured length 22.0 ft. and of average internal diameter 2.469 in., and the larger, of length 38.05 ft. and average internal diameter 3.572 in. The pipes could be closed off in turn by closing one or other of the $2\frac{1}{2}$ in. (nominal) globe valves A and B. The valves A and B were placed as near as possible to the inlet to the surge tank to avoid the presence of dead water regions which would possibly affect the oscillations required to be measured. The friction head-loss in the pipe being used was varied by adjusting the globe valves. It is stated that the value 38.05 ft. of the larger pipe was an effective length made up of 35.45 ft. of 3.572 in. diameter pipe and of 5.1 ft. of $2\frac{1}{2}$ in. diameter connections. Since the friction loss in the pipe is measured directly, the length of the pipe occurs in the formulae only in relation to the mass of water in the pipe, i.e. to its volume. The 5.1 ft. of $2\frac{1}{2}$ in. diameter connections could thus be scaled down to an equivalent length of 2.6 ft. of the 3.572 in. pipe.

From the surge tank inlet the penstock led to the quick-action gate valve C (C also as near the inlet to the surge tank as possible) and thence to outlet at the special valve V simulating the turbine, the outlet being at the same horizontal level as the base of the scale on the surge tank so that the hydraulic "head on the turbine" could be read off directly. The gate valve C was equipped with a special lever arm to facilitate rapid closure.

The valve V consisted of a snub-nosed bullet-shaped plunger set centrally in a 2 in. diameter sharp-edged brass orifice plate flanged on to the end of the pipe. The plunger was attached to the smoothly supported vertical member VR, the end R of which was affixed by set screws to a ball bearing roller which could traverse the right-hand slot in the lever arm L. Traversing similarly the longer left-hand slot in L was a roller to which was attached the vertical member PL; P is shown as a pointer but was actually an annular plate surrounding the surge tank. The water level was followed manually by means of this slider P. It is seen that when the slider is moved up to follow an upward surge of the water the valve V is depressed into the orifice thereby throttling the output from the penstock. For all positions, PQ and RV remain vertical and parallel at the distance 2.5 ft. apart. The fulcrum F of the arm QR was so positioned that a 9-unit upward movement of P caused a 1-unit downward movement of the plunger V and vice versa. It is thus seen that for a suitably shaped plunger, a penstock outflow inversely proportional to the head on the valve could be obtained, i.e. the condition of constant hydraulic horsepower input to the turbine could be realized. The valve was first shaped to a mathematically derived curve and then, to allow for variation in the orifice coefficient arising from the variation of the annular opening as the plunger position was varied, reshaped by trial and error. The calibration values given in Table I and shown graphically in Fig. 3 were finally obtained.

TABLE I

SURGE TANK – VALVE CALIBRATION

H_0, ft.	Pounds collected	Time	w, lb./sec.	Q, c.f.s.	QH_0, ft.^{4}/sec.
0.680	300	143	2.10	0.0336	0.0229
0.810	200	114	1.75(5)	0.0281	0.0228
0.900	200	129	1.55	0.0248	0.0224
1.02	300	210	1.43	0.0229	0.0234
1.05	300	216	1.39	0.0223	0.0234
1.15	300	235	1.28	0.0204	0.0235
1.29	200	181	1.10(5)	0.0177	0.0229
1.38(5)	200	193	1.04	0.0166	0.0230
1.48	200	211	0.0948	0.0152	0.0225
1.595	300	333	0.0901	0.0144(5)	0.0230
1.70	200	240	0.0834	0.0134	0.0227
1.785	200	255	0.0785	0.0126	0.0225
1.90	200	270	0.0741	0.0119	0.0226
2.02	200	284	0.0705	0.0113	0.0228
2.19	100	156	0.0641	0.0103	0.0225
2.33	200	323	0.0619	0.0993	0.0231
2.49	200	338	0.0592	0.0949	0.0236
2.60	200	359	0.0557(5)	0.0893	0.0232

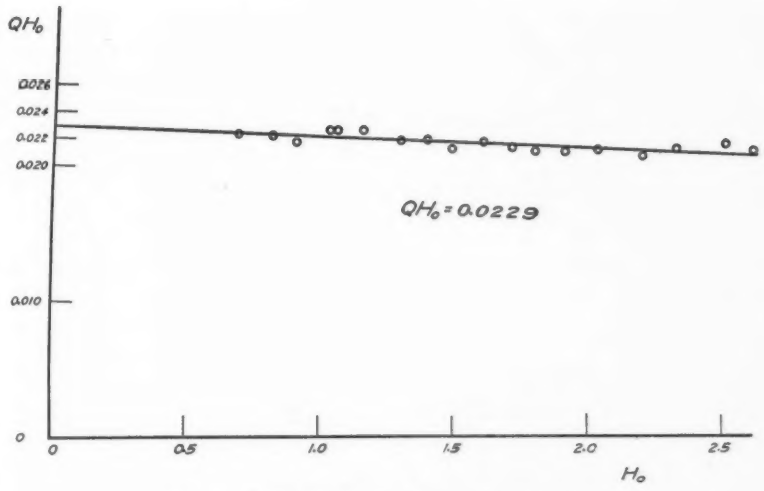

FIG. 3. Calibration curve of power control valve.

Three plexiglass surge tanks were available, the largest of internal diameter 3.510 in. being flanged directly to the inlet pipe as shown in Fig. 2, while the two smaller tanks of internal diameters 2.750 in. and 1.749 in. had hard rubber bungs fitted about their ends, which, when soaped a little, allowed the required tank to be slid down inside the original tank as indicated.

A $\frac{3}{8}$ in. diameter inlet I was provided immediately below the surge tank and a lead taken from it to a Northam variable inductance pressure transducer of range ± 0.5 p.s.i. The output from this was then taken to a Brush Company Amplifier and Oscillograph, so that traces of the wave-forms of the hydraulic oscillations were obtained for the determination of the logarithmic decrement.

EXPERIMENTAL PROCEDURE

The surge tank to be investigated having been set in place, the gate valve C (see Fig. 2) was closed and also one of the globe valves A or B to cut out the pipe not being used. With valve A open and valves B and C closed the water in the pipe was at rest and the water level in the surge tank gave the total head H. The valve C was then opened so that the water level in the surge tank fell to level H_0. It could be rapidly brought to rest by moving the slider P against the oscillations. The globe valve A was adjusted until a value of $h_{f_0} = H - H_0$ giving oscillations of just increasing amplitudes when followed by the slider P was obtained. The valve C was closed, the liquid in the surge tank was damped to rest, and the recorder switched on. The valve C was opened once again and the ensuing oscillations were again followed by the slider. The trace of the wave was obtained and the values of H, h_{f_0}, and the amplitude R' of the first downward surge were noted, the latter being read directly from the scale on the side of the surge tank. The process was repeated with

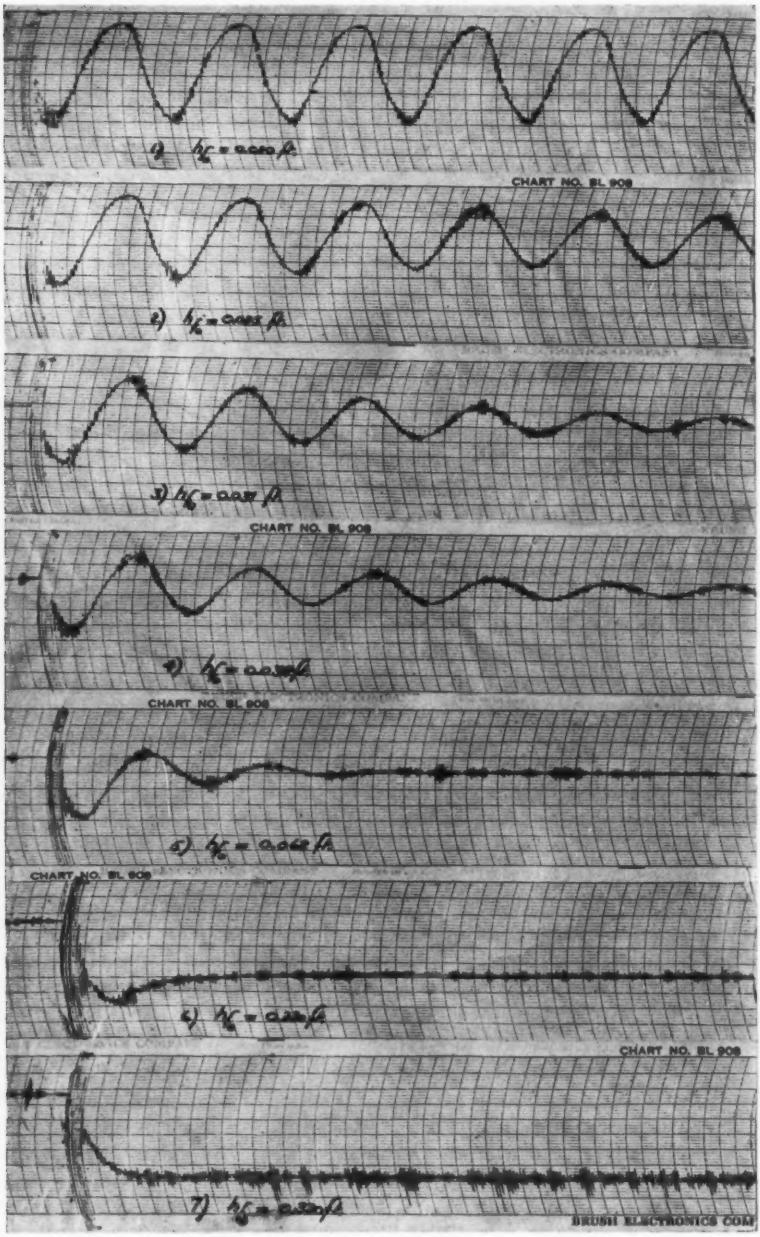

FIG. 4. Oscillation traces for 3.510 in. diameter surge tank operating with 3.572 in. diameter pipe at total head $H = 1.73$ ft.

h_{f_0} increased by increments of 0.01 ft. In this way the traces of the whole series of waves for the given total head H, from the case of built-up oscillation to dead-beat transition and drain, were obtained. See Fig. 4 for a specimen series of such traces.

The values of the decrement d for each h_{f_0} were obtained from the traces. By plotting d against h_{f_0} it was possible to obtain by extrapolation over a short distance the values of h_{f_0} yielding chosen decrements $d = 1.00$, $d = 1.25$, $d = 1.50$, $d = 1.75$, $d = 2.00$, and $d = 2.50$.

The values of h_{f_0} causing dead-beat transitions were obtained directly by inspection of the extremity of the downward surge of the water level as h_{f_0} was increased in increments of 0.005 ft. The values of h_{f_0} causing drainage were determined similarly.

EXPERIMENTAL DATA

From the control valve calibration data shown graphically in Fig. 3 the value

[42] $$QH_0 = 0.0229 \text{ ft.}^4/\text{sec.}$$

was accepted.

It followed that for each pipe cross-section the steady state velocity V_0 could be expressed as

$$V_0 = k_1/H_0,$$

and that for each combination of pipe and surge tank the dimensionless quantity

$$X = h_{f_0} \Big/ \sqrt{\frac{L}{g}\frac{A}{F}}\, V_0$$

could be expressed as

[43] $$X = k_2 h_{f_0} H_0 = k_2(H - H_0)H_0.$$

The values of k_1 and k_2 for the various pipe and surge tank combinations are as set out in Table I.

The values of X $(= k_2(H - H_0)H_0)$ and Y $(= (H - H_0)/H)$ corresponding to the critical case of oscillations of constant amplitude $(d = 1)$ are set out in Table II, and in Tables III, IV, V, VI, and VII the equivalent data for oscillations with decrements $d = 1.25$, 1.50, 1.75, 2.00, and 2.50 respectively. These results are shown graphically in Figs. 5, 6, 7, 8, 9, and 10 and also, for comparison, the corresponding theoretical curves based on the equation

[23] $$pX^2 - \frac{Y}{1-Y} = \frac{\log_e d}{\pi} X.$$

The value of the exponent p was chosen from a Moody chart using an appropriate Reynolds number for the pipe flow.

Thus, from equation [42],

[44] $$V_0 = 0.659/H_0 \text{ ft./sec.}$$

TABLE II

$d = 1$

Pipe length L, ft.	Pipe cross-section A, sq. ft.	Surge tank cross-section F, sq. ft.	Total head H, ft.	$h_{f_0} = H - H_0$, ft.	Y	X
22.00	0.03325	0.06720	1.315	0.055	0.0418	0.1735
			1.580	0.030	0.0190	0.116
			1.463	0.040	0.0274	0.142
			1.555	0.042	0.0270	0.159
			1.659	0.027	0.0163	0.110
		0.04125	1.900	0.029	0.0153	0.106
			1.661	0.040	0.0241	0.127
			1.834	0.032	0.0174	0.113
			1.772	0.018	0.0102	0.062
			1.900	0.033	0.0174	0.121
			1.717	0.037	0.0216	0.122
			2.165	0.022	0.0102	0.0925
			1.505	0.055	0.0366	0.156
		0.01668	2.08	0.043	0.0207	0.109
			1.685	0.094	0.0558	0.186
			1.650	0.129	0.0782	0.228
			1.760	0.095	0.054	0.197
			2.080	0.052	0.025	0.131
			1.970	0.065	0.033	0.154
			1.885	0.073	0.0387	0.165
			2.075	0.046	0.0222	0.116
			1.760	0.110	0.0625	0.226
			1.885	0.075	0.0396	0.169
			1.840	0.100	0.0543	0.216
			1.735	0.110	0.0634	0.222(5)
			1.690	0.120	0.0710	0.235
			2.02	0.050	0.0248	0.123
			1.975	0.060	0.0304	0.143
			1.942	0.062	0.0319	0.146(5)
			1.910	0.070	0.0367	0.160
			1.845	0.075	0.0406	0.165
			1.810	0.082(5)	0.0456	0.177
			1.765	0.1025	0.0581	0.213
			1.785	0.095	0.0533	0.200
			1.795	0.072(5)	0.0404	0.155
			1.60	0.155	0.097	0.28
			1.795	0.085	0.0473	0.182
			1.645	0.135	0.0821	0.255
			1.675	0.115	0.0687	0.225
			1.640	0.125	0.0763	0.236
			1.625	0.140	0.0861	0.260
38.05	0.06958	0.06720	1.730	0.020	0.0116	0.094
			1.597	0.027	0.0169	0.117
			1.803	0.015	0.0083	0.0735
			1.667	0.026	0.0156	0.117
			1.525	0.031	0.0203	0.128
		0.04125	1.713	0.033	0.0192	0.119
			1.517	0.057	0.0376	0.179
			1.650	0.040	0.0242	0.139
			1.392	0.063	0.0453	0.180
			1.328	0.081	0.0610	0.217
			1.345	0.073	0.0542	0.200
			1.290	0.103	0.0798	0.264
		0.01668	1.783	0.086	0.0482	0.200
			1.942	0.062	0.0319	0.160
			1.808	0.085	0.0470	0.201
			1.740	0.098	0.0563	0.221
			1.704	0.101	0.0593	0.222
			1.676	0.113	0.0675	0.242
			1.642	0.126	0.0768	0.262
			1.620	0.130	0.0802	0.265
			1.602	0.134	0.0837	0.270
			1.575	0.133	0.0917	0.263
			1.542	0.147	0.0954	0.281
			1.560	0.140	0.0898	0.268

TABLE III

$d = 1.25$

Pipe length L, ft.	Pipe cross-section A, sq. ft.	Surge tank cross-section F, sq. ft.	Total head H, ft.	$h_{f_0} = H - H_0$, ft.	Y	X
22.00	0.03325	0.06720	1.555	0.045	0.0289	0.169
			1.659	0.038	0.0229	0.154
			1.661	0.048	0.0289	0.196
			1.463	0.044	0.0301	0.156
		0.04125	1.900	0.036	0.0190	0.132
			1.661	0.054	0.0325	0.170
			1.834	0.037	0.0202	0.130
			1.772	0.030	0.0169	0.1025
			1.900	0.041	0.0216	0.149
			1.717	0.049	0.0286	0.160
		0.01668	2.08	0.073	0.0351	0.183
			1.685	0.146	0.0867	0.280
			1.650	0.165	0.100	0.305
			1.760	0.115	0.0653	0.235
			2.080	0.078	0.0375	0.194
			1.970	0.082	0.0417	0.194
			1.885	0.090	0.0477	0.201
			1.685	0.144	0.0854	0.271
			2.075	0.068	0.0327	0.170
			1.760	0.123	0.0699	0.251
			1.885	0.088	0.0457	0.197
			1.710	0.124	0.0724	0.246
			1.760	0.120	0.068	0.245
			1.865	0.095	0.0510	0.210
38.05	0.06958	0.06720	1.730	0.028	0.0162	0.131
			1.597	0.034	0.0213	0.146
			1.803	0.021	0.0116	0.103
			1.667	0.027	0.0162	0.122
		0.04125	1.710	0.046	0.0269	0.165
			1.517	0.063	0.0416	0.197

TABLE IV

$d = 1.50$

Pipe length L, ft.	Pipe cross-section A, sq. ft.	Surge tank cross-section F, sq. ft.	Total head H, ft.	$h_{f_0} = H - H_0$, ft.	Y	X
22.00	0.03325	0.06720	1.661	0.052	0.0313	0.209
			1.463	0.050	0.0342	0.177
			1.555	0.049	0.0315	0.185
			1.659	0.044	0.0265	0.178
		0.04125	1.900	0.042	0.0221	0.153
			1.661	0.067	0.0403	0.209
			1.834	0.045	0.0245	0.158
			1.772	0.043	0.0243	0.146
			1.900	0.048	0.0253	0.174
			1.717	0.062	0.0361	0.201
			1.717	0.063	0.0367	0.204
		0.01668	2.080	0.098	0.0472	0.243
			1.685	0.184	0.1093	0.344
			1.650	0.184	0.1115	0.335
			1.760	0.132	0.0750	0.267
			2.080	0.095	0.0457	0.235
			1.970	0.096	0.0462	0.224
			1.885	0.107	0.0514	0.235
			1.685	0.193	0.1146	0.359
			2.075	0.078	0.0376	0.194
			1.760	0.148	0.0841	0.297
			1.885	0.109	0.0578	0.241
			1.710	0.140	0.082	0.275
			1.760	0.130	0.074	0.265
			1.865	0.109	0.0585	0.240
38.05	0.06958	0.06720	1.730	0.037	0.0214	0.172
			1.597	0.041	0.0257	0.175
			1.803	0.030	0.0166	0.146
			1.667	0.035	0.0210	0.157
		0.04125	1.710	0.059	0.0345	0.214
			1.710	0.056	0.0327	0.199
			1.517	0.074	0.0488	0.230

TABLE V

$d = 1.75$

Pipe length L, ft.	Pipe cross-section A, sq. ft.	Surge tank cross-section F, sq. ft.	Total head H, ft.	$h_{f_0} = H - H_0$, ft.	Y	X
22.00	0.03325	0.06720	1.661	0.057	0.0343	0.229
			1.463	0.057	0.0389	0.200
			1.555	0.055	0.0354	0.206
			1.659	0.049	0.0295	0.197
		0.04125	1.900	0.048	0.0253	0.174
			1.661	0.077	0.0463	0.239
			1.834	0.053	0.0289	0.185
			1.772	0.055	0.0311	0.185
			1.900	0.055	0.0290	0.199
			1.717	0.072	0.0418	0.232
			1.717	0.069	0.0401	0.223
		0.01668	2.08	0.116	0.0557	0.284
			1.650	0.192	0.1164	0.355
			1.760	0.144	0.0818	0.290
			2.080	0.104	0.0500	0.256
			1.970	0.108	0.0548	0.252
			1.685	0.212	0.1258	0.388
			2.075	0.082	0.0395	0.203
			1.760	0.182	0.1034	0.358
			1.885	0.128	0.0678	0.280
38.05	0.06958	0.06720	1.730	0.042	0.0253	0.195
			1.597	0.047	0.0294	0.200
			1.803	0.037	0.0205	0.179
			1.667	0.042	0.0252	0.188
			1.710	0.068	0.0397	0.240
			1.710	0.065	0.0380	0.230
			1.517	0.082	0.0541	0.253

TABLE VI

$d = 2.00$

Pipe length L, ft.	Pipe cross-section A, sq. ft.	Surge tank cross-section F, sq. ft.	Total head H, ft.	$h_{f_0} = H - H_0$, ft.	Y	X
22.00	0.03325	0.06720	1.661	0.0620	0.0373	0.248
			1.463	0.0650	0.0444	0.228
			1.555	0.0620	0.0398	0.231
		0.04125	1.900	0.0530	0.0279	0.192
			1.661	0.0840	0.0505	0.259
			1.834	0.0620	0.0338	0.215
			1.772	0.064	0.0362	0.214
			1.900	0.058	0.0305	0.209
			1.717	0.080	0.0466	0.256
			1.717	0.077	0.0448	0.248
		0.01668	2.080	0.132	0.0635	0.320
			1.650	0.197	0.1193	0.354
			2.080	0.112	0.0539	0.275
			1.970	0.118	0.0567	0.272
			1.685	0.222	0.1318	0.405
			2.075	0.086	0.0414	0.213
			1.885	0.143	0.0758	0.310
			1.710	0.171	0.100	0.330
			1.760	0.143	0.081	0.288
			1.865	0.125	0.067	0.273
			1.91	0.120	0.0628	0.268
38.05	0.06958	0.06720	1.730	0.047	0.0272	0.218
			1.597	0.053	0.0332	0.225
			1.803	0.043	0.0239	0.208
			1.667	0.053	0.0318	0.235
		0.04125	1.710	0.075	0.0438	0.264
			1.710	0.073	0.0427	0.257
			1.517	0.090	0.0593	0.276

TABLE VII

$d = 2.50$

Pipe length L, ft.	Pipe cross-section A, sq. ft.	Surge tank cross-section F, sq. ft.	Total head H, ft.	$h_{f_0} = H - H_0$, ft.	Y	X
22.00	0.03325	0.06720	1.661	0.071	0.0427	0.283
			1.463	0.080	0.0546	0.276
			1.555	0.075	0.0482	0.277
		0.04125	1.661	0.097	0.0584	0.297
			1.834	0.080	0.0436	0.275
			1.772	0.077	0.0436	0.256
			1.900	0.067	0.0352	0.241
			1.717	0.088	0.0513	0.281
		0.01668	2.080	0.156	0.0750	0.373
			2.080	0.122	0.0587	0.298
			1.970	0.133	0.0675	0.304
			1.885	0.170	0.0903	0.363
38.05	0.06958	0.06720	1.730	0.056	0.0324	0.258
			1.597	0.063	0.0394	0.266
			1.801	0.054	0.0300	0.260
			1.667	0.068	0.0408	0.299
		0.04125	1.71	0.087	0.0508	0.303
			1.71	0.085	0.0497	0.297
			1.517	0.106	0.0699	0.382

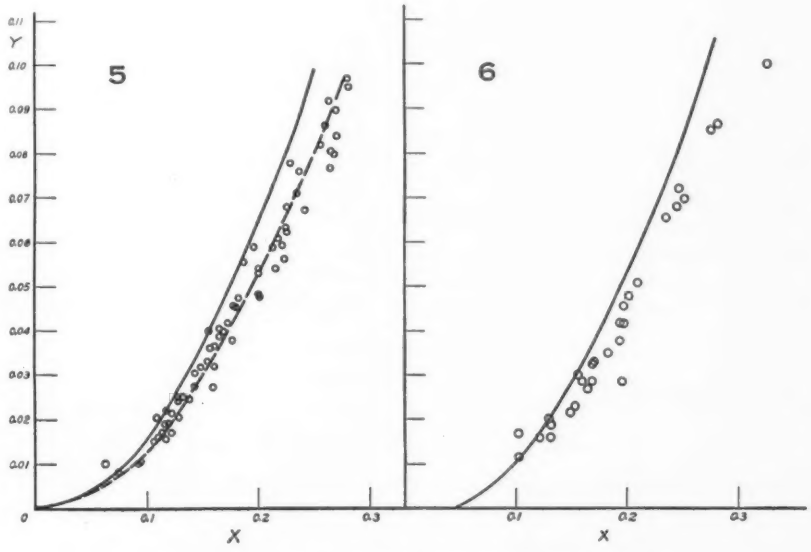

FIG. 5. Characteristic for oscillations of constant amplitude. $pX^2 - \frac{Y}{1-Y} = \frac{\log_e d}{\pi} X$ for $d = 1$ and $p = 1.75$, full curve; for $d = 1$ and $p = 1.40$, dotted curve.

FIG. 6. Characteristic for oscillations of decrement $d = 1.25$. Full curve, $pX^2 - \frac{Y}{1-Y} = \frac{\log_e d}{\pi} X$ for $d = 1.25$ and $p = 1.75$.

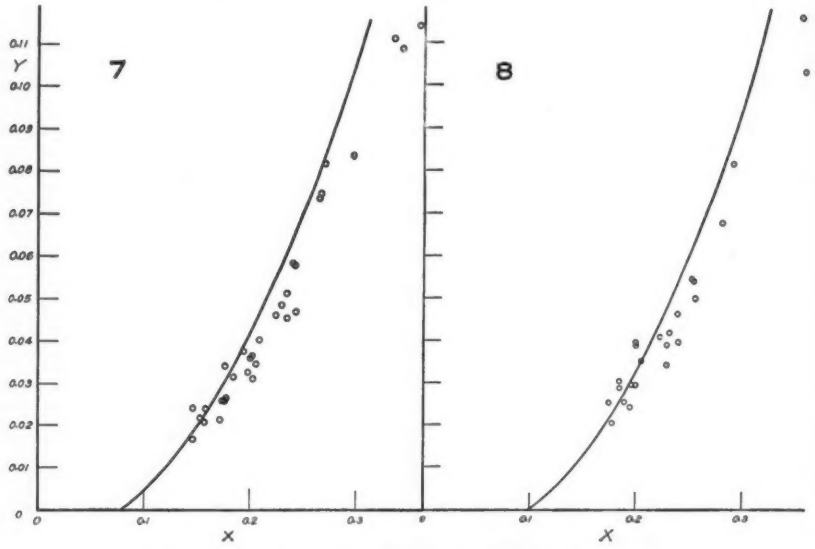

FIG. 7. Characteristic for oscillations of decrement $d = 1.50$.
Full curve, $pX^2 - \frac{Y}{1-Y} = \frac{\log_e d}{\pi} X$ for $d = 1.50$ and $p = 1.75$.
FIG. 8. Characteristic for oscillations of decrement $d = 1.75$.
Full curve, $pX^2 - \frac{Y}{1-Y} = \frac{\log_e d}{\pi} X$ for $d = 1.75$ and $p = 1.75$.

for the smaller pipe, and

[45] $$V_0 = 0.315/H_0 \text{ ft./sec.}$$

for the larger pipe.

Taking the mean water temperature as 60°F. throughout the experiment and the dynamic viscosity of water as 2.39×10^{-5} slug/ft. sec. one obtains

$$N_{Re} = (1.13/H_0) \times 10^4$$

for the smaller pipe, and

$$N_{Re} = (7.86/H_0) \times 10^3$$

for the larger pipe.

For the values of H_0 employed the values of N_{Re} were considered generally large enough to put the pipe flow above the critical region. (It was possible that for the larger pipe at the highest heads the critical unstable region may have been invaded, although there was no evidence of this.) The readings were however taken on the steeper portion of the Moody chart and the average value of the exponent p was assessed to be 1.75.

The full curves of Figs. 5 to 10 are constructed from equation [23] with $p = 1.75$.

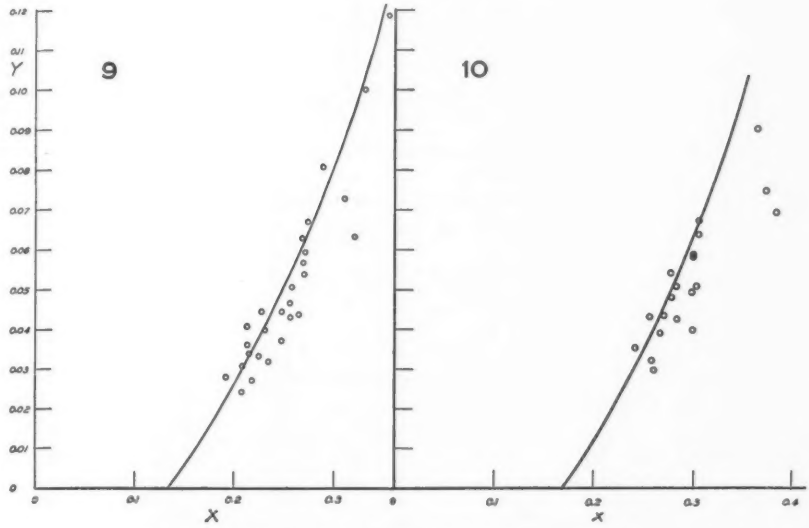

FIG. 9. Characteristic for oscillations of decrement $d = 2.00$.
Full curve, $pX^2 - \frac{Y}{1-Y} = \frac{\log_e d}{\pi} X$ for $d = 2.00$ and $p = 1.75$.
FIG. 10. Characteristic for oscillations of decrement $d = 2.50$.
Full curve, $pX^2 - \frac{Y}{1-Y} = \frac{\log_e d}{\pi} X$ for $d = 2.50$ and $p = 1.75$.

The data for surge tank drainage are set out in Tables VIII, IX, and X corresponding to the three cases $d < 1$, i.e. drainage on the first downward surge of oscillations which would otherwise have demonstrated successively increasing amplitudes; $d > 1$, drainage on first downward surge of oscillations in the region where successive oscillations are of decreasing amplitude; and $d = \infty$, i.e. for drainage from the dead-beat condition.

TABLE VIII

DRAINAGE FOR $d < 1$

Pipe length L, ft.	Pipe cross-section A, sq. ft.	Surge tank cross-section F, sq. ft.	Total head H, ft.	$h_{f_0} = H - H_0$, ft.	Y	X
22.00	0.03325	0.01668	1.520	0.140	0.092	0.240
			1.600	0.155	0.097	0.280
			1.580	0.160	0.100	0.285
			1.595	0.155	0.097	0.278
			1.610	0.135	0.084	0.248
			1.605	0.150	0.0936	0.273
			1.550	0.100	0.0646	0.182
			1.570	0.120	0.0765	0.216
			1.585	0.125	0.0790	0.228
			1.560	0.110	0.0705	0.200
			1.525	0.085	0.0555	0.153
38.05	0.06958	0.01668	1.520	0.130	0.0856	0.248
			1.480	0.110	0.0745	0.206
			1.450	0.100	0.0690	0.185

TABLE IX

DRAINAGE FOR $d > 1$

Pipe length L, ft.	Pipe cross-section A, sq. ft.	Surge tank cross-section F, sq. ft.	Total head H, ft.	$h_{f_0} = H - H_0$, ft.	Y	X
22.00	0.03325	0.04125	1.36	0.220	0.162	0.490
			1.505	0.405	0.270	0.870
			1.380	0.260	0.188	0.570
			1.280	0.190	0.148	0.405
			1.445	0.310	0.214(5)	0.690
			1.490	0.370	0.247	0.810
			1.610	0.480	0.298	1.065
		0.01668	1.840	0.345	0.187	0.640
			1.735	0.255	0.147	0.470
			1.690	0.260	0.154	0.460
			2.020	0.670	0.330	1.130
			1.975	0.655	0.330	1.070
			1.942	0.742	0.382	1.100
			1.845	0.355	0.194	0.660
			1.675	0.270	0.160	0.470
			1.693	0.262(5)	0.155	0.468
			1.620	0.200	0.123	0.355
			1.645	0.205	0.124(5)	0.370
			1.595	0.155	0.097(5)	0.280
			1.680	0.245	0.145	0.437(5)
			1.600	0.160	0.100	0.290
			1.610	0.170	0.106	0.305
			1.615	0.182(5)	0.113	0.330
			1.665	0.235	0.141	0.422(5)
			1.655	0.215	0.130	0.385
			1.690	0.270	0.159	0.475
			1.722(5)	0.292(5)	0.170	0.520
			1.760	0.290	0.165	0.533
			1.782(5)	0.352(5)	0.197	0.630
			1.805	0.390	0.215	0.690
			1.835	0.420	0.228	0.740
			1.875	0.475	0.252	0.830
			1.900	0.500	0.263	0.865
			1.916	0.516	0.268	0.900
			1.950	0.570	0.290	0.980
			1.925	0.535	0.278	0.935
			1.825	0.350	0.191	0.645
			1.780	0.320	0.180	0.580
			1.800	0.370	0.206	0.660
			1.860	0.420	0.215	0.755
			1.910	0.470	0.245	0.845
			1.870	0.440	0.235	0.785
			1.950	0.510	0.262	0.908
			1.980	0.560	0.281	0.985
38.05	0.06958	0.04125	1.517	0.487	0.321	1.234
			1.328	0.230	0.174	0.545
			1.252	0.172	0.137(5)	0.400
			1.290	0.200	0.155	0.470
		0.01668	1.808	0.389	0.214(5)	0.757(5)
			1.783	0.353	0.198	0.692(5)
			1.740	0.345	0.198	0.660
			1.702	0.312	0.183(5)	0.595
			1.676	0.256	0.153	0.497(5)
			1.642	0.212	0.129	0.416(5)
			1.620	0.185	0.114	0.363(5)
			1.602	0.177	0.110(5)	0.346
			1.575	0.170	0.108	0.328
			1.542	0.147	0.095	0.281(5)
			1.560	0.160	0.102(5)	0.307

The critical data to cause a dead-beat transition are given in Table XI. The values from Tables VIII to XI inclusive are plotted in Fig. 11. The full lines in Fig. 11 are the theoretical Thoma line, given by

$$pX^2 - \frac{Y}{1-Y} = 0 \text{ with } p = 1.75,$$

the theoretical dead-beat line

$$X = \frac{2}{p}\left(1 - \frac{p}{4}\frac{Y}{1-Y}\right) \text{ with } p = 1.75,$$

the derived drain-line for oscillatory motion

$$Y = X/(1+p) \text{ for } p = 1.75,$$

and the drain-line from the dead-beat transition state

$$Y = 1/(1+p) \text{ for } p = 1.75.$$

It was required to check how well the frequency $m/2\pi$ of the observed oscillations obeyed the theoretically predicted formula

[19] $$m^2 = n^2\left(1-\frac{pY}{1-Y}\right).$$

TABLE X

DRAINAGE FOR $d = \infty$

Pipe length L, ft.	Pipe cross-section A, sq. ft.	Surge tank cross-section F, sq. ft.	Total head H, ft.	$h_{f_0} = H - H_0$, ft.	Y	X
22.00	0.03325	0.06720	2.310	0.710	0.307	2.837*
			1.890	0.560	0.296	1.860
			1.580	0.410	0.260	1.200
		0.04125	1.772	0.502	0.284	1.245
			2.705	0.865	0.320	3.125*
			1.625	0.465	0.285	1.050
			1.585	0.485	0.305	1.050
			1.545	0.525	0.340	1.050
		0.01668	2.020	0.650	0.320	1.115
			2.060	0.620	0.300	1.040
			2.045	0.695	0.340	1.170
			2.160	0.660	0.306	1.245
			2.300	0.700	0.302	1.400
			2.360	0.700	0.295	1.450
			2.490	0.740	0.295	1.620
			2.410	0.690	0.288	1.480
38.05	0.06958	0.06720	1.597	0.467	0.282	1.450
			1.730	0.470	0.272	1.625
			1.525	0.485	0.318	1.385
		0.04125	1.650	0.470	0.295	1.290
			1.517	0.487	0.321	1.234

**Not plotted.*

TABLE XI

DEAD-BEAT TRANSITION OF WATER LEVEL

$d = \infty$

Pipe length L, ft.	Pipe cross-section A, sq. ft.	Surge tank cross-section F, sq. ft.	Total head H, ft.	$h_{f_0} = H - H_0$, ft.	Y	X
22.00	0.03325	0.06720	1.890	0.290	0.153	1.160
			1.580	0.400	0.253	1.180
			1.550	0.365	0.234	1.085
			1.463	0.408	0.279	1.080
			1.661	0.351	0.210	1.150
		0.04125	1.900	0.380	0.200	1.132
			1.833	0.413	0.216	1.150
			2.165	0.305	0.141	1.110
			2.145	0.325	0.151	1.115
			2.705	0.245	0.090(5)	1.185
			1.715	0.455	0.265	1.125
			2.005	0.345	0.171	1.120
38.05	0.06958	0.06720	1.803	0.298	0.165	1.231
			1.667	0.337	0.202	1.230
			1.597	0.357	0.224	1.220
			1.730	0.320	0.185	1.240
			1.525	0.390	0.256	1.215
		0.04125	1.710	0.430	0.252	1.180

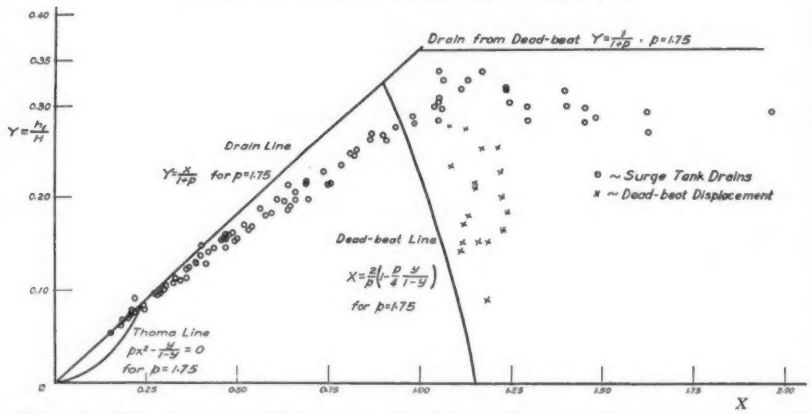

FIG. 11. Plot of calculated Thoma line, "dead-beat" line, and drain lines for $p = 1.75$, and experimental points for surge tank drainage and "dead-beat" displacements.

TABLE XII

Pipe length L, ft.	Pipe cross-section A, sq. ft.	Surge tank cross-section F, sq. ft.	$n^2 = \frac{gA}{LF}$	Observed m frequency	m^2	$\frac{m^2}{n^2}$	$\frac{h_{f_0}}{H_0} = \frac{Y}{1-Y}$
38.05	0.06958	0.06720	0.878	0.827	0.684	0.779	0.0159
				0.827	0.684	0.779	0.0185
				0.827	0.684	0.779	0.0237
				0.816	0.666	0.759	0.0297
				0.796	0.634	0.722	0.0340
				0.786	0.618	0.705	0.0370
				0.796	0.634	0.722	0.0424
				0.786	0.618	0.702	0.0542
		0.04125	1.430	1.030	1.061	0.742	0.0491
				1.013	1.026	0.717	0.0427
				1.013	1.026	0.717	0.0550
				1.013	1.026	0.717	0.0587
				0.997	0.994	0.695	0.0660
				0.981	0.962	0.672	0.0833
22.00	0.03325	0.06720	0.724	0.730	0.533	0.737	0.0615
				0.730	0.533	0.737	0.0513
				0.767	0.588	0.813	0.0453
				0.805	0.648	0.896	0.0362
				0.817	0.667(5)	0.923	0.0362
				0.817	0.667(5)	0.923	0.0297
		0.04125	1.180	0.924	0.854	0.723	0.0647
				0.967	0.935	0.792	0.0540
				0.982	0.964	0.817	0.0480
				0.997	0.994	0.842	0.0381
				1.013	1.026	0.869	0.0336
				1.030	1.061	0.899	0.0260
				0.923	0.852	0.722	0.0740
				0.952	0.906	0.767	0.0580
				0.952	0.906	0.767	0.0520
				0.967	0.935	0.792	0.0454
				1.013	1.026	0.869	0.0357
				1.013	1.026	0.869	0.0302
				1.047	1.097	0.929	0.0126
				1.047	1.097	0.929	0.0184
				0.952	0.906	0.768	0.0732
				0.952	0.906	0.768	0.0598
				0.982	0.964	0.817	0.0533
				0.997	0.994	0.842	0.0470
				0.997	0.994	0.842	0.0406
		0.01668	2.917	1.257	1.580	0.542	0.166
				1.257	1.580	0.542	0.162
				1.257	1.580	0.542	0.154
				1.310	1.716	0.589	0.146
				1.337	1.768	0.607	0.138(5)
				1.396	1.948	0.668	0.116
				1.396	1.948	0.668	0.105
				1.427	2.036	0.698	0.0977
				1.400	1.960	0.674	0.124
				1.460	2.132	0.731	0.100
				1.496	2.237	0.767	0.100
				1.496	2.237	0.767	0.0898

Values of m^2/n^2, where m was determined from the oscillation traces and n $(=\sqrt{gA/LF})$ took on the value appropriate to the particular pipe – surge tank relation, against $Y/(1-Y)$ $(=h_{f_0}/H_0)$ are set out in Table XII and shown graphically in Fig. 12. Once again they are compared with the curve representing equation [17] for the case $p = 1.75$.

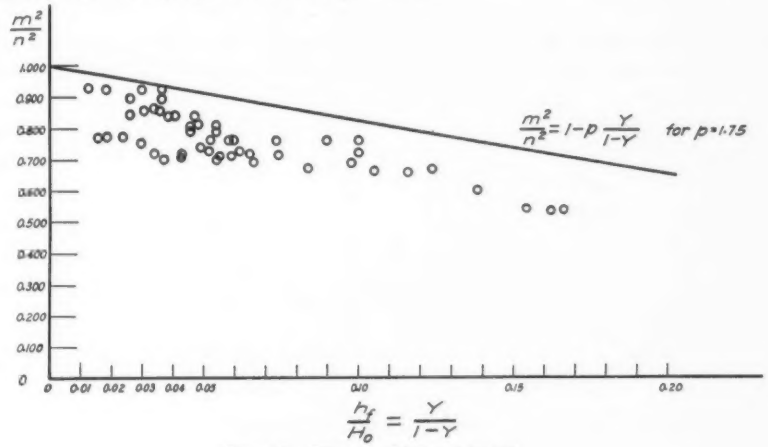

FIG. 12. Plot of m^2/n^2 and h_f/H_0.

TABLE XIII

d	h_{f_0}	X	Z_{th}	R'	Z_{obs}	$\frac{Z_{th}}{Z_{obs}} = \frac{R_{obs}}{R_{th}}$
1.00	0.025	0.092	0.992	0.275	0.992	1.00
	0.042	0.133	0.982	0.345	0.916	1.07
	0.034	0.122	0.985	0.326	0.865	1.14
	0.029	0.103	0.989	0.300	0.943	1.05
	0.020	0.094	0.991	0.240	0.886	1.12
	0.050	0.126	0.984	0.430	0.920	1.07
	0.025	0.108	0.988	0.262	0.883	1.12
	0.024	0.098	0.990	0.255	0.923	1.07
	0.033	0.125	0.984	0.272	0.967	1.02
	0.090	0.187	0.965	0.630	0.765	1.26
1.25	0.120	0.245	0.956	0.600	0.817	1.17
	0.150	0.287	0.937	0.695	0.752	1.25
	0.085	0.200	0.973	0.475	0.895	1.09
	0.043	0.153	0.986	0.295	0.957	1.03
	0.025	0.117	0.993	0.235	0.910	1.09
	0.034	0.120	0.993	0.295	0.960	1.03
	0.054	0.171	0.982	0.333	0.952	1.03
	0.110	0.226	0.964	0.610	0.798	1.21
	0.140	0.269	0.946	0.665	0.813	1.16
	0.037	0.159	0.975	0.255	0.916	1.06
1.50	0.180	0.329	0.936	0.690	0.794	1.18
	0.061	0.191	0.984	0.329	0.972	1.01
	0.044	0.154	0.992	0.285	1.002	0.99
	0.038	0.177	0.988	0.222	0.970	1.02
	0.090	0.223	0.975	0.405	0.997	0.98
	0.047	0.190	0.984	0.234	1.060	1.02
1.75	0.055	0.206	0.986	0.263	1.017	0.97
	0.135	0.294	0.959	0.490	0.937	1.020
	0.067	0.217	0.984	0.302	1.023	0.96
	0.065	0.230	0.980	0.300	0.942	1.04
	0.070	0.247	0.975	0.300	0.945	1.03
2.00	0.064	0.222	0.988	0.265	1.088	0.91
	0.110	0.270	0.975	0.390	1.045	0.93
	0.057	0.241	0.984	0.240	0.985	1.00
	0.043	0.208	0.990	0.200	1.034	0.96
	0.084	0.259	0.978	0.378	0.858	1.14
2.50	0.087	0.278	0.982	0.290	1.078	0.91
	0.081	0.280	0.982	0.272	1.064	0.92
	0.135	0.308	0.974	0.435	1.010	0.96
	0.235	0.407	0.942	0.620	0.932	1.01
	0.054	0.249	0.989	0.206	1.053	0.94

Finally to compare the observed magnitudes of the first downward surges with the values predicted by the linear equation, the values of Z_{th}/Z_{obs}, where

$$[38] \qquad Z_{th} = \frac{h_{f_0}}{RX} = (1-X^2)-(1-X^2)\left(\frac{\log_e d}{2\pi}\right)^2+2X\left(\frac{\log_e d}{2\pi}\right)\left(1-\left(\frac{\log_e d}{2\pi}\right)^2\right)$$

and Z_{obs} is the observed $h_{f_0}/R'X$ at the same d and X, and values of R', the observed first amplitude, are set out in Table XIII and shown graphically in Fig. 13.

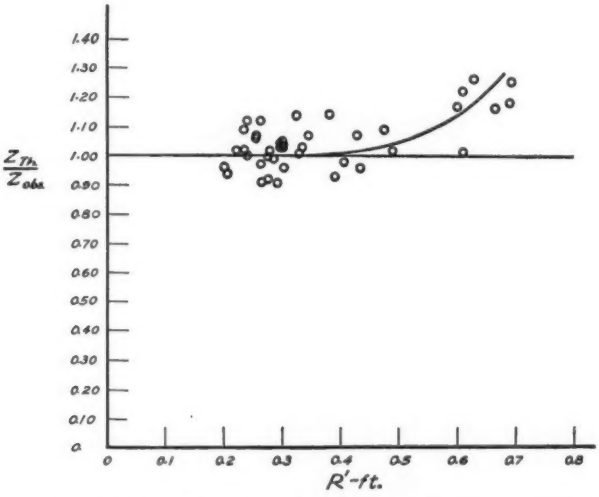

FIG. 13. Plot of Z_{th}/Z_{obs} against observed amplitude of first downward surge R'.

ANALYSIS OF RESULTS

It remains to inspect the theoretical and experimental results compared in Figs. 4 to 12 and to draw conclusions as to the ranges of validity of the predictions of the solution of the linear differential equation.

(1) *The Thoma Criterion for Oscillations of Constant Amplitude*

Referring to Fig. 5 it is seen that the experimental results lie generally a little to the right of the line predicted by the equation

$$[14] \qquad pX^2-\frac{Y}{1-Y} = 0 \qquad \text{for } p = 1.75,$$

and that they may be considered to fit the theoretical equation if p is taken as 1.4.

An inspection of the Moody chart for the range of Reynolds numbers employed shows that p cannot be as low as 1.4.

It is noted that the error is on the "danger" side in that the values of X and Y predicted to give oscillations of constant amplitude have in fact yielded oscillations that increase exponentially with time.

For a contributory cause of this discrepancy one may look back to an approximation made in the theory. The Thoma condition is actually given by

$$pX^2 - \frac{Y}{1-Y} V_0^{p-2} = 0 \qquad [46]$$

but for the sake of expressing the condition graphically in the XY space the approximation

$$V_0^{p-2} = 1$$

was made.

In the experiment, $V_0 = 0.659/H_0$ for the smaller pipe and $V_0 = 0.315/H_0$ for the larger pipe, and it is noted that for all readings H_0 was always greater than 1 ft. It follows that V_0 was always less than 1 f.p.s. so that with $p < 2$ the stability characteristic obtained from equation [46] lies to the right of that obtained from equation [14] and is therefore nearer the experimental curve.

Thus taking V_0 as 0.7 say, X has the value 0.27 instead of 0.25 for $Y = 0.10$, a value which is close to the experimental value.

It is noted that for values of V_0 greater than 1 f.p.s. such as will occur in the prototype, the curve given by equation [14] will be to the right of that given by equation [46], that is, the curve predicted as the critical criterion is actually a safe one. The approximation will have caused an error on the side of safety.

(2) *The Criteria for the Oscillations to Have Given Decrements*

Referring to Figs. 6 to 10, it is seen that as the logarithmic decrement is increased the theoretical characteristics given by

$$pX^2 - \frac{Y}{1-Y} = \frac{X}{\pi} \log_e d \qquad [23]$$

move to the right faster than the experimentally determined curves. In other words, if p was chosen as 1.4 to give the best fit at $d = 1$, then for larger values of d the experimental points would lie to the left of the predicted curve, the damping of the oscillations would not be as great as predicted.

The reason for this would again appear to be a theoretical approximation in that the more exact expression is

$$pX^2 - \frac{Y}{1-Y} = \frac{X}{\pi} (1-\rho) \log_e d, \qquad [25]$$

where ρ is a positive function of d, p, and Y, less than unity. Values of X obtained from equation [25] for given values of Y will be generally less than the corresponding values obtained from equation [23].

(3) *The Criteria for Drainage of the Surge Tank and for Dead-beat Transition of the Water Level*

An inspection of Fig. 11 shows that the deduced characteristic $Y=X/(1+p)$ for drainage from oscillatory motion predicts the experimental results for low values of X and Y (e.g. the case of drainage for $k < 0$) but for $X > 0.4$, $Y > 0.15$, the line lies generally above the experimental data, the discrepancy increasing for increasing X and Y.

It is again emphasized that the condition $Y = X/(1+p)$ was deduced only as a sufficient condition for drainage, that is, it is implied that the surge tank will certainly drain for values of X and Y satisfying it, but also perhaps for some slightly lower value of Y.

Another likely cause of the discrepancy at the higher values of Y is the fact that it is in this region that the neglected powers of w become important since h_{f_0} is now a relatively large proportion of H.

The discrepancies between theory and experiment observed at the dead-beat characteristic, and at the characteristic for drainage from the dead-beat state may perhaps be attributed to the linear equation no longer holding with the same accuracy.

It is mentioned that certain experimental difficulties were encountered in determining the conditions for drainage from the dead-beat state. The motion of the water level was sluggish yet critical in that any failure to follow it exactly with the slider would either stop its motion abruptly (slider slightly behind water level) or else cause a sudden overaccelerated drainage (slider slightly leading water level).

(4) *The Frequency of the Oscillations*

From Fig. 12 it is seen that the observed frequency m of oscillation of the water level is fairly uniformly less than that predicted by the equation

$$[19] \qquad \frac{m^2}{n^2} = 1-p\frac{Y}{1-Y} = 1-p\frac{h_{f_0}}{H_0}$$

for $p = 1.75$.

The experimental curve may be accepted as a line of the theoretically predicted slope -1.75, but making an intercept on the m^2/n^2 axis of about 0.9 instead of unity. It is noted from Table XII that for the lower values of $Y/(1-Y)$ the discrepancy was greater when the larger pipe was used. Since the large pipe (nominal diameter $3\frac{1}{2}$ in. and length 38 ft.) included about 5 ft. of $2\frac{1}{2}$ in. diameter connection (these being allowed for in computing its effective length, see section "Description of the Surge Tank Model") and also an additional elbow, it would seem likely that the frequencies were lowered by hydraulic damping in the pipe. The same may have occurred to a lesser degree as a result of the elbows in the smaller pipe.

(5) *The Amplitude of the First Downward Surge*

From Fig. 13 where the values of Z_{th}/Z_{obs}, where $Z_{th} = h_{f_0}/RX$ as calculated from equation [38], are plotted against the observed amplitude of the first

downward surge, R', it is seen that, allowing for the rather considerable scatter, Z_{th}/Z_{obs} stays constant at the value unity until R' reaches the value 0.5 ft., after which the curve turns upwards.

The reason for the scatter is that while allowance is made for the variation of k (or d) in equation [38], the magnitude of the first downward surge as measured experimentally is not R' but $R'e^{-kt_1}$ where t_1 is the time for the water to come to its first minimum. For the larger values of k this factor e^{-kt_1} may be appreciable.

The up-turning of the curve can possibly be attributed to the failure of the linear equation to apply to large displacements.

SUMMARY AND CONCLUSION

On the limited basis of the linear differential equation, characteristics for stability of the surge tank, for oscillations of given decrement, for drainage, and for a dead-beat transition of the water level were obtained. To allow for cases in model or prototype where the Reynolds number was not sufficiently high to ensure constancy of the Fanning (D'Arcy) friction factor for the flow in the pipe from the reservoir, the curves were obtained for a general pipe head-loss law of the form cV^p.

At the price of being able to represent the characteristics completely on an XY space, where X and Y are dimensionless parameters, respectively the ratio of the pipe friction loss in feet to the "free" amplitude of oscillation of surge-tank water level and the ratio of the pipe friction loss to the total head, the approximation $V_0^{\frac{1}{2}p-1} = 1$ had to be made in determining the Thoma condition for oscillations of constant amplitude. An approximation also had to be made in determining the curves for oscillation with a given decrement.

A sufficient condition for drainage valid for all X was obtained from the coefficient of w in the linear equation, and a more stringent condition was deduced to hold at the lower values of X yielding oscillatory motion. It was emphasized that the neglecting of terms involving higher powers of w may to a certain extent invalidate these results and also the derived condition for a dead-beat displacement of the water level.

A model was built to test the theory. The condition of constant hydraulic power input to the turbine was achieved by means of a bullet-shaped throttling device operated through a lever arm from a slider with which the water level in the surge tank could be followed manually. Traces of the wave-form of the oscillations were obtained from a recorder operating from the hydraulic pressure at the base of the surge tank.

Allowing for the deliberate theoretical approximations, satisfactory agreement between theory and experiment was obtained for the condition for oscillations of constant amplitude and for oscillations of a prescribed factor of decrement. As far as surge tank drainage was concerned, satisfactory agreement between theory and experiment was obtained only for the lower values of the parameters X and Y.

Allowing for frequency variations due to damping as a result of bends

and necks in the pipe from the reservoir, the frequency of the oscillation varied with friction generally as predicted by the linear equation.

There was evidence that the linear equation is inadequate to describe surge phenomena of large displacement.

ACKNOWLEDGMENT

Acknowledgment is made to the National Research Council of Canada whose research Grant G-514 made possible the development of this model and its associated apparatus.

REFERENCES

1. PAYNTER, H. M. Trans. ASME, 118: 962. 1953.
2. RICH, G. R. Hydraulic transients. McGraw-Hill Book Company, Inc., New York. 1951. p. 110.
3. THOMA, D. Sur Theorie des Wasserschlosses bei selbstatig geregelten Turbinenanlagen. Oldenburg, München, Germany. 1910.

COMPOSITION OF THE LIQUID PORTION OF FROZEN MILK[1]

By H. Tessier and Dyson Rose

Studies on the relation of lactose crystallization to casein precipitation in frozen milk indicate that the composition of the highly concentrated liquid phase of frozen milk influences the rate of casein precipitation (1, 2, 3). It was therefore desirable to estimate the composition of this liquid phase.

Collection of unfrozen liquid from frozen milk is difficult but some concentrated salt solution was obtained from milk by centrifuging during freezing, and sufficient solution for analysis could be collected by centrifuging an ultrafiltrate of concentrated milk during freezing. Skim milks and concentrates prepared from them by low temperature evaporation were therefore filtered under pressure through dialysis membranes supported on stainless steel screens. The ultrafiltrates of skim milks were analyzed directly. Fifty milliliter aliquots of ultrafiltrates from the concentrates were chilled, seeded to ensure ice formation from the top downward, and frozen while centrifuging at 500 R.C.F. for 24 hr. in a room at −12.5° C. (sample temperatures at equilibrium were −6° to −8° C.). The frozen upper portions of the samples were then withdrawn from the tubes, and the unfrozen portions (about 8 ml.) were held at 4° C. for a few hours to allow lactose to crystallize. The lactose was then sedimented at room temperature and the clear supernatants were analyzed.

Because separation of unfrozen liquid from the ice was not quantitative, the concentration effected by freezing could not be determined from volume estimates. However, since the chloride salts of milk are soluble at the concentration and temperature studied recovery of the other components was calculated relative to chloride concentration (Table I). About 80% of the sodium

TABLE I

Analysis of ultrafiltrates of skim milk and of the liquid portion of frozen ultrafiltrates

(Averages for three samples)

	Ultrafiltrate of skim milk	Liquid portion of frozen ultrafiltrate from concentrated milk	Recovery,* %
pH	6.7	5.8	—
Chloride	34.9 m*M*	459 m*M*	*100*
Citrate	8.0 "	89 "	84
Phosphate	10.5 "	84 "	61
Sodium	19.7 "	218 "	84
Potassium	38.5 "	393 "	78
Calcium	9.1 "	59 "	50

**Recoveries are calculated relative to chloride.*

[1]*Issued as N.R.C. No. 3928.*

and potassium, and about half the calcium remained in solution. Total cation concentration of the unfrozen portion varied from 0.6 to 0.8 *M* in the three samples analyzed. Precipitation of alkaline calcium phosphate increased the acidity of the unfrozen portion to pH 5.8. Direct freezing of milk during centrifugation yielded an unfrozen portion of pH 5.9, indicating that the buffering action of milk proteins does not prevent this pH shift.

While not in themselves sufficient to coagulate casein, salt concentrations and acidities corresponding to those of the liquid found in these unfrozen portions do decrease the stability of casein suspensions. Since only small amounts of lactose crystallized during the freezing of the ultrafiltrates, these unfrozen portions were essentially representative of the liquid phase of frozen milk at the beginning of a storage period. Further freezing of water as a result of lactose crystallization during storage would increase the acidity and salt concentration, and the chronological relation between casein precipitation and lactose crystallization (2, 3) suggests that this increase causes casein coagulation.

1. Rose, D. Can. J. Technol. 34: 145. 1956.
2. Tessier, H., Rose, D., and Lusena, C. V. Can. J. Technol. 34: 131. 1956.
3. Tummerman, L., Fram, H., and Cornely, K. W. J. Dairy Sci. 37: 830. 1954.

Received December 30, 1955.
Division of Applied Biology,
National Research Laboratories,
Ottawa, Canada.

AN ADHESION TEST FOR ELECTROPLATES

By J. D. McIntyre* and A. F. McMillan

The problem of testing the degree of adhesion of copper plating on metals arose in this laboratory. The literature (1) on the matter showed that there are no accurate, quantitative, simple methods for the measurement of adhesion. The following technique, developed to meet this need, measures the adhesion of copper plate in the shear direction, provided that the adhesion is not greater than the strength of solder. In addition this test may be used to measure the shear strength of solder.

A special aluminum "C-type" clamp with a hole of ½ in. diameter drilled in the upper face (Fig. 1) is used to clamp the plate whose adhesion is to be measured. The plate is masked with a piece of 1/8 in. aluminum sheet in which is accurately drilled a hole with a surface area of 1/16 sq. in. The plate and the mask are clamped, with the hole in the mask concentric with the hole in the clamp. The assembly is then heated by holding it by a pair of crucible tongs on the surface of a molten 50% lead – 50% tin solder solution at 250° C. Two drops of a zinc ammonium chloride flux solution (British Air Ministry DTD 81)

*Present address is the University of Toronto, Toronto, Ontario.

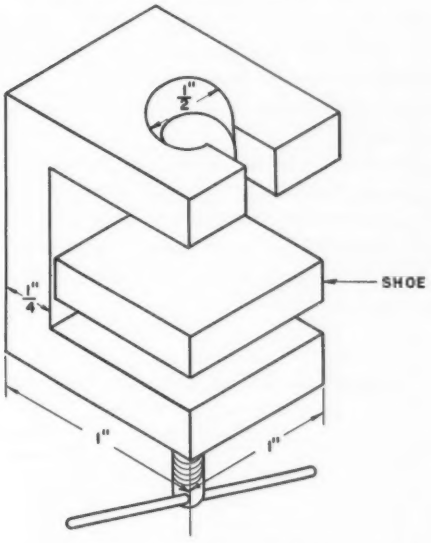

FIG. 1. Aluminum C-clamp.

are dropped on the exposed area of the plate with an eye-dropper and the assembly lowered into the solder. A heated cylindrical copper plug (½ in. long, ¼ in. diameter) is then quickly dipped in the flux solution and placed in the hole in the mask with a pair of tweezers so that the solder flows evenly around its edges. Excess solder is poured out the slot in the side of the clamp, and the assembly is quickly cooled by dipping in water, care being taken not to wet

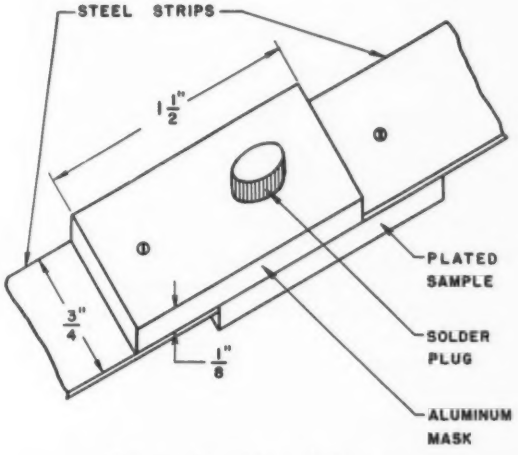

FIG. 2. Assembly ready for test.

the solder plug. After the solder has come in contact with the plate the operations are performed as rapidly as possible, since copper is soluble in molten solder. If this procedure is carried out correctly, a tight fitting reinforced solder plug is obtained. No filleting of the solder can occur, and the solder area of the plate is accurately defined.

Two stainless steel straps are bolted on, one to the mask, the other to the sample (Fig. 2), and are clamped in the tensile test machine. The shear stress is the force at which the solder – plate – basis metal bond breaks.

Samples cut from the same piece of copper plated aluminum were tested by this technique, and the results are shown in Table I. The maximum per cent deviation from the mean is 4.6.

TABLE I

ADHESION TEST FOR COPPER PLATED ALUMINUM

Test No.	Breakage force (lb.)	% Deviation from mean
1	295	4.2
2	270	−4.6
3	284	0.4
Average	283	

In Table II are shown some results obtained when this technique was used on copper plated aluminum whose adhesion was too strong for this type of test. The results may thus serve as an illustration for a determination of solder strength. The maximum per cent deviation from the mean is 4.3.

TABLE II

SOLDER STRENGTH TEST

Test No.	Breakage force (lb.)	% Deviation from mean
1	310	2.3
2	310	2.3
3	290	−4.3
Average	303	

ACKNOWLEDGMENTS

The authors acknowledge permission of the Chairman, Defence Research Board, to publish. The material in this note was part of the work carried out under D.R.B. Project D 12–75–20–01 at the Naval Research Establishment.

1. FERGUSON, A. L. and STEPHAN, L. F. Am. Electroplaters' Soc. Ser. Nos. 1 and 2. 1946.

RECEIVED JANUARY 13, 1956.
NAVAL RESEARCH ESTABLISHMENT,
DEFENCE RESEARCH BOARD,
DARTMOUTH, N.S.